# BUILDING THE CELL'S ANTENNA:
# PROTEIN TARGETING TO THE CILIARY MEMBRANE

A Dissertation Presented

By

John Alexander Follit

Submitted to the Faculty of the
University of Massachusetts Graduate School of Biomedical Sciences, Worcester
in partial fulfillment of the requirements for the degree of

DOCTOR OF PHILOSOPHY

MAY, 11th 2012

BIOMEDICAL SCIENCE

BUILDING THE CELL'S ANTENNA:
PROTEIN TARGETING TO THE CILIARY MEMBRANE

A Dissertation Presented
By

John Alexander Follit

The signatures of the Dissertation Defense Committee signify
completion and approval as to style and content of the Dissertation

(Signature)
Gregory J. Pazour, Thesis Advisor

(Signature)
Mary Munson, Member of Committee

(Signature)
Peter M. Pryciak, Member of Committee

(Signature)
Jaime A. Rivera-Perez, Member of Committee

(Signature)
Jagesh V. Shah, Member of Committee

The signature of the Chair of the Committee signifies that the written dissertation meets
the requirements of the Dissertation Committee

(Signature)
David G. Lambright, Chair of Committee

The signature of the Dean of the Graduate School of Biomedical Sciences signifies
that the student has met all graduation requirements of the school.

(Signature)
Anthony Carruthers, Ph.D.,
Dean of the Graduate School of Biomedical Sciences

Interdisciplinary Graduate Program
May, 11th 2012

## Dedication

For my mother...
"Are we having fun yet?"

**Acknowledgements**

I gratefully acknowledge my colleagues without whose contributions this thesis would not be possible, especially my thesis advisor Gregory Pazour, past and present members of the Pazour and Witman Labs and the members of my dissertation committee.

Finally, I would like to thank my family and friends for their constant love and support - without all of you this journey would not be possible.

Thank you all.

## Abstract

Protruding from the apical surface of nearly every cell in our body lies a specialized sensory organelle - the primary cilium. Eukaryotic cells use these ubiquitous structures to monitor the extracellular environment, defects in which result in an ever-growing list of human maladies termed ciliopathies including obesity, retinal degeneration and polycystic kidney disease. The sensory functions of primary cilia rely on the unique complement of receptors concentrated within the ciliary membrane. Vital to the proper functioning of the cilium is the cell's ability to target specific proteins to the ciliary membrane yet little is known how a cell achieves this highly polarized distribution. IFT20, a subunit of the intraflagellar transport particle is localized to the Golgi complex that is hypothesized to sort proteins to the ciliary membrane. We show that IFT20 is anchored to the Golgi complex by the golgin protein GMAP-210 and mice lacking GMAP210 die at birth with a pleiotropic phenotype that includes growth restriction and heart defects. Cilia on GMAP210 mutant cells have reduced amounts of the membrane protein polycystin-2 localized to them suggesting IFT20 and GMAP-210 function together in the sorting or transport of proteins to the ciliary membrane. To better understand the mechanism of ciliary protein trafficking, we identify a ciliary targeting sequence (CTS) contained within fibrocystin, the gene mutated in autosomal recessive polycystic kidney disease, and investigate a series of proteins required for the delivery of this sequence to the primary cilium. We demonstrate the small G protein Rab8 interacts with the CTS of fibrocystin and controls the ciliary levels of the CTS. Arf4 is another small G protein deemed a key regulator of ciliary protein trafficking. We show Arf4 binds the CTS of fibrocystin but is not absolutely required for trafficking of the fibrocystin CTS to cilia. *Arf4* mutant mice are embryonic lethal and die at mid-gestation likely due to defects in the non-ciliated visceral endoderm, where the lack of Arf4 caused defects in cell structure and apical protein localization. This suggests Arf4 is not only important for the efficient transport of fibrocystin to cilia, but also plays critical roles in non-ciliary processes. Together this work aims to elucidate the mechanisms of protein targeting to the ciliary membrane.

## Table of Contents


Title Page i
Approval Page ii
Dedication iii
Acknowledgements iv
Abstract v
Table of Contents vi
List of Figures viii
List of Tables ix

**CHAPTER I**
Introduction 1
Protein trafficking to the ciliary membrane 2
Intraflagellar transport and the strange case of IFT20 3
Ciliary targeting sequences 4
Proteins implicated in ciliary trafficking 10

**CHAPTER II**
**The Golgin GMAP210/TRIP11 Anchors IFT20 to the Golgi Complex**
Preface 17
Abstract 19
Author Summary 20
Introduction 21
Results
- Identification of IFT20 interacting proteins 25
- Identification of the IFT20 binding site on GMAP210 26
- Generation of a GMAP210 mutant mouse 32
- Cellular function of GMAP210 42

Discussion 51
Materials and Methods 59

**CHAPTER III**
**The Cytoplasmic Tail of Fibrocystin Contains a Ciliary Targeting Sequence**
Preface 65
Abstract 67
Introduction 68
Results & Discussion
- The cytoplasmic tail of fibrocystin contains a ciliary targeting signal 69
- Trafficking of the CTS is regulated by Rab8 79
- The CTS interacts with Rab8 82
- Comparison of ciliary targeting to apical and basolateral targeting 91

Materials and Methods 92

**CHAPTER IV**
**Arf4 Is Required for Mammalian Development but Dispensable for Ciliary Assembly**
Abstract 99
Author Summary 100
Introduction 101
Results
Arf4 interacts with the ciliary targeting sequence of fibrocystin 104
Arf4 is required for efficient delivery of the fibrocystin C-terminal tail to the cilium 110
Arf4 mutant mice are embryonic lethal 114
Arf4 expression is highest in the visceral endoderm 117
Arf4 is required for visceral endoderm function 120
Discussion 126
Materials and Methods 133

**CHAPTER V**
**Discussion**
GMAP210 and IFT20 as a ciliary sorting module 140
Implications and future directions of GMAP/IFT20 research 141
Identification of a fibrocystin ciliary targeting sequence 143
The fibrocystin CTS interacts with Rab8 and Arf4 143
Palmitoylation, lipid microdomains and CTS trafficking 144
Protein interactions and CTS trafficking 150
The role of Arf4 in ciliary vs. general trafficking 151
Closing remarks 153

**Bibliography** 154

## List of Figures


| | | |
|---|---|---|
| Figure 2.1: | Identification of GMAP210 as and IFT20 binding protein. | 27 |
| Figure 2.2: | Identification of the IFT20 binding site on GMAP210. | 30 |
| Figure 2.3: | Golgi binding site in GMAP210. | 33 |
| Figure 2.4: | Generation of a GMAP210 mutant mouse. | 36 |
| Figure 2.5: | Characterization of the GMAP210 mutant mouse phenotype. | 39 |
| Figure 2.6: | Lung cell types. | 43 |
| Figure 2.7: | Characterization of the GMAP210 cellular phenotype. | 46 |
| Figure 2.8: | GMAP210 mutant cilia. | 49 |
| Figure 3.1: | The cytoplasmic tail of fibrocystin contains a ciliary targeting sequence. | 70 |
| Figure 3.2: | Characterization of the CTS of fibrocystin. | 73 |
| Figure 3.3: | The CTS is associated with lipid. | 76 |
| Figure 3.4: | Colocalization between the CTS-GFP and various markers of the endomembrane system. | 80 |
| Figure 3.5: | Effect of Rab8 on the trafficking of the fibrocystin CTS. | 83 |
| Figure 3.6: | Fluorescence images of cells expressing the FLAG-tagged Rab proteins used in Figure 3.7 with the GFP-CTS. | 86 |
| Figure 3.7: | Rab8 interacts with the fibrocystin CTS. | 89 |
| Figure 4.1: | Arf4 interacts with the ciliary targeting sequence of fibrocystin. | 105 |
| Figure 4.2: | Arf4 expression inhibits CTS trafficking. | 108 |
| Figure 4.3: | Arf4 knockdown delays CTS trafficking to the primary cilium. | 112 |
| Figure 4.4: | Arf4 mutant mice are embryonic lethal. | 115 |
| Figure 4.5: | Arf4 mutant mice have functional nodal cilia. | 118 |
| Figure 4.6: | Arf4 expression is concentrated in the visceral endoderm during development. | 121 |
| Figure 4.7: | Arf4 mutant embryos have defects in the visceral endoderm. | 124 |
| Figure 5.1 | Model of Rab8 and Arf4 trafficking. | 145 |
| Figure 5.2 | Palmitoylated cysteines are required for proper CTS localization but dispensable for Arf4 binding. | 148 |

## List of Tables


| | | |
|---|---|---|
| Table 1.1: | Ciliary targeting sequences capable of delivering heterologous proteins to the cilium. | 5 |
| Table 4.1: | qPCR Primers | 138 |

# CHAPTER I

## Introduction

Cilia are subcellular organelles composed of a microtubule- based cytoskeleton surrounded by an extension of the plasma membrane and exist in motile and non-motile forms. The functions of motile cilia and flagella have long been recognized. The coordinated beating of cilia lining our respiratory tract clear mucus allowing us to breathe and propulsion of the male gamete required for fertilization of a human embryo are two of the most widely recognized functions of motile cilia. Another class of cilia exists that compensate for their lack of flashy motility with their association with an ever-growing list of human maladies; these are known as the primary cilia.

The darlings of countless electron microscopists, primary cilia were once viewed as a cellular anomaly, a curious vestige of our primitive past (Alberts, 1994). Protruding from the apical surface of nearly every cell in our body, a solitary non-motile primary cilium endures. Recent studies in the field of cilia biology have thrust this once neglected organelle firmly into the spotlight of a fascinating realm of cell biology. Defects in cilia structure or function result in a number of human diseases including obesity, cognitive deficits, polycystic kidney disease and retinal degeneration (Fliegauf et al., 2007; Pazour and Witman, 2003; Wheatley, 1995). This introduction serves to highlight the key features of the primary cilium with special focus given to current understanding of the mechanisms by which ciliary proteins are trafficked to this organelle.

## Protein trafficking to the ciliary membrane

Sight and smell, the detection of visual and olfactory stimuli, depend upon proper functioning of cilia. To perceive extracellular cues, the ciliary membrane is replete with an ever-growing number of trans-membrane receptors (Nachury et al., 2010). The ability of the cell to target and concentrate a specific set of receptors to the ciliary membrane is of upmost importance as the gene products of numerous human disease genes localize to cilia (Pazour and Bloodgood, 2008). Defects in receptors present on the ciliary membrane result in a pleiotropic class of human disorders termed ciliopathies (Waters and Beales, 2011). The diverse functions of cilia underlie the broad range of disorders associated with ciliary dysfunction including obesity, cognitive deficits, blindness and polycystic kidney disease (Fliegauf et al., 2007; Pazour, 2004). The numerous sensory functions of primary cilia rely on a unique complement of receptors that are targeted and concentrated within the ciliary membrane. While continuous with the apical plasma membrane, the ciliary membrane is a specialized subdomain of the plasma membrane that surrounds the ciliary axoneme (Rohatgi and Snell, 2010). Trans-membrane receptors destined for the ciliary membrane are first synthesized in the endoplasmic reticulum, sorted at the Golgi complex and subsequently delivered to the cilium (Nachury et al., 2010). The subsequent chapters explore the mechanisms underlying ciliary protein targeting.

## Intraflagellar transport and the strange case of IFT20

The primary cilium is composed of a microtubule-based axoneme consisting of nine outer doublets surrounded by an extension of the plasma membrane deemed the ciliary membrane. Intraflagellar transport (IFT) is the bi-directional movement of protein complexes along these microtubule tracks within a cilium (Kozminski et al., 1993). IFT is required to build, maintain and ultimately disassemble the cilium by transporting required axonemal subunits from the site of synthesis in the cell body to the growing tip of the cilium (Ishikawa and Marshall, 2011; Rosenbaum and Witman, 2002). Purification and subsequent characterization of IFT complexes from the biflagellar green algae *Chlamydomonas* revealed two multi-subunit complexes termed IFT Complex A and B (Cole et al., 1998). The IFT complexes are highly conserved in mammals. This fact led to a discovery identifying defects in IFT88, known to be required for ciliary assembly in *Chlamydomonas*, as the causative mutation in the *orpk* mouse model of polycystic kidney disease (PKD). This provided the first link between primary cilia and PKD (Pazour et al., 2000). A pool of IFT proteins is concentrated at the base of the cilium and IFT complexes in transit along the cilium are observed as punctate staining decorating the cilium (Rosenbaum and Witman, 2002).

One IFT protein is unique in its subcellular localization. The IFT Complex B subunit IFT20 is concentrated at the Golgi complex and exhibits dynamic movement between the Golgi and cilium (Follit et al., 2006). In addition to soluble proteins required to build the axoneme, the ciliary membrane is decorated with trans-membrane proteins synthesized by the endoplasmic reticulum, sorted at the Golgi complex and trafficked to

the ciliary membrane. Unique among the IFT proteins, the Golgi localization of IFT20 suggested that it might play a role in sorting proteins at the Golgi destined for the cilium. Early RNAi based studies demonstrated that partial knocking down of IFT20 resulted in decreased levels of the ciliary membrane channel polycystin-2 (Follit et al., 2006). The second chapter of this dissertation builds on these findings and further explores the role of IFT20 at the Golgi complex.

## Ciliary targeting sequences

Intraflagellar transport is known to move soluble axonemal precursors from their site of synthesis in the cell body to the growing tip of the cilium. Ciliary function also relies on specific receptors localized to the ciliary membrane and many of these trans-membrane receptors undergo IFT-like movement within the cilium. However, with the exception of IFT20, the majority of IFT proteins are believed to transport cargo within the cilium, but little is known regarding the intracellular transport of trans-membrane receptors to the cilium (Nachury et al., 2010; Pazour and Bloodgood, 2008).

To understand the mechanisms required for ciliary protein targeting a number of groups have identified targeting sequences in known ciliary proteins. A ciliary targeting sequence (CTS) is a domain within a protein necessary and sufficient to target said protein to the cilium. The CTS is often a transferrable module capable of conferring ciliary targeting to a previously non-ciliary protein; in fact this ability is required to validate potential ciliary targeting sequences.

**Table 1.1 Ciliary targeting sequences capable of delivering heterologous proteins to the cilium** [modified from (Nachury et al., 2010)].

| Protein | Function | Lipidation | CTS (key residues in bold) | Reference |
|---|---|---|---|---|
| **Polycystin-1** | Unknown | Not Determined | **KV**H**P**SST | Ward et. al (2011) |
| **Fibrocystin** | Unknown | Palmitoylated | **C**LV**CCWFKKSKTRKIKPE** | Follit et. al (2010) |
| **Cystin** | Unknown | Myristoylated | T**AS**E**GG**TA | Tao et. al (2009) |
| **Polycystin-2** | Cation Channel | Not Determined | MVNSS**RV**Q**P**QQPGDA | Geng et. al (2006) |
| **Rhodopsin** | Photon Receptor | Palmitoylated | SSSQ**VSP**A | Tam et. al (2000) |
| **SSTR3** | Somatostatin Receptor | Not Determined | **A**PS**CQ** + **A**PA**CQ** | Berbari et. al (2008); Jin et. al (2010) |
| **5HT6** | Serotonin Receptor | Not Determined | **A**TAG**Q** | Berbari et. al (2008) |

Rhodopsin is a seven-span transmembrane receptor that is concentrated in the highly specialized photoreceptor cilium and is required for light detection in the first steps of the visual system. Mutations present in the last five residues of rhodopsin (QVSPA) result in severe autosomal dominant retinal degeneration and deletion of this motif impairs trafficking of rhodopsin (Berson et al., 2002). Tam et. al identified a CTS present in the c-terminal tail of rhodopsin by fusing the last eight amino acids of rhodopsin to membrane- anchored GFP or the cytoplasmic tail of structurally similar but non-ciliary localized AAR and demonstrating trafficking of this heterologous protein to the rod outer segment (ROS) (Tam et al., 2000). Interestingly truncations/mutations to the QVSPA caused an accumulation of these proteins within the rod inner segment (RIS)

and reduced, but did not prevent targeting to the ROS, suggesting additional residues may be involved in Rhodopsin trafficking to the ROS.

Defects in the ciliary-localized transmembrane receptors polycystin-1, polycystin-2 and fibrocystin result in polycystic kidney disease (Pazour et al., 2002b; Ward et al., 2003; Yoder et al., 2002). Characterized by the over proliferation and poor differentiation of the ciliated kidney epithelia, this progressive degenerative disorder afflicts between 1:1000 (ADPKD) and 1:20,000 (ARPKD) persons worldwide (Chapin and Caplan, 2010; Harris and Torres, 2009). Geng et. al identified a (RVxP) sequence present in polycystin-2 that shared similarity with the CTS of rhodopsin (Geng et al., 2006). In an elegant series of experiments, Geng et. al demonstrated that the first 72 amino acids of polycystin-2 are both necessary and sufficient to direct the non-ciliary PKD2L1, albeit weakly, to primary cilia. Using a second heterologous fusion with the transferrin receptor, Geng et. al further refined the CTS to the first 15 amino acids of polycystin-2. Conserved residues including the RVxP motif were identified and subsequently mutated confirming the importance of these residues within the CTS of polycystin. Truncations to the N-terminal amino acids (Δ5-72) or mutations (R6G, V7A, P9A) resulted in heterologous protein accumulation within the endoplasmic reticulum (ER) and endo H insensitivity, suggesting the mutant proteins may be misfolded and unable to exit the ER. Of note, the RVxP motif is not conserved in *C. elegans* although this orthologue of polycystin-1 is known to localize to cilia indicating an alternative pathway may be present in *C. elegans* (Bae et al., 2006).

G protein-coupled receptors serve a vast array of sensory functions and play vital roles in both our sense of taste and smell (Takeda et al., 2002). The seven trans-membrane span receptors must be properly localized within the cell including several isoforms that are concentrated to the ciliary membrane including the third isoform of the somatostatin receptor (SSTR3) and the sixth isoform of the serotonin receptor (5HTR6) (Brailov et al., 2000; Hamon et al., 1999; Handel et al., 1999; Schulz et al., 2000). Taking advantage of closely related but non-ciliary localized Sstr5 and 5Htr7 and using a well-designed series of domain swapping experiments, Berbari et. al demonstrated the third intracellular loop (i3) of Sstr3 or 5Htr6 was necessary and sufficient to direct the previously plasma membrane localized Sstr5 or 5Htr7 receptors to the ciliary membrane (Berbari et al., 2008). Sequence alignment and analysis highlighted a unique (AxS/AxQ) motif present in the i3 loop of both Sstr3 and 5Htr6; subsequent mutation of the conserved A and Q residues to F drastically reduced ciliary localization of each construct. Using the (AxS/AxQ) to screen a library of i3 loops from all human GPCRs, the authors identified a number of known ciliary receptors including opsin, and identified four additional GPCRs of unknown cellular localization. In support of the (AxS/AxQ) motif as a predictor of ciliary GPCRs, the authors demonstrated one of their identified receptors (Mchr1) indeed localizes to cilia in both mouse brain and cultured kidney cells.

Following the identification of the i3 loop CTS, Jin et. al used the i3 loop of SSTR3 in a ciliary trafficking assay in which the authors fused the i3 loop of Sstr3 to the transmembrane and extracellular domain of CD8a creating a single span trans-membrane chimera (Jin et al., 2010). The CD8a/Sstr3(i3) traffics efficiently to the cilium and

confirms a CTS is located within the Sstr3(i3) domain. However the previously identified A and Q residues were not required for the ciliary localization of this CD8a/Sstr3(i3). Rather, Jin et al. describe two conserved cysteines adjacent to the Q are required for ciliary localization of the CD8a/Sstr3(i3) chimera. The observed differences suggest that the context in which the i3 CTS is presented is important in ciliary trafficking, as Jin et. al suggests the original A/Q mutations may result in a misfolded protein subject to ER retention. Unfortunately Berbari et. al do not discuss the effect of the A/Q mutations on the subcellular localization and possible ER retention of either Sstr3 or 5Htr6 as this information would be useful in assessing the possible function of this sequence.

Proper presentation and requisite sorting of CTSs may involve important post-translational modifications, since many ciliary-localized receptors are known to be lipid modified including rhodopsin(Emmer et al., 2010; Nachury et al., 2010; Pazour and Bloodgood, 2008). In some cases, lipid modifications are inseparable from CTS activity as is the case with the CTS of fibrocystin and the peripheral membrane protein cystin (Follit et al., 2010; Tao et al., 2009). Initially identified as the causative mutation in *Cys1*$^{cpk}$ mouse model of autosomal recessive polycystic kidney disease. Tao et. al demonstrate that cystin localizes to cilia in both embryonic mouse kidneys and cultured kidney cells and often note an interesting accumulation of cystin at the ciliary tip (Tao et al., 2009). To better understand the ciliary targeting of cystin, the authors performed deletion analysis to identify a CTS in the first 50 amino acids of cystin, which is N-terminally myristoylated and associated with the lipid microdomain marker flotillin-1.

Mutations that block myristoylation prevent lipid microdomain association and subsequent ciliary localization of cystin; however a similarly myristoylated protein HIV Gag does not localize to the cilium, demonstrating that myristoylation is necessary but not sufficient for ciliary localization of cystin. Using the N-terminal myristoylated first 30 amino acids of HIV Gag followed by amino acids 22-50 of cystin, the authors further refine the CTS. Sequence analysis identified a conserved AxEEG motif that when mutated blocks ciliary localization of cystin or chimeric cystin/gag. When combined with myristoylation, the AxEEG motif constitutes a functional CTS and suggests an intriguing link with lipid modifications as a primary sorting step in ciliary trafficking.

Mutated in 85% of autosomal dominant polycystic kidney disease, the PKD1 gene encodes, polycystin-1, a 12-span transmembrane receptor that localizes to the ciliary membrane (Yoder et al., 2002). To identify the CTS of polycystin-1, Ward et. al constructed a heterologous fusion of the last 112 intracellular residues of polycystin-1 fused to the trans-membrane domain of CD7 and extracellular domain of CD16 that localizes to the primary cilium (Ward et al., 2011). The authors identified a conserved KVxP motif that is similar to the rhodopsin and polycystin-2 CTS, residing within the final 20 residues of polycystin-1, and demonstrated that deletion of the final 20 amino acids or mutagenesis of the KVxP motif prevented ciliary targeting of CD16/7/Pkd1. However it is important to point out any mutation to the putative polycystin-1 CTS resulted in an accumulation of protein with the ER, again complicating the interpretation of results. To support a role for the KVxP motif in ciliary trafficking, Ward et al fused the KVHPSST motif to a similar CD16/CD7 construct containing the full C-terminal tail

of CD7 and show this chimera traffics to 100% of cilia. Once again, it is important to point out that the authors show their CD16/CD7 construct without the putative CTS traffics to 50% of cilia, an unusual localization since entry into the cilium is generally regarded as a tightly regulated process. Furthermore, the authors failed to perform a critical mutagenesis experiment in the same CD16/CD7 construct that would distinguish between a bona fide CTS and a mutation that results in an unfolded and subsequently ER-retained protein.

In Chapter III we identify a CTS in the cytoplasmic tail of fibrocystin, the gene product mutated in autosomal recessive polycystic kidney disease, and examine salient features including lipid modification and interaction with the small G protein Rab8 (Follit et al., 2010).

## Proteins implicated in ciliary trafficking

The identification of ciliary targeting sequences is a significant first step in understanding how trans-membrane proteins are directed to the cilium. Once a CTS is identified, the focus turns to better understanding the mechanisms that drive the CTS sequence to the ciliary membrane. One approach is to identify proteins and/or complexes that specifically interact with a CTS and that are themselves required for cargo delivery to the cilium. Here we examine recent findings linking candidate proteins to known CTSs and provide biochemical and functional data in support.

Rhodopsin trafficking to the photoreceptor cilium is one of the best-studied examples of protein trafficking to a ciliary membrane. The C-terminal tail of rhodopsin

harbors a VxPx CTS; mutations within this region cause rhodopsin mislocalization and lead to severe retinal degeneration (Deretic, 2006). To better understand the mechanism of rhodopsin trafficking, Deretic and colleagues used two rhodopsin peptides, one corresponding to the C-terminal tail and another that lacked the VxPx CTS, to search for rhodopsin interacting proteins. Using a combination of photo-activatable crosslinkers and GST pulldown assays, the authors identified the small G protein Arf4 to be a protein that specifically interacted with the full-length rhodopsin peptide but not the peptide lacking the VxPx motif. Antibodies to Arf4 or rhodopsin inhibited rhodopsin transport carrier (RTC) formation in an in vitro assay and suggested a functional role for Arf4 in RTC formation (Deretic et al., 2005).

Based on this work, Mazelova et. al. confirmed the VxPx motif is required for RTC formation in the same cell free assay; using a combination of co-localization and co-fractionation experiments, additional components of this trafficking pathway were identified including the small G protein Rab11, an effector FIP3 and the GTPase activating protein ASAP1 (Mazelova et al., 2009). In a series of loosely controlled immunoprecipitations, Mazelova and colleagues showed some evidence for a Arf4/Rab11/FIP3/ASAP1 complex and demonstrated that perturbation of any of these proteins inhibits RTC budding. To support a functional role for this complex in rhodopsin trafficking, transgenic frogs harboring a mutation in Arf4 that inhibited ASAP1 mediated GTP hydrolysis exhibited rhodopsin trafficking defects (Mazelova et al., 2009). Taken together these results suggest a possible role for an

Arf4/Rab11/FIP3/ASAP1 complex, however the authors fail to provide a direct link to the functional effect these proteins may have on rhodopsin trafficking.

Based on the Arf4/rhodopsin model of ciliary trafficking Ward et. al asked if a similar trafficking module is required for polycystin-1 delivery to cilia (Ward et al., 2011). A series of in vitro GST binding and immunoprecipitation studies demonstrated interactions between Arf4 and the CTS of polycystin-1. Removal of the predicted Arf4 binding site KVHPSST resulted in a 50% reduction in its ability to bind to polycystin-1. Additional deletion analysis of the CTS revealed a similar reduction in polycystin-1/Arf4 where each successive deletion results in 50% less polycystin-1 binding to Arf4. The authors concluded the KVHPSST sequence is required for Arf4 binding and constitutes a functional CTS. However, the data indicated additional truncations to the C-terminal tail of polycystin-1 have similar graded effect on ciliary trafficking. This suggests there are other functional motifs present in the C-terminal tail of polycystin in addition to the indicated KVHPSST. The authors then used a series of poorly controlled and unconvincing IPs to suggest a Rab6/Rab11/ASAP1 complex exists in mammalian cells, however functional data to support these claims is absent. RNAi mediated knockdown of two putative polycystin-1 CTS interacting proteins, Arf4 and Rab8, resulted in an approximately 50% reduction in polycystin-1 CTS positive cells and provides some functional support for the authors' conclusions. Additional experiments are required to investigate and validate the potential roles of Arf4, Rab8 and especially Rab6/Rab11/ASAP1 and possible consequences related to ciliary protein trafficking.

Intraflagellar transport (IFT) is required for the transport of soluble axonemal precursors from their site of synthesis in the cell body to the point of assembly at the growing tip of the cilium (Ishikawa and Marshall, 2011; Rosenbaum and Witman, 2002). Bhowmick et. al asked if IFT-based mechanisms may also move trans-membrane cargo within the cilium (Bhowmick et al., 2009). Based on a yeast two-hybrid screen with IFT Complex B subunit IFT88 as bait, and confirmed through reciprocal immunorecipitation studies, the authors identified IFT Complex B members and the co-chaperone protein MRJ and its binding partner HSC70 as IFT88 interacting proteins. The ciliary-localized MRJ was also able to pull down the trans-membrane guanylyl cyclase 1 (GC1) from bovine retinal extracts. To investigate whether these MRJ/GC1 complexes also contained IFT Complex B proteins, the authors performed a series of co-immunoprecipitations that showed a weak interaction with MRJ/GC1 and a number of IFT proteins. The addition of ATP significantly increased interactions with MRJ/Hsc70/IFT complexes with trans-membrane receptors GC1 and rhodopsin, providing the most convincing evidence for an IFT/trans-membrane cargo interaction. Further research is needed to explore the role of ATP on MRJ/Hsc70 interactions with IFT and possible effects on trans-membrane cargo.

Previously we discussed the unique distribution of another IFT protein, IFT20, which is found in the Golgi complex in addition to the canonical basal body and ciliary localization (Follit et al., 2006). Data presented in Chapter II and in previous work suggest that IFT20 may play a role in ciliary protein targeting, as reduction in IFT20 or IFT20's binding partner GMAP210 results in decreased ciliary levels of polycystin-2 (Follit et al., 2008). To further investigate the role of IFT20 in ciliary trafficking, Keady

et. al examined the effect of deleting IFT20 in mouse photoreceptors (Keady et al., 2011). Using a tamoxifen inducible Cre to delete IFT20 in the retina, rhodopsin rapidly becomes mislocalized within the photoreceptors. Immunogold labeling indicates rhodopsin accumulates in the Golgi complex suggesting that IFT20 may be involved in rhodopsin trafficking and sorting at the Golgi. A series of GST-pulldowns and immunoprecipitations demonstrated that IFT20 interacts with the C-terminal tail of both opsin and rhodopsin in addition to the IFT Complex B members IFT57, IFT52 and IFT54. In contrast to reported rhodopsin binding to Arf4, the VxPx motif appears dispensable for interactions with IFT Complex B proteins. Finally the authors asked if IFT20, the only Golgi localized IFT protein, interacted with opsin independent of IFT Complex B. Use of the GMAP210 binding domain for IFT20 binding (discussed in Chapter II) the authors pulldown IFT20 and opsin but not other IFT proteins. This confirms an opsin interaction with IFT20 that is independent of IFT Complex B, presumably at the Golgi Complex.

Cilia are required for myriad sensory functions. Consequently, defects in ciliary function often result in pleiotropic symptoms as is the case in Bardet-Biedel Syndrome (BBS). Characterized by retinal degeneration, polydactylyly, obesity and kidney cysts, Bardet-Biedel Syndrome is associated with ciliary dysfunction caused by defects in any of 14 known BBS genes (Fliegauf et al., 2007). A number of the BBS proteins form a stable complex called the BBSome that has been implicated in vesicular trafficking to cilia (Nachury et al., 2007). In an elegant series of experiments, Jin et al. demonstrate that the small G protein BBS3(Arl6) recruits the BBSome to the cilium in cultured cells and

drives its association with membranes in vitro in a GTP dependent manner (Jin et al., 2010). Using structure based algorithms and drawing corollaries to the Arf1/coatamer complex, the authors suggest the BBSome functions as a coat recruited by BBS3 that is required for the entry of trans-membrane receptors to the cilium. In support of this, the authors demonstrate that the BBSome directly interacts with CTS of Sstr3 and that this interaction is required for entry of the Sstr3 CTS to primary cilia in hippocampal neurons and cultured cells. Although the BBS3/BBSome fails to form vesicles from membrane in vitro and does not meet the classical requirements of a bona fide coat, this is the best evidence to date of the direct CTS recognition by large protein complex and subsequent trafficking into the cilium.

Further support of BBS functions in ciliary protein trafficking includes the identification of another BBS interacting protein Lztfl1 (Seo et al., 2011). Seo et. al created a functional BBS4 LAP tagged transgenic mouse and purified the BBSome from mouse testis and identified Leucine zipper transcription factor-like 1 (Lztfl1). Unlike BBS proteins Lztfl1 is not localized to the basal body or cilium and is, instead, concentrated in the cytoplasm where it appears to sequester the BBSome. A combination of over-expression and knockdown studies indicates a high level of Lztfl1 reduces ciliary levels of several BBS proteins and knockdown of Lztfl1 increases ciliary levels of BBS proteins. Finally the authors report Lztfl1 knockdown increased ciliary levels of the trans-membrane receptor smoothened and demonstrate BBSome binding to the c-terminal tail of smoothened. The authors speculate that altered BBSome function caused by Lztfl1 knockdown results in abnormal ciliary accumulation of smoothened. Further

experiments are needed to determine if smoothened accumulation is a result of increased delivery or a failure to remove smoothened from the cilium by BBS proteins.

This introduction highlights the vital role of the primary cilium in numerous sensory functions – sensory functions that depend on the specific receptors targeted to the ciliary membrane. The recent advances in the field of ciliary protein trafficking highlight this exciting and rapidly evolving field of cell biology. The subsequent chapters represent significant contributions to the understanding of ciliary protein trafficking.

# CHAPTER II

## The Golgin GMAP210/TRIP11 Anchors IFT20 to the Golgi Complex

### Preface

Originally published in Plos Genetics*, Chapter II describes the role of a golgin protein GMAP-210 in anchoring IFT20 to the golgi complex and the requirement of GMAP-210 in mouse development. Cardiac defects evident in GMAP-210 (*Trip11*) knockout embryos were investigated in collaboration with Cecilia Lo and Rajeev Samtani who added significant technical and analytical contributions to this work including the data in Figure 2.5. GMAP-210 lung defects were characterized by Jovenal T. San Agustin who contributed data to Figure 2.6. Fenghui Xu provided assistance in cloning some of the GMAP-210 constructs and Julie Jonassen conducted rtPCR and statistical analysis of the GMAP-210 expression levels. Finally, this chapter was co-authored primarily with Greg Pazour.

*The Golgin GMAP210/TRIP11 anchors IFT20 to the Golgi complex. Follit JA, San Agustin JT, Xu F, Jonassen JA, Samtani R, Lo CW, Pazour GJ. *PLoS Genet.* 2008 Dec;4(12):e1000315. Epub 2008 Dec 26. PMID: 19112494

**The Golgin GMAP210/TRIP11 Anchors IFT20 to the Golgi Complex**

John A. Follit, Jovenal T. San Agustin, Fenghui Xu, Julie A. Jonassen[1], Rajeev Samtani[2], Cecilia W. Lo[2] and Gregory J. Pazour[‡]

Program in Molecular Medicine
University of Massachusetts Medical School
Biotech II, Suite 213
373 Plantation Street
Worcester, MA 01605

[1]Department of Physiology
University of Massachusetts Medical School
55 Lake Avenue North
Worcester MA 01655

[2]Laboratory of Developmental Biology
National Heart Lung Blood Institute
National Institutes of Health
Bethesda, MD 20892

## Abstract

Eukaryotic cells often use proteins localized to the ciliary membrane to monitor the extracellular environment. The mechanism by which proteins are sorted specifically to this subdomain of the plasma membrane is almost completely unknown. Previously we showed that the IFT20 subunit of the intraflagellar transport particle is localized to the Golgi complex in addition to the cilium and centrosome and hypothesized that the Golgi pool of IFT20 plays a role in sorting proteins to the ciliary membrane. We show here that IFT20 is anchored to the Golgi complex by the golgin protein GMAP210/Trip11. Mice lacking GMAP210 die at birth with a pleiotropic phenotype that includes growth restriction, ventricular septal defects of the heart, omphalocele, and lung hypoplasia. Cells lacking GMAP210 have normal Golgi structure but IFT20 is no longer localized to this organelle. GMAP210 is not absolutely required for ciliary assembly, but cilia on GMAP210 mutant cells are shorter than normal and have reduced amounts of the membrane protein polycystin-2 localized to them. This work suggests that GMAP210 and IFT20 function together at the Golgi in the sorting or transport of proteins destined for the ciliary membrane.

## Author Summary

The primary cilium is a sensory organelle used by cells to monitor the extracellular environment. In mouse, severe defects in primary cilia lead to embryonic lethality while less severe defects cause a pleiotrophic phenotype that includes cystic kidney disease, retinal degeneration, obesity, and hydrocephaly among others. The sensory functions of cilia rely on proteins localized to the ciliary membrane, which is continuous with the plasma membrane of the cell. Cells have the ability to specifically localize proteins to the ciliary membrane to the exclusion of the rest of the plasma membrane. Little is known about how this is accomplished. In prior work, we showed that the ciliary assembly protein IFT20 is localized to the Golgi complex in addition to the cilium and proposed that it is involved in sorting or transport of membrane proteins to the cilium. In this work we show that IFT20 is anchored to the Golgi complex by the golgin GMAP210. Mice defective in GMAP210 die at birth with lung and heart defects. Cells from these animals have ciliary defects suggesting that IFT20 and GMAP210 function together at the Golgi complex in the trafficking of ciliary membrane proteins.

## Introduction

Most vertebrate cells have a non-motile primary cilium projecting from their surface (Satir and Christensen, 2007; Wheatley, 1995). Defects in these organelles lead to a wide range of developmental disorders and diseases ranging from embryonic lethality in severe cases to polycystic kidney disease and retinal degeneration with less extreme alleles. These non-motile primary cilia are thought to be sensors of the extracellular environment. A number of receptors and channels have been localized to the ciliary membrane including the opsin photoreceptors of the vertebrate retina, the odorant receptors of the olfactory system, the SSTR3 isoform of the somatostatin receptor (Handel et al., 1999), smoothened and patched, transmembrane receptors in the hedgehog signaling pathway (Corbit et al., 2005; Rohatgi et al., 2007), the PDGFRα isoform of the platelet derived growth factor receptor (Schneider et al., 2005), and the polycystins and fibrocystin, products of the human polycystic kidney disease genes (Hou et al., 2002; Pazour et al., 2002b; Yoder et al., 2002).

Little is known about how the ciliary membrane is assembled and maintained despite the fact that this membrane is vitally important for the sensory functions of cilia. While the ciliary membrane is continuous with the plasma membrane of the cell it is a separate domain with a unique complement of proteins localized to it (Bloodgood, 1990). The mechanism separating the ciliary membrane domain from the rest of the apical plasma membrane is likely to involve a membrane-cytoskeletal complex called the ciliary necklace (Gilula and Satir, 1972). The proteins that make up these complexes are as yet

unknown, but probably help form the diffusional barrier separating the two zones. There is also a zone of condensed lipid at the base of the cilium that may contribute to the barrier (Vieira et al., 2006). Membranous vesicles containing ciliary membrane proteins appear to dock on the plasma membrane just outside of the cilium (Bouck, 1971; Papermaster et al., 1985). Recent studies are beginning to identify the protein machinery required for trafficking to the ciliary membrane. In *C. elegans*, progress has been made in identifying proteins required for transport of membrane proteins into the dendrite, which is a prerequisite step for ciliary membrane targeting in this organism, but proteins required specifically at the cilium are still unknown (Bae et al., 2006). In vertebrates, Rab8 appears to regulate the transport of membrane proteins to the cilium as expression of dominant negative Rab8 causes opsin-containing vesicles to accumulate at the base of the cilium (Moritz et al., 2001) and also prevents the formation of cilia in cultured cells (Nachury et al., 2007). Defects in proteins required for polarization of mammalian cells such as FAPP2 (Vieira et al., 2006), Crumbs3-CLPI (Fan et al., 2007), annexin-13, and syntaxin-3 (Torkko et al., 2008) also perturb ciliogenesis, but whether these are acting directly on transport of ciliary proteins or indirectly in the formation of the apical domain is not known (Vieira et al., 2006). Smoothened transport in mammalian cells requires beta-arrestin (Kovacs et al., 2008) although this is not required for transport of polycystin-2 in *C. elegans* (Bae et al., 2006).

Intraflagellar transport (IFT) is responsible for assembling the non-membrane portions of the cilium (reviewed in (Rosenbaum and Witman, 2002; Scholey, 2003)) but its role in movement of membrane proteins is not clear. During IFT, large complexes,

composed of ~20 proteins are transported along the ciliary microtubules under the membrane (Cole et al., 1998; Piperno and Mead, 1997). The complexes are thought to carry proteins from their site of synthesis in the cell body to sites of assembly in the cilium. The IFT particles traffic along the microtubule axoneme just under the flagellar membrane and probably interact with the membrane (Kozminski et al., 1993; Pazour et al., 1998). The nature of the connection between the ciliary membrane and the particle is not obvious as none of the known IFT particle proteins have any predicted transmembrane domains (Cole, 2003). In *C. elegans*, membrane channels move in cilia at rates that are comparable to those of IFT, suggesting that IFT moves proteins within the ciliary membrane (Qin et al., 2005) and in *Chlamydomonas*, movement of a membrane associated kinase into the cilium requires IFT (Pan and Snell, 2003). Levels of the transmembrane protein, polycystin-2, are elevated in cilia when the IFT88 subunit is mutated in *C. elegans* (Qin et al., 2001), mouse (Pazour et al., 2002b), and *Chlamydomonas* (Huang et al., 2007) suggesting that IFT88 may be more important for removing polycystin-2 from the cilium than inserting it into the cilium.

We previously showed that one of the IFT particle proteins, IFT20, is localized to the Golgi complex as well as to the cilium and the peri-basal body pool. We hypothesized that IFT20 plays a role in the sorting or transport of membrane proteins processed through the Golgi complex and destined for the ciliary membrane. This idea was based on the observation that IFT20 moved between the Golgi and ciliary compartments and the demonstration that partial reduction of IFT20 by RNAi reduced the level of the membrane protein polycystin-2 in cilia (Follit et al., 2006). In this work we

sought to further our understanding of the function of the Golgi-associated pool of IFT20 by identifying proteins that interact with IFT20 at the Golgi complex. To do this, we immunoprecipitated an IFT20-containing complex from mouse kidney cells and used mass spectrometry (MS) to identify one of the subunits as a golgin known as GMAP210 or TRIP11. This peripheral membrane protein was previously shown to be localized to the Golgi complex by a number of groups (Barr and Egerer, 2005). Beyond localization to the Golgi complex, there is little agreement in the literature about the function of this protein in mammals and it has been proposed to play roles ranging from regulating gene expression, controlling Golgi structure, and polarized secretion. To understand the *in vivo* function of GMAP210, we generated a GMAP210 mutant mouse. The mutant mice are viable until birth, when they die from a pleiotrophic phenotype that includes growth retardation and lung and heart defects. Cells derived from these animals do not have structural defects in their Golgi complexes indicating that this protein is not required for Golgi organization. However, IFT20 is displaced from the Golgi complex in mutant cells indicating that GMAP210 anchors IFT20 to the Golgi membrane. In addition, the mutant cells have slightly shorter cilia and have significantly less polycystin-2 in these cilia. This suggests that GMAP210 functions with IFT20 in the trafficking of proteins to the ciliary membrane.

# Results

## Identification of IFT20 interacting proteins

IFT20 is the only IFT particle protein known to be associated with the Golgi complex (Follit et al., 2006). The identification of proteins that interact with IFT20 at the Golgi membrane is likely to yield new information about the function of IFT20. To this end, we generated stable mouse kidney cell lines expressing FLAG-tagged IFT20 and as controls, FLAG-tagged IFT25 and FLAG-tagged GFP (Figure 2.1A). IFT25 is a small IFT complex B subunit that is not Golgi associated (Follit et al., 2009). FLAG-IFT20 localizes predominantly to the Golgi complex, whereas FLAG-IFT25 localizes to the cilium and basal body region as well as the cell body. FLAG-GFP is found in the cell body and is not enriched at either the cilium or Golgi complex. To identify candidate proteins that potentially interact with FLAG-tagged proteins, FLAG-tagged proteins were immunoprecipitated (IPed) from cell lysates using FLAG antibody coupled to agarose, fractionated by SDS-PAGE and the gels silver stained (Figure 2.1B). Proteins found in all three lanes are background proteins that non-specifically bound to the resin whereas proteins found in the IFT20 and IFT25 extracts are likely to be IFT complex B proteins. This appears to be the case since the ~200 kD band found in both the IFT20 and IFT25 lanes was identified by mass spectrometry (MS) as IFT172. Two bands were identified in the IFT20 extract but not in either of the controls suggesting that these are IFT20 interacting proteins that are not part of complex B. We were not able to identify the larger band (indicated by an asterisk), but MS identified the smaller band as a golgin protein known in mammals as Thyroid Hormone Receptor Interacting Protein 11

(TRIP11) (Chen et al., 1999), Golgi Microtubule Associated Protein 210 (GMAP210) (Rios et al., 2004), and Clonal Evolution Related Protein (CEV14) (Abe et al., 1997). The yeast orthologue is known as RUD3p (Gillingham et al., 2004).

To verify the interaction between IFT20 and GMAP210, we used a monoclonal antibody against GMAP210 (Clone 15, BD Transduction Laboratories) to perform inverse IPs. This antibody recognizes a single protein in extracts made from human cells (Figure 2.1C, starting material) but does not recognize the mouse orthologue. Extracts of human retinal pigmented epithelial (RPE) cells were IPed using the GMAP210 monoclonal Ab and a GFP monoclonal Ab (JL-8, Clontech) as a negative control. The GMAP210 Ab but not the GFP Ab precipitated IFT20 (Figure 2.1C). The IP extracts also were probed with our collection of antibodies directed against mouse IFT proteins that also recognize the human orthologues. Even though all of these proteins were present in the extract, only IFT20 was precipitated by the GMAP210 antibody (Figure 2.1C). This corroborates the identification of GMAP210 as an IFT20-binding protein and indicates that IFT20 and GMAP210 interact independently of IFT complex B. Furthermore, IFT20 and GMAP210 extensively co-localize at the Golgi complex as would be expected for interacting proteins (Figure 2.1D).

**Identification of the IFT20 binding site on GMAP210**

To map the IFT20 binding site on GMAP210, we tested whether IPing FLAG-tagged fragments of GMAP210 also brought down IFT20 and whether these FLAG-GMAP210 fragments could displace IFT20 from the Golgi apparatus by competing with native GMAP210 for binding to IFT20. The identity of the Golgi-targeting sequence within

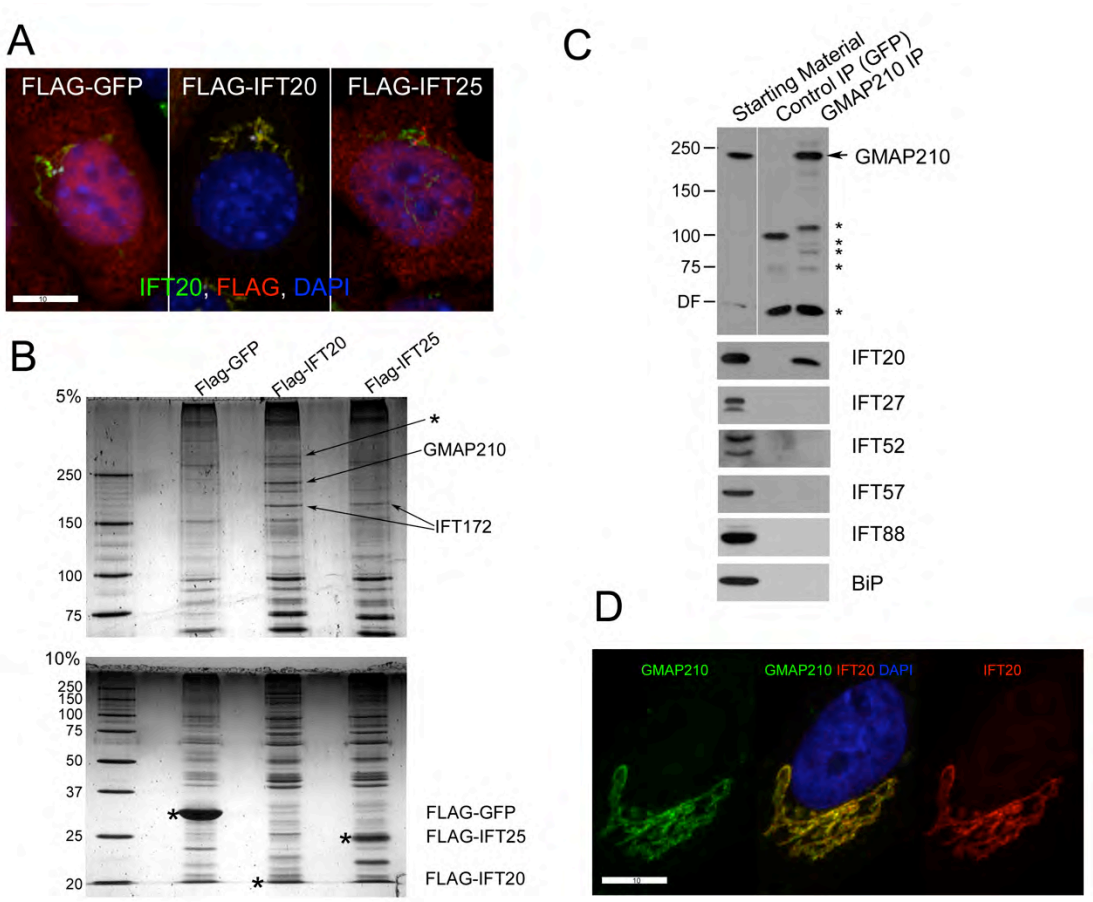


**Figure 2.1: Identification of GMAP210 as an IFT20 binding protein.**

**Figure 2.1: Identification of GMAP210 as an IFT20 binding protein.**

**A.** Stable mouse kidney cells lines expressing FLAG-tagged GFP, IFT20, and IFT25 were generated, fixed and stained with DAPI (blue) and antibodies to IFT20 (green) and FLAG (red). Scale bar is 10 μm. **B.** FLAG IPs from these lines were analyzed by silver stain after SDS-PAGE. The bait proteins are marked with * on the 10% (lower) gel. The bands marked with arrows were analyzed by MS. The large band (*) was not identified. **C.** Inverse IP. Human RPE cells were IPed with antibodies to GFP and GMAP210 (monoclonal antibody clone 15) and analyzed by western blotting. The GMAP210 antibody precipitated GMAP210 and IFT20 but not any of the other IFT proteins or the negative control protein BiP even though all were present in the starting material. * mark proteins introduced in the IP. **D.** GMAP210 and IFT20 extensively colocalize in human RPE cells. GMAP210 (green) was detected by monoclonal Ab clone 15. IFT20 (red), DAPI (blue). Scale bar is 10 μm.

GMAP210 is controversial, with the targeting sequence variably being located to the N- or C-terminal ends of the protein (Barr and Egerer, 2005) so we also examined the cellular distribution of our FLAG-tagged GMAP210 constructs. Data are graphically displayed in Figure 2.2A, key examples of IF and IP that document the IFT20 binding site are shown in Figures 2.2B and 2.2C while IF data supporting the Golgi localization are shown in Figure 2.3. Initially, we expressed GMAP210 as two fragments split at the junction between the coiled-coil and Grab domains (JAF157 and JAF172, Figure 2.2A). Both fragments localized to the Golgi-complex, although the N-terminal fragment (JAF172) also was found in the cytoplasm (Figure 2.3A). The C-terminal fragment (JAF157) did not affect the localization of native IFT20 or bring down IFT20 in an IP. The N-terminal fragment (JAF172) precipitated IFT20 and partially displaced IFT20 from the Golgi complex indicating that it contains an IFT20 binding site (Figure 2.3A). We then split the JAF172 fragment into two smaller fragments. The N-terminal JAF175 fragment partially localized to the Golgi complex indicating that there are Golgi-targeting domains at both the N- and C-terminal ends of the protein (Figure 2.2A, Figure 2.3). Thus our results explain the apparent discrepancy in the literature (Barr and Egerer, 2005), which can be ascribed to a non-systematic analysis of the protein in previous studies (Chen et al., 1999; Gillingham et al., 2004; Infante et al., 1999). We did not precisely map the Golgi-binding domain at the N-terminus, but it is likely to involve the ALPS domain that has recently been shown to bind curved membranes (Drin et al., 2008). The JAF174 fragment displaced IFT20 from the Golgi and was able to IP IFT20 indicating that it contained the IFT20 binding site (Figure 2.2A, 2.3). Expression of these

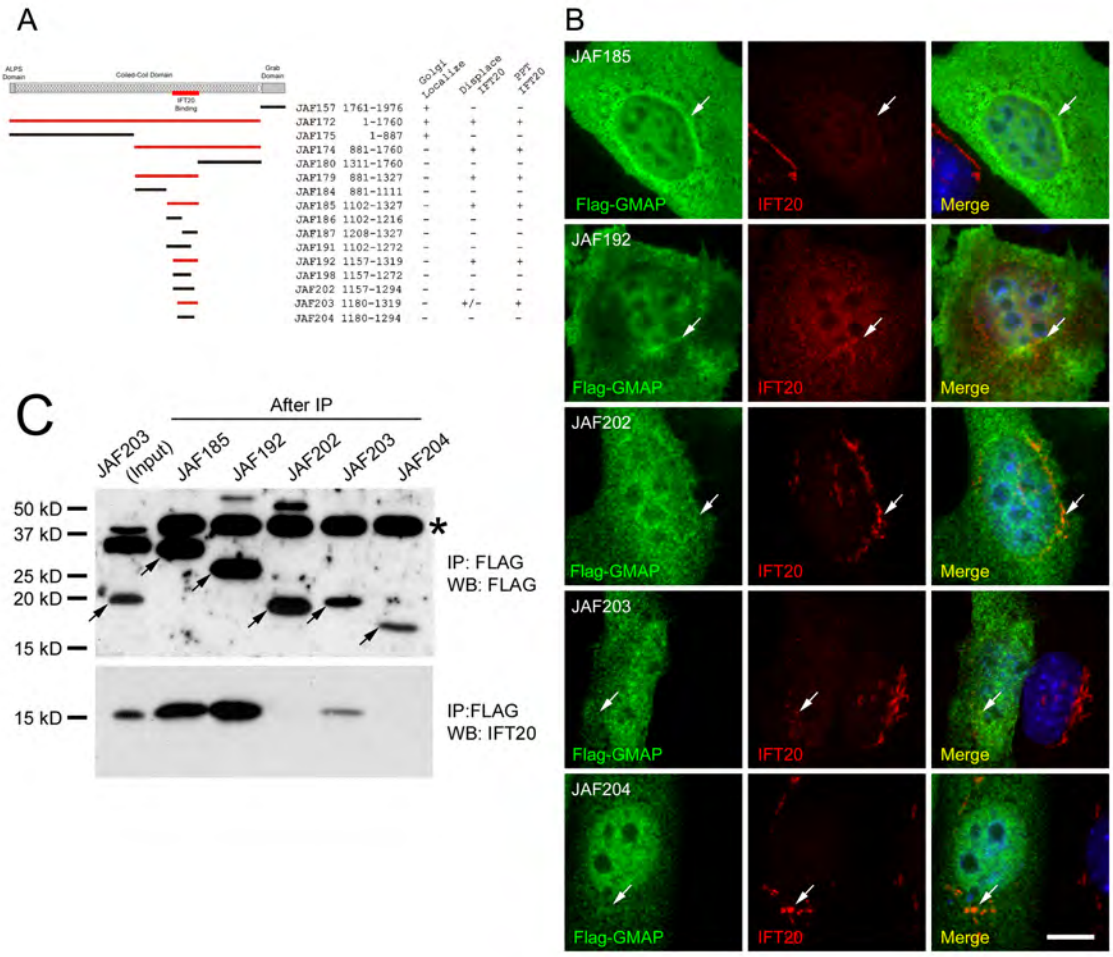


**Figure 2.2: Identification of the IFT20 binding site on GMAP210.**

**Figure 2.2: Identification of the IFT20 binding site on GMAP210.**

**A.** Schematic map of GMAP210 and summary of the data. Fusion proteins that bind IFT20 are drawn red while those that did not are black. The numbers following the plasmid names are the residues of GMAP210 in the construct. The behavior of the fusion proteins is summarized on the right. **B.** Selected images of cells expressing the fusion proteins illustrating the main points from Figure 1.2A. GMAP210 fragments were detected with FLAG antibody staining (green), endogenous IFT20 with our antibody (red) and nuclei with DAPI (blue). Note that fragments of GMAP210 containing the IFT20 binding site (JAF185, JAF192, JAF203) did not bind to the Golgi on their own but did displace IFT20 from the Golgi complex. Scale bar is 10 μm. **C.** Co-IP of IFT20 by selected GMAP210 fragments to illustrate main points from Figure 1.2A. The top panel shows the GMAP210 fusion proteins after IP with FLAG. The bottom panel show these IPs probed with the IFT20 antibody to determine if the fragment of GMAP210 is capable of binding IFT20. The smallest fragment capable of binding IFT20 is encoded by JAF203 although the fragment encoded JAF192 is more effective. The band marked with * is a cross reacting protein IPed and detected by the FLAG antibody. Arrows mark the GMAP210-FLAG fusion proteins. JAF203 (Input) is the starting material to illustrate the level of IFT20 in these cells while the remaining lanes are after IP.

GMAP210 fragments did not alter Golgi structure (Figure 2.3B). We progressively split the JAF174 fragment into smaller pieces and tested their ability to IP IFT20 and displace IFT20 from the Golgi complex. The smallest fragment of GMAP210 that IPed IFT20 and displaced IFT20 from the Golgi contained residues 1180 to 1319 (JAF203) (Figure 2.2). However, this peptide was not as effective as the slightly larger 1157 to 1319 fragment (JAF192). In all cases, the ability to IP IFT20 correlated with the ability to displace IFT20 from the Golgi complex (Figure 2.2). In contrast, the ability of the GMAP210 fragment to localize to the Golgi complex was not correlated with the presence of the IFT20 binding site. This suggests that GMAP210 localization to the Golgi complex is not dependent on IFT20. This appears to be the case as cells lacking IFT20 still localize GMAP210 to the Golgi complex.

The amino acid sequence of the IFT20 binding domain in GMAP210 is 95% identical between humans and mice while overall the two proteins are 80% identical, suggesting that there is selective pressure maintaining the IFT20-binding sequence. The IFT20 binding site is not found in the *Caenorhabditis* or *Drosophila* GMAP210 homologues.

**Generation of a GMAP210 mutant mouse**

To begin to understand the *in vivo* function of GMAP210, we obtained mouse gene trap ES cell line AJ0490 from the Sanger Institute (Skarnes et al., 2004) and used these cells to generate a mutant mouse. Cell line AJ0490 contains a splice acceptor site and a β-galactosidase-neomycin resistance gene fusion inserted into intron 4 of GMAP210. There also is an insertion of 531 bp derived by duplication from chromosome 16 at the

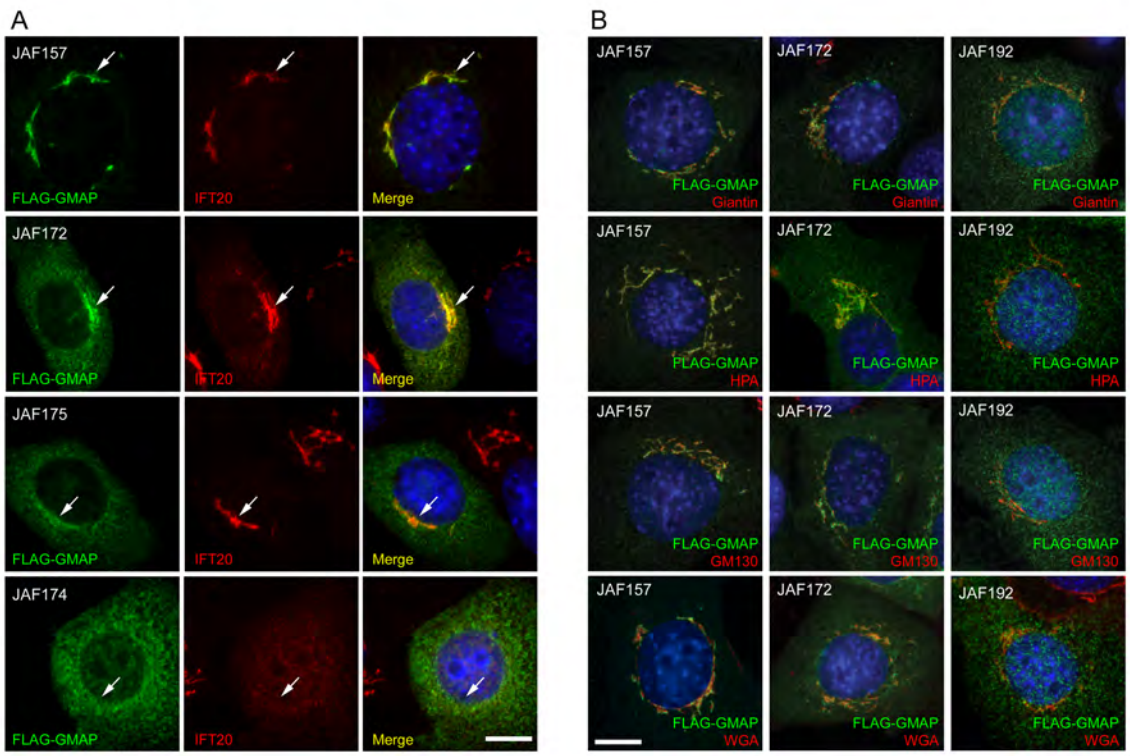


**Figure 2.3: Golgi binding site in GMAP210.**

**Figure 2.3: Golgi binding site in GMAP210.**

**A.** Selected images to illustrate the Golgi binding site in GMAP210. See Figure 1.2A for schematic drawing of the constructs and summary of data. GMAP210 fragments were detected with FLAG antibody staining (green), endogenous IFT20 with our antibody (red) and nuclei with DAPI (blue). Note that both the N- (JAF172) and C- (JAF157) terminal ends of GMAP210 bound to the Golgi. Splitting the N-terminal fragment into two halves separated the N-terminal Golgi binding site (in JAF175) from the IFT20 binding site (in JAF174). Scale bar is 10 μm. **B.** Selected images to show that expression of FLAG-tagged GMAP210 fragments does not disperse the Golgi complex. Cells expressing the N-terminal coiled-coil domain (JAF172), the C-terminal grab domain (JAF157) and the IFT20 binding domain (JAF192) stained with DAPI (blue), FLAG (green), and giantin (top row), HPA (second row), GM130 (third row) or WGA (fourth row) in red. Scale bar is 10 μm. Note that Golgi complex is still organized in ribbons when these constructs are expressed.

junction between the vector and intron 4 (Figure 2.4A). In spite of this duplication, the rest of the gene appears intact as measured by PCR of exons and selected other regions of genomic DNA (Figure 2.4A). Sequencing of cDNA made from the AJ0490 allele indicates that the first four GMAP210 exons are spliced to the 5' end of the b-galactosidase message, potentially producing a fusion protein containing the first 197 residues of GMAP210 fused to the N-terminus of β-galactosidase. Real time RT-PCR of mRNA from e18.5 lungs indicates that the message derived from exons upstream of the insertion is found at about the same level as controls but significantly less message is made from the exons downstream of the insertion (Figure 2.4C).

Since the commercially available GMAP210 clone 15 Ab did not detect mouse GMAP210, we generated a rabbit polyclonal directed against the C-terminal tail of the mouse protein. In extracts made from wild type and heterozygous mouse cells, this antibody recognizes a band of ~200 kD that is likely to be GMAP210 and a cross reacting band of ~60 kD. The observation that the 200 kD band is missing in the homozygous mutants, without the presence of any new smaller bands, suggests that the downstream exons in the mutant allele are not translated significantly (Figure 2.4D). In addition, immunofluorescence analysis of MEFs from mutant animals did not show any staining with this antibody whereas GMAP210 was readily detected at the Golgi complex in the control MEFs (Figure 2.4E). This data suggests that the AJ0490 allele is either null or a strong hypomorph.

The GMAP210 gene trap allele causes a neonate lethal phenotype as all homozygous mutant animals were found either dead or close to death on the morning of

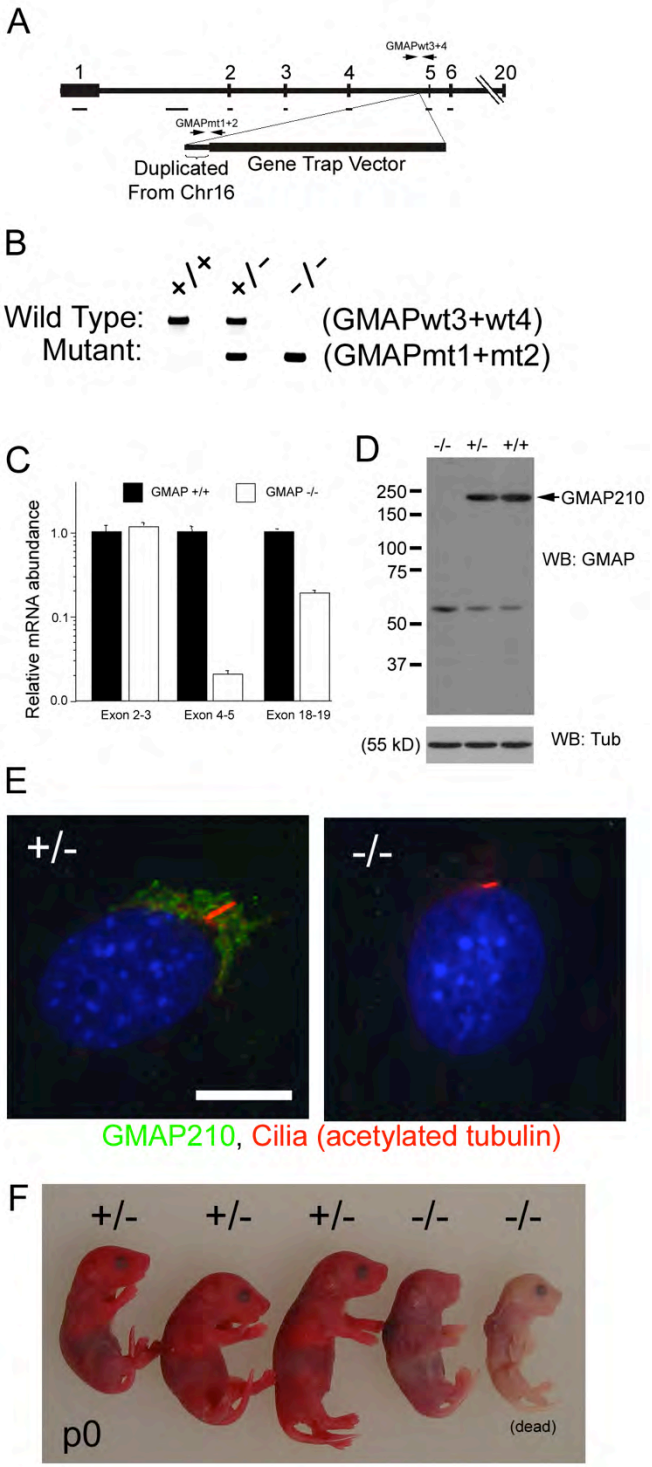


**Figure 2.4: Generation of a GMAP210 mutant mouse.**

**Figure 2.4: Generation of a GMAP210 mutant mouse.**

**A.** Schematic drawing of the GMAP210 AJ0290 allele. This allele contains the gene trap vector plus 531 base pairs of DNA duplicated from chromosome 16 inserted into the fourth intron. Exons are numbered above the bar. The lines under the exons and intron 1 indicate fragments of genomic DNA that were verified to be present by PCR. Positions of genotyping primers are indicated by the pairs of arrows. **B.** Genotyping primers (see materials and methods and diagram in A) spanning the insertion site were designed to detect the wild-type allele while primers in the insertion were used to detect the mutant allele. **C.** Real Time qPCR was used to measure the relative transcript levels in lung for parts of the message upstream of the insertion site (exons 2-3), at the insertion site (exons 4-5), and downstream of the insertion site (exons 18-19). GMAP data were expressed relative to GAPDH mRNA and normalized to wild-type expression for each primer pair. n=9-10 mice/point. Note the logarithmic scale on the ordinate axis ** $p < 0.01$, unpaired t-tests. **D.** Western blotting of MEF cells generated from homozygous mutant, heterozygous and homozygous wild-type embryos. Antibody was generated against the C-terminal end of the protein and detects GMAP210 and a smaller non-specific band at ~60 kD. Tubulin was used as a loading control. **E.** Embryonic fibroblasts from heterozygous (+/-) and homozygous (-/-) mutant embryos stained with GMAP210 (green) and acetylated a-tubulin (red) antibodies plus DAPI (blue). Scale bar is 10 μm. **F.** Photo of a new born liter of animals. The fourth animal from the left was alive at the time of the photo, while the right most animal had died prior. Genotypes are above the animals.

their birth and none survived past postnatal day 0 (p0) (25 +/+, 56 +/-, 14 -/- from 18 litters. +/+ and +/- were genotyped at various ages between p0 and p21, all -/- were genotyped at p0). Mutants on p0 never achieve the healthy pink color of normal littermates but rather appear cyanotic or pale bluish pink (Figure 2.4F). Mutants that were found alive were inactive but occasionally made a convulsive or a gasping like movement. Less than expected numbers of homozygous mutants were found but this is likely due to cannibalism of dead pups, since roughly Mendelian numbers of mutant embryos (44 +/+, 50 +/- , 33 -/- from 18 litters) were found at embryonic day 18.5 (e18.5), one day prior to birth. Mutant embryos at e18.5 were smaller than normal, weighing on average 70 $\pm$ 9% (n=6 litters) of what +/- and +/+ embryos weigh. In addition, the mutants usually had their mouths open with protruding tongues, suggesting craniofacial anomalies, and some exhibited an omphalocele or abdominal wall hernia, indicating a body wall closure defect (Figure 2.5A). The omphalocele has also been observed by D. Beier in an independently identified allele (Smits et al., 2010). We observed no evidence of polydactyly, left-right patterning defects or hydrocephaly, which are common phenotypes also associated with cilia defects.

To understand the pathology causing neonatal lethality in the mutant animals, we fixed embryos at e18.5, the day prior to birth, and examined them histologically. The abdominal organs did not appear to be greatly affected by the absence of GMAP210 and we did not detect any abnormalities in the kidney or pancreas. However in the thoracic cavity, both the heart and lungs were affected. To characterize the heart defect, 5 mutant and control animals were fixed in formalin and the hearts analyzed using episcopic

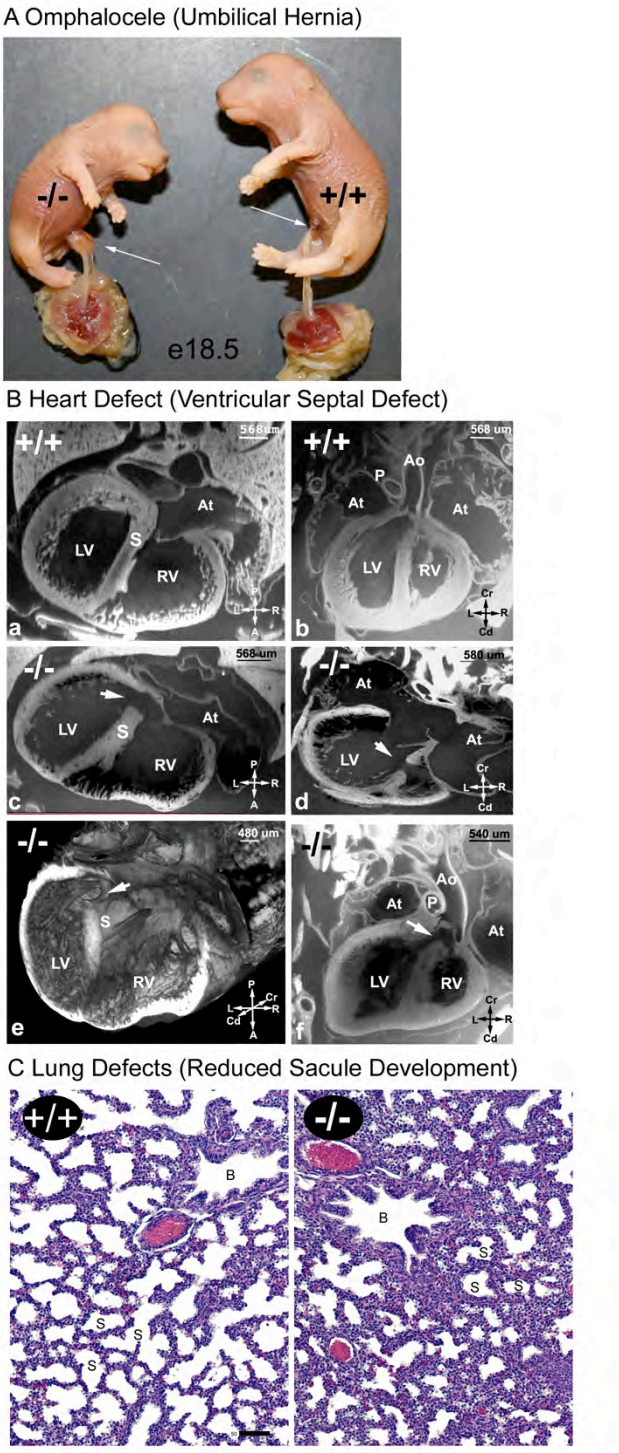


**Figure 2.5: Characterization of the GMAP210 mutant mouse phenotype.**

**Figure 2.5: Characterization of the GMAP210 mutant mouse phenotype.**

**A Gross Morphology of GMAP210 Mutants.** Image of a pair of e18.5 embryos. Note the open mouth and omphalocele (arrow) on the mutant embryo**. B Cardiovascular defects in the GMAP210 Mutants. (Ba-Bb, wild type)** EFIC images of a wild type e18.5 embryo showing normal septation of the ventricular chambers (Ba), contrasting with the VSD seen in mutant embryo shown in (Bc). The aorta (Ao) connects with the left ventricle (LV) (Bb), which contrasts with the mutant embryo shown in (Bf) with an overriding aorta that connects to both ventricles via a VSD. **(Bc-Be, mutant)** EFIC images of a mutant embryo at e18.5. In the transverse imaging plane (Bc), a large muscular ventricular septal defect (white arrow) can be seen situated posteriorly. Examination in the frontal plane (Bd) showed a second muscular ventricular septal defect (white arrow) positioned anteriorly. Three dimensional reconstruction of the heart (Be) shows the posterior ventricular septal defects (white arrow). **(Bf, mutant)** Another mutant fetus at E18.5 examined by EFIC imaging was found to have a ventricular septal defect (white arrow) associated with a overriding aorta (Ao). Pulmonary stenosis was indicated with a reduction in the size of the pulmonary outflow (P) compared to the aorta (Ao). There was also apparent thickening of the ventricular chamber walls. This constellation of defects is consistent with Tetralogy of Fallot. At: atrium, LV: left ventricle, RV: right ventricle, S: septum, Cr: cranial, CD: caudal, L: left, R: right, A: anterior, P: posterior. **C Lung.** Hematoxylin and eosin staining of e18.5 embryonic lungs. The larger airways are marked with B and the saccules are marked with S. Note the smaller saccule space and thicker inter saccule mesenchyme in the mutant at e18.5. Scale bar is 50 μm for e18.5 and 100 μm for e15.5.

fluorescence image capture (EFIC) (Rosenthal et al., 2004). With EFIC imaging, we generated serial 2D image stacks and 3D reconstructions that allowed detailed examination of the cardiac anatomy in multiple imaging planes. All five mutant hearts showed ventricular septal defects (VSD). Normally, at e18.5 ventricular septation is complete, allowing for separate pulmonary vs. systemic circulation from the right vs. left ventricles (Figure 2.5Ba,b +/+). However in the mutants, muscular VSDs are found at the anterior and posterior walls of the heart, which would cause inappropriate mixing of blood (Figure 2.5Bc-f -/-). In one mutant, a VSD was observed in conjunction with an overriding aorta, which is an abnormal positioning of the aorta between the right and left ventricle. This was accompanied by a narrowing of the pulmonary outflow (pulmonary stenosis) and thickening of the ventricular chamber walls (Figure 2.5Bf). Together this constellation of defects is consistent with Tetralogy of Fallot (Figure 2.5Bf), which in humans, is a relatively common but serious congenital heart condition. The lungs showed the normal four right and one left lobe structure suggesting that the early stages of development had occurred normally. However, at e18.5 the mutant animals had notably smaller saccules with thicker inter-saccule mesenchyme (Figure 2.5C). Mutants had about one third as much saccule space as littermate controls (Wild type = 33.6 $\pm$ 9%, Mutant = 12.9 $\pm$ 5%, n=5 animals for each genotype). At e18.5 mouse lungs are normally in the terminal sac stage of development. During this stage, which lasts from e17.5 to p5, the lung mesenchyme thins to bring the capillaries next to the prospective alveoli and the alveolar type I and II cells differentiate (Bridges and Weaver, 2006). During their differentiation, the Type I cells flatten to reduce the distance between the

capillaries and the air exchange surface of the saccule and the Type II cells produce surfactant for secretion into the saccules. Staining control and mutant lungs with markers for the Type I and II epithelial cells indicates that both types of cells are present. However in the mutant lungs, the Type II surfactant secreting cells are not as clearly interdigitated between the Type I cells and the SP-C staining is more punctate and distributed throughout the cell rather than being located at the apical end as it is in the control lungs (Figure 2.6B). Staining with PECAM1, to mark the endothelial cells of the capillaries, indicates that capillaries are forming in the mutant lungs like the wild type but in the mutant lungs the capillaries are less associated with the saccules (Figure 2.6A). EM analysis indicates that the type I cells are less flattened in the mutant lungs as compared to the controls (Figure 2.6C). Quantitative PCR was used to examine the expression levels of a number of lung development genes. Genes examined included sonic hedgehog (SHH), which is critical for branching morphogenesis, VEGF-A, which is a regulator of vascular development, Hif1a and its binding partner ARNT, which regulate transcription of VEGF-A and other genes, SP-C, which encodes a surfactant molecule critical for lung function at birth, and the selenium binding protein, SelenBP1, which is up regulated just before birth (Bonner et al., 2003). No differences were seen between the mutant and control animals (data not shown).

**Cellular function of GMAP210**

To begin to understand GMAP210s function in cells, we generated embryonic fibroblasts (MEFs) and kidney (MEKs) cells from e18.5 animals. All three genotypes (+/+, +/-, -/-) grew at similar rates and outwardly appeared indistinguishable. Since GMAP210 was

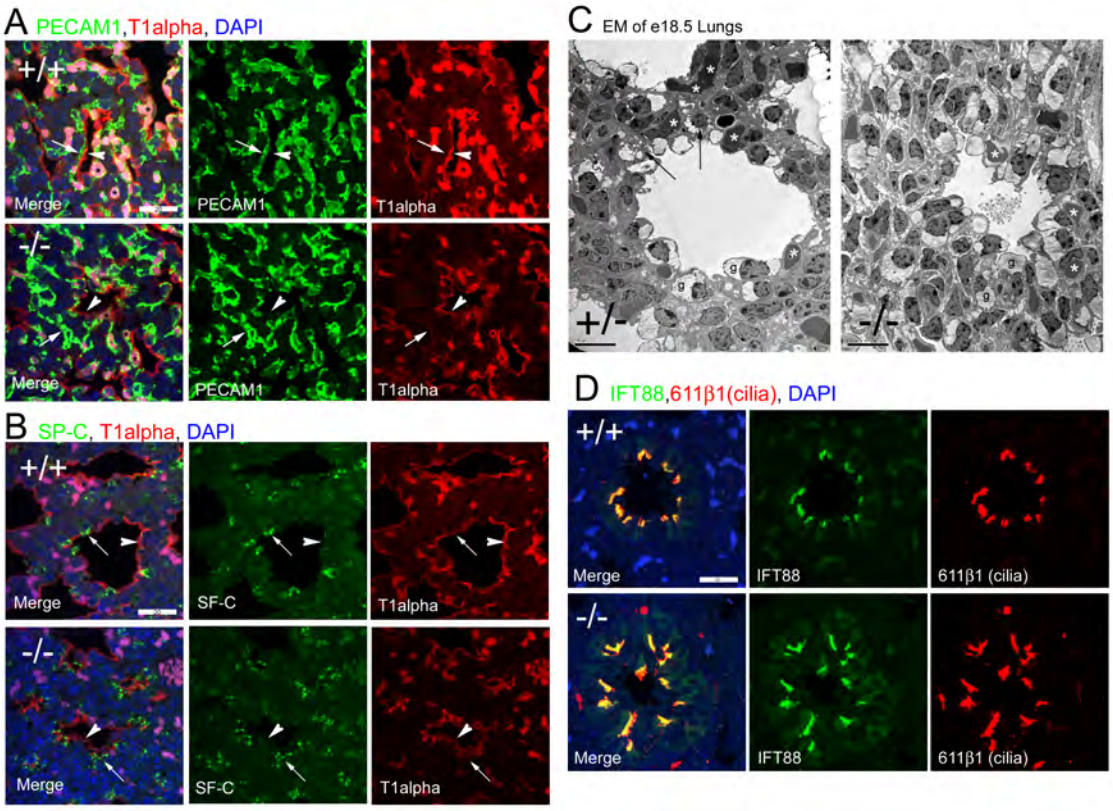


**Figure 2.6: Lung Cell Types.**

**Figure 2.6: Lung Cell Types.**

**A.** PECAM1 (green, arrow) and T1α (red, arrowhead) staining of e18.5 embryos. * mark selected red blood cells. Scale bar is 20 μm. **B.** Surfactant C (SP-C, green, arrow) and T1α (red, arrowhead) staining of e18.5 embryos. Blue is DAPI plus autofluorescence. * mark selected red blood cells. Scale bar is 20 μm. **C.** Transmission EM of e18.5 lungs. Type II cells are marked with arrows. Glycogen is marked with g. Scale bar is 10μm. **D.** IFT88 (green) and 611β1 (red) staining of multi-ciliated cells in e18.5 lungs. Blue is DAPI plus autofluorescence. Scale bar is 20 μM.

identified as an IFT20 binding partner, we sought to understand how the lack of GMAP210 affected IFT20 and cilia formation. Wild-type MEKs and MEFs (not shown) localize IFT20 to the Golgi apparatus (Figure 2.7A, Wild Type) as we described earlier for other cell types (Follit et al., 2006). However, IFT20 is completely dispersed from the Golgi complex in cells lacking GMAP210 (Figure 2.7A Mutant). This is not simply an indirect result caused by dispersal of the Golgi as the cis-medial and trans compartments of the Golgi complex appear normal in the GMAP210 mutant cells by *Helix pomatia* agglutinin (HPA), golgin97, wheat germ agglutinin (WGA), giantin, and GM130 staining (Figure 2.7B). The dispersal of IFT20 from the Golgi complex is caused by the lack of GMAP210 because re-expression of FLAG-tagged GMAP210 restores IFT20 to the Golgi complex (Figure 2.7A Rescue). IFT20 protein levels are slightly reduced in the mutant cells suggesting that some IFT20 is degraded when GMAP210 is absent with the rest being distributed throughout the cell. In addition to being localized to the Golgi complex, IFT20 is also found at the centrosome (Follit et al., 2006). We were unable to detect GMAP210 at the centrosome in either the mutant or wild-type cells (Figure 2.7C top row) and consistent with this observation, the centrosomal pool of IFT20 is not affected in the GMAP210 mutant cells (Figure 2.7C bottom row). This suggests that IFT20 is not required to be trafficked through the Golgi complex in order to be assembled into an IFT particle.

We previously showed that IFT20 is required for ciliary assembly (Follit et al., 2006). GMAP210 in contrast, is not absolutely required for cilia assembly (Figure 2.4E, 2.7A, Figure 2.6D). Quantification showed that GMAP210 mutant cells are ciliated

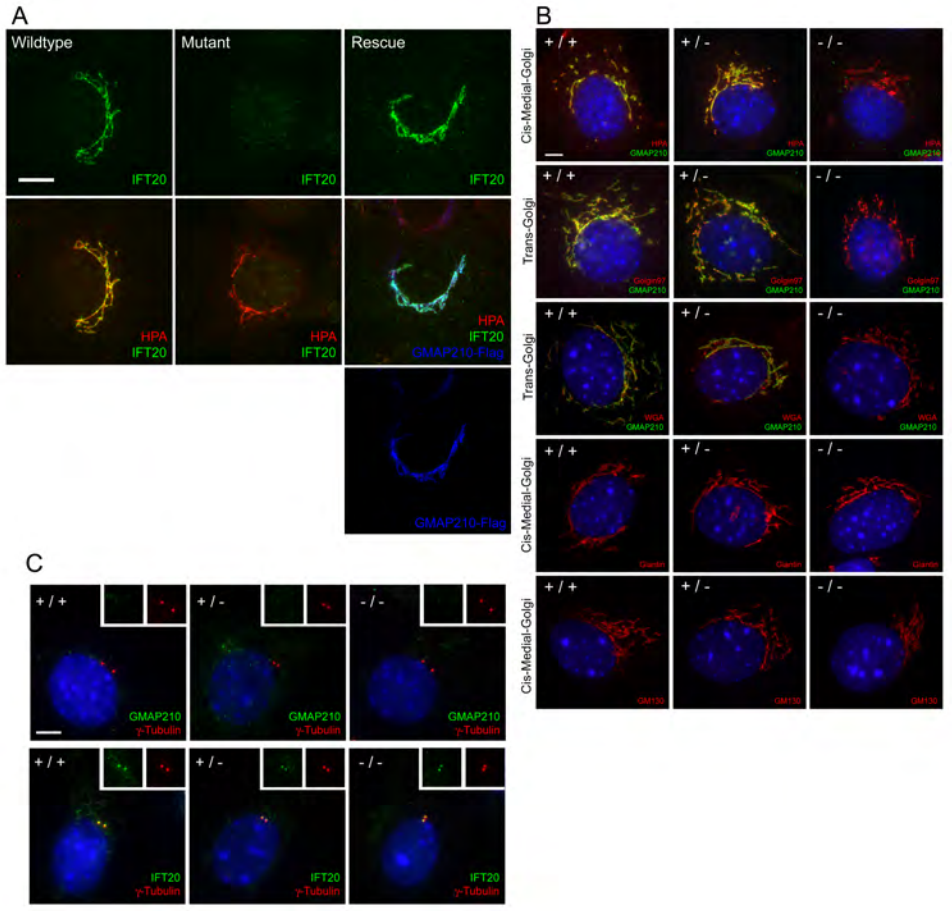


**Figure 2.7: Characterization of the GMAP210 cellular phenotype.**

**Figure 2.7: Characterization of the GMAP210 cellular phenotype.**

**A.** MEK cells labeled with IFT20 (green), the cis-medial Golgi marker HPA (red) and FLAG (blue). Scale bar is 10 μm. **B.** MEK cells labeled with Golgi markers HPA, Golgin97, WGA, Giantin, and GM130 (red). The Golgi compartment stained by each marker is listed on the left side of the row. Cells also are labeled with DAPI (blue) and GMAP210 (green) if the markers are compatible. Scale bar is 5 μm. **C.** MEK cells were fixed with methanol and labeled with DAPI (blue), the centrosome marker gamma tubulin (red), and either GMAP210 (green, top panel) or IFT20 (green, bottom panel). Insets show the green and red channels of the centrosome region. Note that the methanol fixation extracts most of the Golgi pools of IFT20 and GMAP210 (see [32]). Scale bar is 5 μm.

nearly as well as control cells, and the level of ciliation did not increase upon re-expression of FLAG-tagged GMAP210 (Figure 2.8B, left panel). However we did note that the cilia on the GMAP210 mutant cells were often shorter than those on control cells. Measurement of cilia length on MEK cells indicated that the cilia are only about 2/3 as long as cilia on control cells. The length difference can be restored by expression of FLAG-tagged GMAP210 indicating that this result is specifically caused by the lack of GMAP210 (Figure 2.8B, right panel). This suggests that GMAP210 is involved in ciliary assembly.

One of the proposed roles of GMAP210 is in ER to Golgi transport (Pernet-Gallay et al., 2002) and there is clear evidence in yeast for the involvement of the homologue Rud3p and Rud3p-interacting proteins in membrane protein transport (Kim et al., 1999; Powers and Barlowe, 2002). Partial knockdown of IFT20 by RNAi reduced the amount of the membrane protein polycystin-2 on cilia suggesting that the Golgi pool of IFT20 was important for transport or retention of polycystin-2 in cilia
(Follit et al., 2006). To test the involvement of GMAP210 in ciliary transport, we measured the ciliary levels of polycystin-2 in wild-type and mutant MEKs (Figure 2.8C, D). The level of polycystin-2 in the mutant cilia was reduced to about one quarter the amount seen in the control line. The results are also displayed as polycystin-2 per unit of ciliary length to show that this is not an indirect effect of having shorter cilia on the mutant cells (Figure 2.8D right panel). To test if the decrease in ciliary polycystin-2 was specifically due to the lack of GMAP210, we transfected in FLAG-tagged GMAP210 and measured the levels of ciliary polycystin-2 in the rescued cells. Rescue with FLAG-

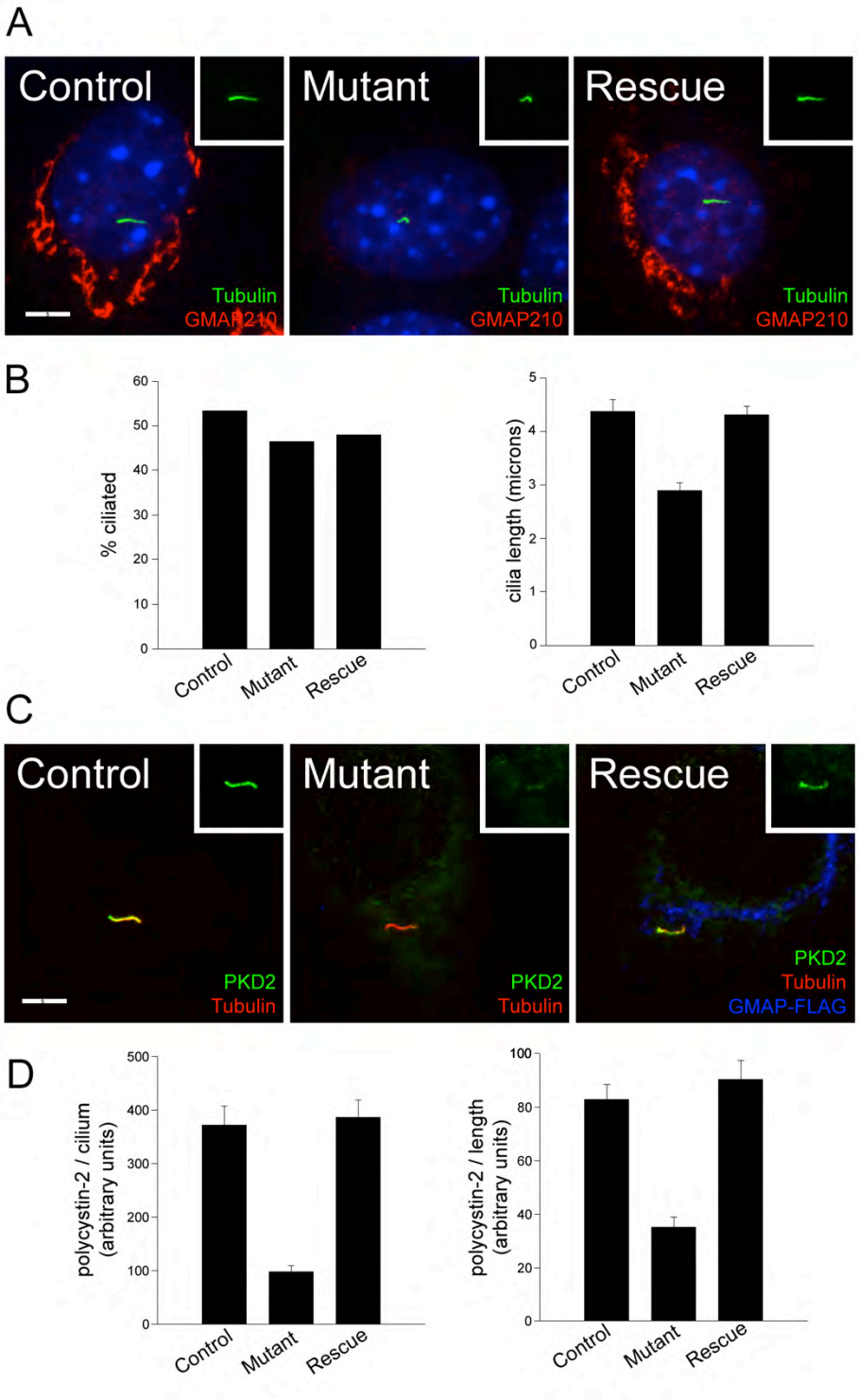


**Figure 2.8: GMAP210 mutant cilia.**

**Figure 2.8: GMAP210 mutant cilia.**

**A.** MEK cells labeled with GMAP210 (red), the acetylated tubulin marker 611b1 to mark cilia (green) and DAPI (blue). Scale bar is 5 μm. Insets show the acetylated tubulin channel. **B.** Extent of ciliation (left panel) and cilia length (right panel) of the MEK cells after 48 hrs of serum starvation. n=50 cilia for each genotype. **C.** MEK cells labeled with polycystin-2 (PKD2, green), the acetylated tubulin marker 611b1 to mark cilia (red) and FLAG (blue). Scale bar is 5 μm. Insets show the polycystin-2 channel. **D.** Quantification of ciliary polycystin-2 levels in control, mutant and rescued MEK cells. Polycystin-2 data are plotted per cilium on the left and corrected for length differences on the right. Error bars represent standard error of the mean (n=46-50 cilia measured for each line). ** $p < 0.01$.

tagged GMAP210 was able to restore ciliary polycystin-2 levels to wild type levels (Figure 2.8C, D). These results indicate that GMAP210 is important for efficient targeting of polycystin-2 to the cilium.

## Discussion

IFT20 is unique among the known IFT particle proteins in that it is the only one shown to localize to the Golgi complex in addition to the basal body and cilium, where the other IFT particle proteins are found. As such, it is in a unique position to coordinate the sorting or transport of ciliary membrane proteins. In prior work, we showed that an RNAi-mediated reduction of IFT20 that depleted the Golgi pool but did not greatly affect the basal body pool was sufficient to block ciliary assembly suggesting that the Golgi pool of IFT20 played an important role in ciliary assembly. We also showed that cells with a moderate reduction of IFT20 could still assemble cilia, but these cilia had less polycystin-2 in them supporting a role for IFT20 in the sorting or transport of ciliary membrane proteins (Follit et al., 2006). In the present work, we sought to further our understanding of the function of the Golgi-associated pool of IFT20 by identifying proteins that interact with IFT20 at the Golgi complex. This analysis identified a protein called GMAP210 that binds to IFT20. Cells lacking GMAP210 fail to localize IFT20 to the Golgi complex, indicating that this protein is the linker that holds IFT20 to the Golgi. These cells can still form cilia, but they are shorter than normal and have reduced amounts of polycystin-2. Mice lacking GMAP210 die at birth likely from heart and lung defects.

As discussed below, previously published *in vitro* studies have implicated GMAP210 in a wide variety of processes ranging from Golgi structure to regulating gene expression, so the ability of GMAP210 mutant embryos to progress through embryonic development was unexpected. When examined just prior to birth, the major organs, with the exception of the lungs and heart, appear fairly normal and do not show signs of cystic disease. Our finding that ciliary levels of polycystin-2 are reduced in cells derived from the GMAP210 mutant animals would suggest that these animals should develop kidney cysts. However, in other work, we found that mice lacking cilia due to a mutation in IFT20 do not show signs of cystic disease until five to ten days after birth. When the IFT20 mutant kidneys are examined at e18.5, cilia are absent but there is no sign of cysts or even dilation of the kidney tubules (Jonassen et al., 2008). Thus, it is likely that if the GMAP210 mutant animals were to live for a few weeks longer they would develop cystic kidney disease, but instead, animals die at birth before cysts have time to develop within the kidneys.

GMAP210 mutants exhibit serious congenital heart defects (VSD and Tetralogy of Fallot) that are a likely cause of the neonatal lethality observed in these animals. These disorders are common in humans, where it is estimated that as many as 1% of live births have congenital heart defects with VSDs being the most common form (Hoffman and Kaplan, 2002). Tetralogy of Fallot accounts for 10% of human congenital heart disease and is the leading cause of cyanotic congenital heart disease in newborns (Shinebourne et al., 2006). VSDs and malalignment of the great arteries also are observed in mice with mutations in *Vangl2, Dvl2,* and *Scrib*. These genes are members

of the planar cell polarity pathway (PCP), which regulates cell polarity and polarized cell movement via non canonical Wnt signaling (Hamblet et al., 2002; Phillips et al., 2005; Phillips et al., 2007); for review see (Henderson et al., 2006). It is thought that formation of the ventricular septum is mediated by compaction of the trabeculae, with growth of the muscular septum generated by addition of sheets of trabeculae (Ben-Shachar et al., 1985). Cre mediated cell lineage tracing indicates the ventricular septum is derived from cells originating from the ventral aspect of the primitive ventricle, with closure of the ventricular foramen mediated by dorsal migration of this precursor cell population (Stadtfeld et al., 2007). These cell migration events could be regulated by PCP signaling and thus VSDs might arise in animals with defects in PCP components. Similarly, the outflow tract alignment defects in the *Vangl2* mutant hearts may involve inhibition of polarized cell migration associated with myocardialization of the outflow tract. In the *Scrib* mutants, PCP defects are suggested to cause abnormalities of cardiomyocyte organization, which may result in abnormal trabeculation and ventricular noncompaction (Phillips et al., 2007). Cilia mutants often show defects in PCP (Jonassen et al., 2008; Jones et al., 2008; Ross et al., 2005). For example, the deletion of IFT20 in the kidney collecting duct disrupts PCP by randomizing the orientation of the cell division plane (Jonassen et al., 2008). These observations suggest cardiac defects in the GMAP210 mutants could arise from dysregulated PCP signaling due to defects in the cilia. Cilia are present in the developing mouse heart from e9.5 onward and defects in ciliary assembly cause severe heart development defects including malformation of the trabeculae that normally contribute to the formation of the ventricular septum (Slough et al., 2008). In

the GMAP210 mouse, the cilia are not absent but are likely missing key sensory receptors, analogous to the reduction of polycystin-2 in the kidney cilia (Figure 2.8).

The lung phenotype of the GMAP210 mutant mouse is similar to several mouse models of infantile respiratory distress syndrome caused by defects in signaling between cells of the developing lungs such as the Wnt5a (Li et al., 2002) and the nitric oxide synthase (eNOS) mutant (Han et al., 2004). The Wnt5a mutant mouse is neonatal lethal and shares a number of features with the GMAP210 mutant mouse, including the thickened mesenchyme, reduced saccule space and a failure to organize its capillaries under the saccule epithelium. Wnt5a is a secreted ligand thought to be produced by both the mesenchyme and epithelial cells of the lung to regulate lung development (Li et al., 2002). It is of significance to note that Wnt5a mediates non canonical Wnt signaling in the PCP pathway. Thus the observed disorganization of the alveoli may reflect a disturbance of PCP signaling related to ciliary dysfunction. Similarly, the eNOS mouse is neonatal lethal and has reduced saccule space with thickened mesenchyme. In this case, it is thought that signaling between the endothelial and epithelial cells via eNOS influences development of the lung (Han et al., 2004). Recent studies suggest NO production in endothelial cells is regulated by shear stress transduced through the cilia, with polycystin-1 cleavage associated with loss of responsiveness to high shear stress (Nauli et al., 2008). Thus it is also possible that abnormal regulation of NO production due to ciliary abnormalities in the GMAP210 mutant may play a role in the lung defects. Based on the reduced amount of polycystin-2 in the kidney cilia, we speculate that the

cilia present in the developing lung may be deficient in membrane-localized receptors and hence unable to respond to cues from the environment.

GMAP210 is a member of the golgin family of proteins. Golgins are thought to function in the formation of the Golgi matrix, which organizes the Golgi membranes and regulates membrane trafficking. Members of this family typically have large coiled-coil regions and GRIP and GRAB domains that bind to small GTPases in the ARF and ARL subfamilies (Short et al., 2005). In addition, GMAP210 contains an ALPS domain, which is an amphipathic helix that binds preferentially to curved membranes. In GMAP210 the ALPS domain is at the N-terminus and is separated from the GRIP and GRAB domains at the C-terminus by a long stretch of coiled-coil suggesting that it may be able to hold small vesicles on the end of a long tether (Drin et al., 2008). Clear homologues of GMAP210 are found throughout the vertebrates and in organisms as distantly related as *Drosophila* and *Caenorhabditis*. The yeast orthologue is reported to be Rud3p as this protein shares the same domain structure being largely coiled-coil with Grab and Grab-associated domains (Gillingham et al., 2004). However sequence identity between the yeast and mouse proteins is low (20-24%, BLAST E= 1e-9). BLAST analysis does not identify a *Chlamydomonas* homologue, but XP_001702340 is a coiled-coil protein containing Grab and Grab-associated domains and thus may be the *Chlamydomonas* orthologue. The IFT20 binding domain localizes within a 163 amino acid region of the GMAP210 coiled-coil domain. This sequence is well conserved throughout the vertebrate kingdom but is not present in the yeast, *Drosophila* or *Caenorhabditis* proteins nor is it found in the putative *Chlamydomonas* GMAP210

homologue. At this point, it is not known if IFT20 associates with the Golgi complex in *Drosophila*, *Caenorhabditis* or *Chlamydomonas* but if it does, it is likely to use a different mechanism. It is possible that the sorting mechanism of ciliary membrane proteins is fundamentally different in vertebrate cells as compared to *Caenorhabditis* or *Drosophila* since the cilia assembled by IFT in these invertebrates are found on dendrites and so ciliary trafficking requires sorting to dendrites before sorting to cilia. In vertebrates, this arrangement is found in olfactory sensory neurons but the majority of cells assemble their cilia directly from the cell body and do not require sorting to dendrites first. Dendritic sorting shares features with sorting to the basal-lateral domain (Dotti and Simons, 1990) whereas most vertebrate cilia project from the apical surface if the cell is polarized.

The proposed functions of GMAP210 in the literature fall into disparate categories of organizing the microtubule cytoskeleton, organizing the Golgi complex, regulating gene expression, and playing roles in vesicular transport. Many of these studies have either not been repeated independently or are controversial. For example, Barr and Egerer called into question the role of GMAP210 as a microtubule associated protein involved in Golgi organization (Barr and Egerer, 2005) and our data indicating that cells lacking GMAP210 still form normal Golgi structures further brings this result into question. The strongest data on the role of GMAP210 suggests that it plays roles in vesicular trafficking within the endomembrane system. In yeast, Rud3p, the GMAP210 homologue (with the caveats described above), was identified as a suppressor of mutations causing defective ER to Golgi transport (Kim et al., 1999). Deletion of Rud3p

causes glycosylation defects but the gene is not essential for viability (Kim, 2003). Erv14p is required to localize Rud3p to the Golgi membrane (Gillingham et al., 2004). Erv14 in yeast and its orthologue Cnih in *Drosophila* appear to play critical roles in polarized secretion. In yeast, Erv14 mutants retain the transmembrane protein Axl2p in the ER rather than inserting at the bud site (Powers and Barlowe, 2002). In *Drosophila*, Cnih mutants retain the membrane protein Gurkin in the endoplasmic reticulum instead of secreting it at the anterodorsal corner of the oocyte (Bokel et al., 2006). Mammals have four Erv14/Cnih homologues but very little is known about their function. It will be interesting to learn if any of the Erv14/Cnih homologues are required for localization of mouse GMAP210 and IFT20 to the Golgi complex. In mammalian cells, overexpression of GMAP210 blocked the secretion of alkaline phosphatase into the medium and inhibited the retrograde transport of a KDEL-containing substrate from the Golgi to the ER (Pernet-Gallay et al., 2002).

The proposed function of GMAP210 in polarized secretion of proteins is interesting in the context of GMAP210 anchoring IFT20 to the Golgi complex and in being required for localization of polycystin-2 to cilia. Polarized secretion at the bud site in yeast and at the base of the cilium in other eukaryotes may be evolutionarily related and share common components. It has been proposed that the entire IFT process evolved from the coated vesicle transport system (Jekely and Arendt, 2006). Whether this is true remains to be determined. However, it is likely that transport of membrane proteins to the ciliary membrane evolved as a specialized form of transport to the apical plasma membrane. We proposed earlier that IFT20 may function to mark vesicles that are

destined for the ciliary membrane (Follit et al., 2006). The unique ability of GMAP210 to bind IFT20 and anchor it to the Golgi membrane in addition to its ability to bind curved membranes (Drin et al., 2008) puts GMAP210 in a position to play a key role in sorting proteins to the ciliary membrane.

# Materials and Methods

## Mammalian cell culture

IMCD3 (ATCC) and hTERT-RPE cells (Clontech, Palo Alto, CA) were grown in 47.5% DMEM (high glucose for IMCD3, low glucose for hTERT-RPE), 47.5% F12, 5% fetal bovine serum, with penicillin and streptomycin at 37° C in 5% $CO_2$. Cells were transfected by electroporation (Biorad, Hercules CA). Stable cell lines were selected by supplementing the medium with 400 μg/ml of G418 (Sigma, St. Louis, MO). Clonal lines were selected by dilution cloning after drug selection.

Primary mouse embryonic fibroblasts (MEF) were generated by dispersing e18.5 embryos in trypsin then plating in 45% DMEM (high glucose), 45% F12, 10% fetal bovine serum, with penicillin and streptomycin. Mouse embryonic kidney (MEK) cells were made by trypsin, collagenase, and DNAse dispersion (Freshney, 2000) of e18.5 kidneys and grown in the same medium as the MEFs. 24 hrs after the MEKs were initially plated, the medium was supplemented with 150 mM NaCl and 150 mM urea to select against fibroblasts and maintained until the fibroblasts were gone.

## Immunofluorescence microscopy

Cells for immunofluorescence microscopy were grown, fixed, and stained as described (Follit et al., 2006) except that the paraformaldehyde fixation time was reduced to 15 min. For embryonic lung immunofluorescence, lungs from e18.5 embryos were fixed overnight at 4 $^0$C with 4% paraformaldehyde in PBS and embedded in paraffin. Sections were treated with the antibodies after antigen retrieval. Labeling of the GMAP210 and

PECAM-1 antibodies was enhanced with a biotin-streptavidin layer. For electron microscopy, the lungs were fixed in 4% paraformaldehyde and 2% glutaraldehyde.

Primary antibodies used included anti-tubulins (611β1, GTU-88, Sigma, St. Louis MO), anti-FLAG (Sigma), anti-MmIFT20, anti-MmIFT52, anti-MmIFT57, anti-MmIFT88 (Pazour et al., 2002a), anti-MmPKD2 (Pazour et al., 2002b), anti-human GMAP210 (clone 15, BD Transduction Laboratories), anti-T1α (8.1.1, DSHB, Univ. Iowa), anti-PECAM1 (M-20, Santa Cruz Biotechnology), anti-SP-C (FL-197, Santa Cruz Biotechnology), anti-golgin97 (CDF4, Molecular Probes). Anti-giantin, anti-GM130 (gifts from M. Fritzler, Univ. of Calgary), Anti-MmGMAP210 was made by expressing the C-terminal end of GMAP210 in bacteria (residues 1761-1976, same fragment as in JAF157, Figure 2.2) as a maltose binding protein fusion and injecting into rabbits. Antibodies were affinity purified against the same fragment expressed as a glutathione S-transferase fusion. Alexa 488 conjugated *Helix pomatia* agglutinin and wheat germ agglutinin was from Molecular Probes (Eugene, OR).

Widefield images were acquired by an Orca ER camera (Hamamatsu, Bridgewater, NJ) on a Zeiss Axiovert 200M microscope equipped with a Zeiss 100X plan-Apochromat 1.4 NA objective. Images were captured by Openlab (Improvision, Waltham, MA) and adjusted for contrast in Adobe Photoshop. If comparisons are to be made between images, the photos were taken with identical conditions and manipulated equally. For the quantification of polycystin-2 in the cilia, the length, area, and average fluorescence intensity of the cilia was measured using the measurement tools of Openlab. To determine significance of differences, data were logarithmically transformed to

normalize variance, subjected to one-way analysis of variance, followed by post-hoc analysis with a Tukey-Kramer test (SuperANOVA, Abacus Concepts, Berkeley CA). Confocal images were acquired by a Nikon TE-2000E2 inverted microscope equipped with a Solamere Technology modified Yokogawa CSU10 spinning disk confocal scan head. Z-stacks were acquired at 0.5 micron intervals and converted to single planes by maximum projection with MetaMorph software. Bright field images were acquired using a Zeiss Axioskop 2 Plus equipped with an Axiocam HRC color digital camera and Axiovision 4.0 acquisition software.

**Protein analysis**

FLAG-tagged IFT20, IFT25, GMAP210, and GFP were constructed by PCR amplifying the open reading frames and inserting them into p3XFLAG-myc-CMV-26 (Sigma, St. Louis, MO). FLAG IPs were carried out on stable cell lines expressing FLAG-Tagged IFT20 (JAF134), IFT25(JAF143), GFP(JAF146) or GMAP210 (full length = JAF205, shorter fragments are listed in Figure 2.2). Cells were rinsed once with cold PBS and lysed in Cell Lytic M + 0.1 % NP40 (Sigma), 0.1% CHAPSO (BioRad), plus Complete Protease Inhibitor (Roche) at 4° Celsius. Lysates were centrifuged at 18,000 g for 10 minutes and clarified lysates were incubated with Agarose beads coupled with FLAG M2 antibody (Sigma) for one hour. FLAG beads were washed 3 times with Wash Buffer (50 mM Tris, 150 mM NaCl, pH 7.4) plus 1% NP40. Bound FLAG proteins were eluted with 200 mg/ml 3X FLAG peptide (Sigma).

**Mouse Breeding**

ES cell line AJ0490 was obtained from the Sanger Center and injected into C57Bl6J blastocysts to generate chimeric mice. Chimeric mice were backcrossed to the C57Bl6J inbred line and the animals used in this study were a mix of 129 and C57Bl6 backgrounds. Embryonic ages were determined by timed mating with the day of the plug being embryonic day 0.5. Genotyping was carried out with the following primer pairs: GMAPwt3 AAACAGGAGCATTTCCGAGA + GMAPwt4 AAGACATGCGCCACTATGC (product size = 295 bp in wild type) and GMAPmt1 GGGCATCCACTTCTGTGTTT + GMAPmt2 TGTCCTCCAGTCTCCTCCAC (product size = 168 bp in mutant) (Figure 2.4B). Mouse work was approved by the UMMS IACUC.

**Quantification of Saccule Area**

Pregnant mice were euthanized by isoflurane overdose, their uteri were removed and submerged in ice cold PBS. While remaining submerged in cold PBS, the embryos were dissected from the uteri and their chests opened. The lungs were then fixed, paraffin embedded, sectioned, stained with H&E, and photographed at 4X magnification. The percent of open space (excluding bronchioles and vasculature) was calculated using the measure particle function of ImageJ.

**mRNA analysis**

Individual lungs were dissected and frozen at -80$^{o}$C in RNAlater (Qiagen Inc, Valencia, CA) until RNA was isolated with RNeasy kits (Qiagen), including on-column DNA

digestion. First strand cDNA was synthesized from 1 μg of total lung RNA per mouse, using a SuperScript II First-Strand Synthesis System (Invitrogen, Carlsbad, CA) and random hexameric primers. PCR primers were designed to produce amplicons between 100-150 nucleotides in length, using the online primer3 web PCR primer tool (http://fokker.wi.mit.edu/primer3/input.htm) and the IDT Primer Express software tool (http://www.idtdna.com/Scitools/Applications/Primerquest/). PCR primers were synthesized by Integrated DNA Technologies Inc (Coralville, IA) and are listed in Table S1. Real-time qRT-PCR analysis was performed using the ABI Prism 7500 sequence detection system (Applied Biosystems, Foster City, CA). Each reaction contained 2.5 ng first strand cDNA, 0.1μM each specific forward and reverse primers and 1X Power SYBR Green (Applied Biosystems, Foster City, CA) in a 15 μl volume.

**Accession numbers**

Mouse IFT20 = NM_018854, Mouse GMAP210/TRIP11 = XM_001001171.

## Acknowledgements

We thank Dr. R. Bloodgood (Univ. of VA) for critical comments on this work, Dr. J. Leszyk (UMMS Proteomic Mass Spectrometry Core), M. Keeler, Dr. S. Jones (UMMS Transgenic Mouse Core), and Dr. P. Furcinitti (UMMS Digital Imaging Core Facility) for assistance during this work. We also thank Dr. P. Odgren for use of his bright field microscope, Drs. C. Mello and J. Claycomb for assistance with real time PCR, and Dr. M. Fritzler (Univ. of Calgary) for reagents.

# CHAPTER III

## The Cytoplasmic Tail of Fibrocystin Contains a Ciliary Targeting Sequence

### Preface

Originally published the Journal of Cell Biology*, Chapter III identifies a ciliary targeting sequence (CTS) within the transmembrane receptor fibrocystin and characterizes the interaction of this CTS with the small G protein Rab8. First co-author Lixia Li performed deletion and alanine scanning mutagenesis to identify the CTS and was responsible for lipid flotation experiments and contributed significant data to Figures 3.2, 3.3. Yvonne Vucica assisted in cloning and supplied reagents. Gregory Pazour conducted Rab8/CTS overexpression experiments providing the data in Figure 3.5. Finally, this chapter was written in collaboration with Lixia Li and Gregory Pazour.

***** The cytoplasmic tail of fibrocystin contains a ciliary targeting sequence. Follit JA, Li L, Vucica Y, Pazour GJ. *J Cell Biol.* 2010 Jan 11;188(1):21-8. Epub 2010 Jan 4. PMID: 20048263

**The Cytoplasmic Tail of Fibrocystin Contains a Ciliary Targeting Sequence**

John A. Follit[*], Lixia Li[1*], Yvonne Vucica[2], and Gregory J. Pazour

Program in Molecular Medicine
University of Massachusetts Medical School
373 Plantation Street
Worcester MA 01605 USA

[1]Current Address
Merck Research Laboratories
33 Ave Louis Pasteur
Boston, MA 02115

[2]Current Address
CSL Bioplasma
189 Camp Road
Broadmeadows, VIC 3047, Australia

[*]These authors contributed equally to this study.

## Abstract

Sensory functions of primary cilia rely on ciliary-localized membrane proteins but little is known about how these receptors are targeted to the cilium. To further our understanding of this process, we dissected the ciliary targeting signal (CTS) of fibrocystin, the human autosomal recessive polycystic kidney disease gene product. We show that the fibrocystin CTS is an 18 residue motif localized in the cytoplasmic tail. This motif is sufficient to target GFP to cilia of ciliated cells and targets GFP to lipid rafts if the cells are not ciliated. Rab8, but not a number of other Rabs implicated in ciliary assembly, binds to the CTS in a co-immunoprecipitation assay. Dominant negative Rab8 interacts more strongly than wild type or constitutively active Rab8 and co-expression of this dominant negative mutant Rab8 blocks trafficking to the cilium. This suggests that the CTS functions by binding regulatory proteins like Rab8 to control its own trafficking through the endomembrane system and on to the cilium.

## Introduction

The primary cilium is a ubiquitous eukaryotic organelle that plays vital roles in the development of mammals and in the etiology of diseases such as polycystic kidney disease and blindness. It is thought that primary cilia function as cellular antennae to monitor the extracellular environment and report this information back to the cell. This small organelle is composed of hundreds of proteins assembled onto a microtubule-based cytoskeleton that projects from the surface of the cell and is surrounded by an extension of the plasma membrane. Although contiguous with the plasma membrane, the ciliary membrane is unique as cells have the ability to localize receptors and other membrane proteins specifically to this domain. This polarized distribution of proteins is required for the cilium to carry out its sensory function but little is known about how the cell achieves this distribution.

To learn more about the mechanism of ciliary targeting of membrane proteins, we characterized the ciliary targeting sequence (CTS) in fibrocystin. Fibrocystin is the gene product of the human autosomal recessive polycystic kidney disease gene, *PKHD1* (Onuchic et al., 2002; Ward et al., 2002). Patients with defects in this gene develop severe cystic kidney disease along with defects in lung, pancreas and liver. Fibrocystin is a large (>4000 residues) single-pass transmembrane protein that is predicted to be entirely extracellular except for a short ~190 residue C-terminal tail. Fibrocystin has been localized to cilia and centrosomes in mammalian cells (Menezes et al., 2004; Wang et al.,

2004; Ward et al., 2003; Wu et al., 2006; Zhang et al., 2004) and a *Chlamydomonas* homolog was found in cilia (Pazour et al., 2005).

## Results and Discussion

### The cytoplasmic tail of fibrocystin contains a ciliary targeting signal

To understand how fibrocystin is targeted to cilia, we characterized its CTS. To date, CTSs have been identified in a small number of proteins but comparison of these does not reveal common motifs. However, all are found in intracellular domains (Pazour and Bloodgood, 2008). Thus, we reasoned that even though fibrocystin is large, it is mostly extracellular with only a short cytoplasmic tail and this is the likely position of its CTS. To test this idea, we made two constructs fusing the C-terminal end of fibrocystin to reporter proteins (Fig 3.1A). In the first (JAF16), we fused the C-terminal 503 residues of fibrocystin to a fragment of CD8. This construct contains the extracellular domain of CD8 fused to fibrocystin just prior to its membrane spanning domain and is predicted to have the same membrane topology as native fibrocystin. CD8 is a well characterized membrane protein often used in chimerics to identify targeting domains (Xia et al., 2001). In the second construct (JAF99), we fused the last 193 residues of fibrocystin to the C-terminal end of GFP. This construct lacks most of the predicted membrane spanning residues but contains the entire cytoplasmic tail. After transfection into cells, both constructs can localize to cilia (Fig 3.1B, Fig 3.2Aa). In addition to cilia, JAF16 also is found in the endoplasmic reticulum. In non-ciliated cells, JAF16 remains in the endoplasmic reticulum while JAF99 is found throughout the cell in small punctate spots

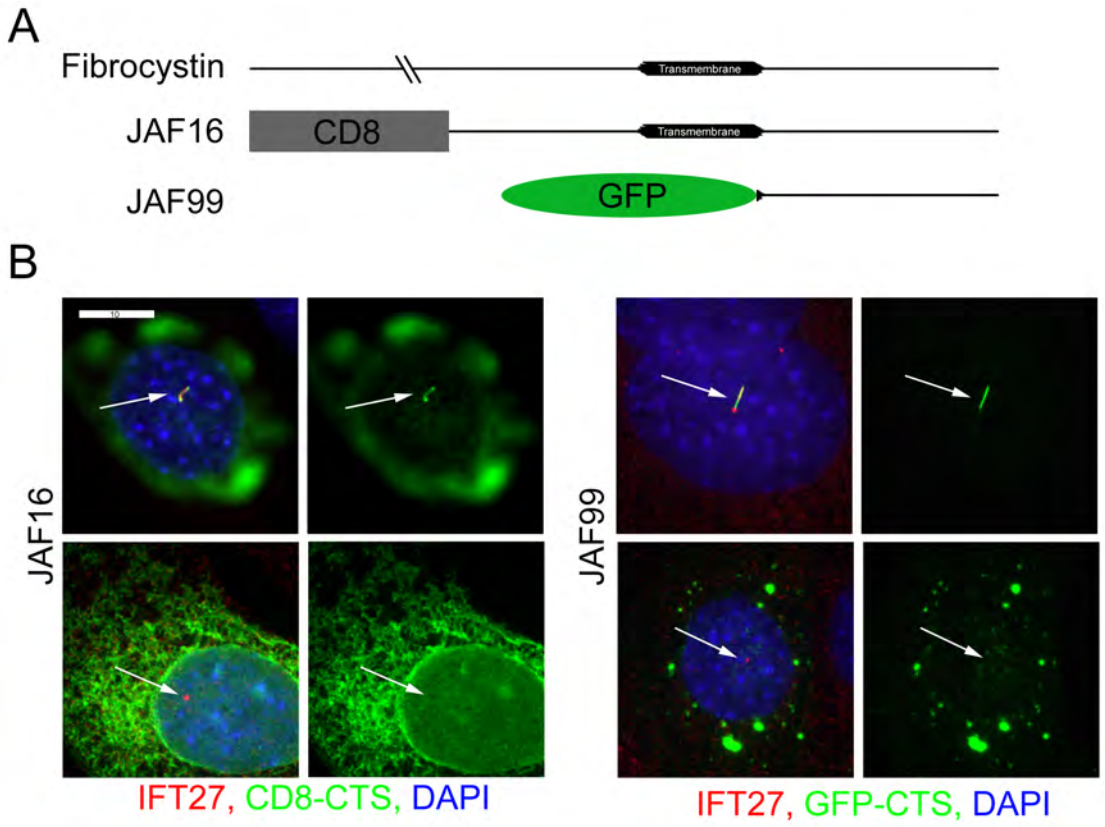


**Figure 3.1. The cytoplasmic tail of fibrocystin contains a ciliary targeting sequence.**

**Figure 3.1. The cytoplasmic tail of fibrocystin contains a ciliary targeting sequence.** **A.** Diagram of fibrocystin and the two initial constructs made to characterize the CTS. The CD8 fragment contains a signal sequence that directs the N-terminal end to the extracellular space and an epitope recognized by the CD8 antibody. The JAF16 construct is expected to have the same membrane topology as native fibrocystin. The JAF99 construct contains only the last residues of the predicted transmembrane domain and the cytoplasmic tail fused to GFP. **B.** Cellular distribution of these two constructs in IMCD3 cells. Both constructs have the ability to traffic to cilia (top row). The left panels are three color merges while the right panel in each pair shows only the CD8-CTS and GFP-CTS channels. IFT27 marks either the cilia (arrow, top row) or centrosome (arrow, bottom row). Note that JAF16 directs CD8 to both the cilium (arrow) and the endoplasmic reticulum (below the focal plane in the top image). Scale bar is 10 mm and relevant for all images in panel.

(Sup Fig 3.1, Fig 3.2Aa'). These results indicate that a CTS is located within the C-terminal 193 residues of fibrocystin.

To determine what part of the cytoplasmic tail is responsible for ciliary targeting, we constructed a series of GFP fusions containing smaller portions of the tail and quantitated their ability to localize to cilia (Fig 3.2A, B). This analysis indicated that 18 residues near the N-terminal end of the cytoplasmic tail were sufficient to target GFP to the cilium of ciliated cells or to punctate spots in non-ciliated cells. The large size of fibrocystin prevented us from determining if these residues are required for trafficking of native fibrocystin to cilia. Thus it is currently unknown if this is the only CTS within the protein. If the GFP fusion construct did not contain the 18 residue CTS, the GFP was distributed throughout the cell or concentrated in the nucleus. We did not carefully demarcate the nuclear targeting sequence but the fusion containing residues 63-193 was able to efficiently concentrate in the nucleus, while the 40-68 fusion could localize to the nucleus but was also found in the cytoplasm. Other work also mapped a nuclear targeting sequence to the region between residues 80 and 104 (Hiesberger et al., 2006).

Examination of the CTS in fibrocystins from other species indicates that it is highly conserved in mammals and moderately conserved in chicken (Fig 3.2C). The sequence is not conserved in the fibrocystin-related protein, fibrocystin-L from mammals or other species. BLAST searches with the CTS did not identify any novel proteins containing similar sequences. The fibrocystin CTS does not contain a VxP motif that has been proposed to be a generic ciliary targeting sequence (Deretic et al., 2005; Geng et al., 2006) nor does it contain an Ax[S/A]xQ motif identified in several G-protein coupled

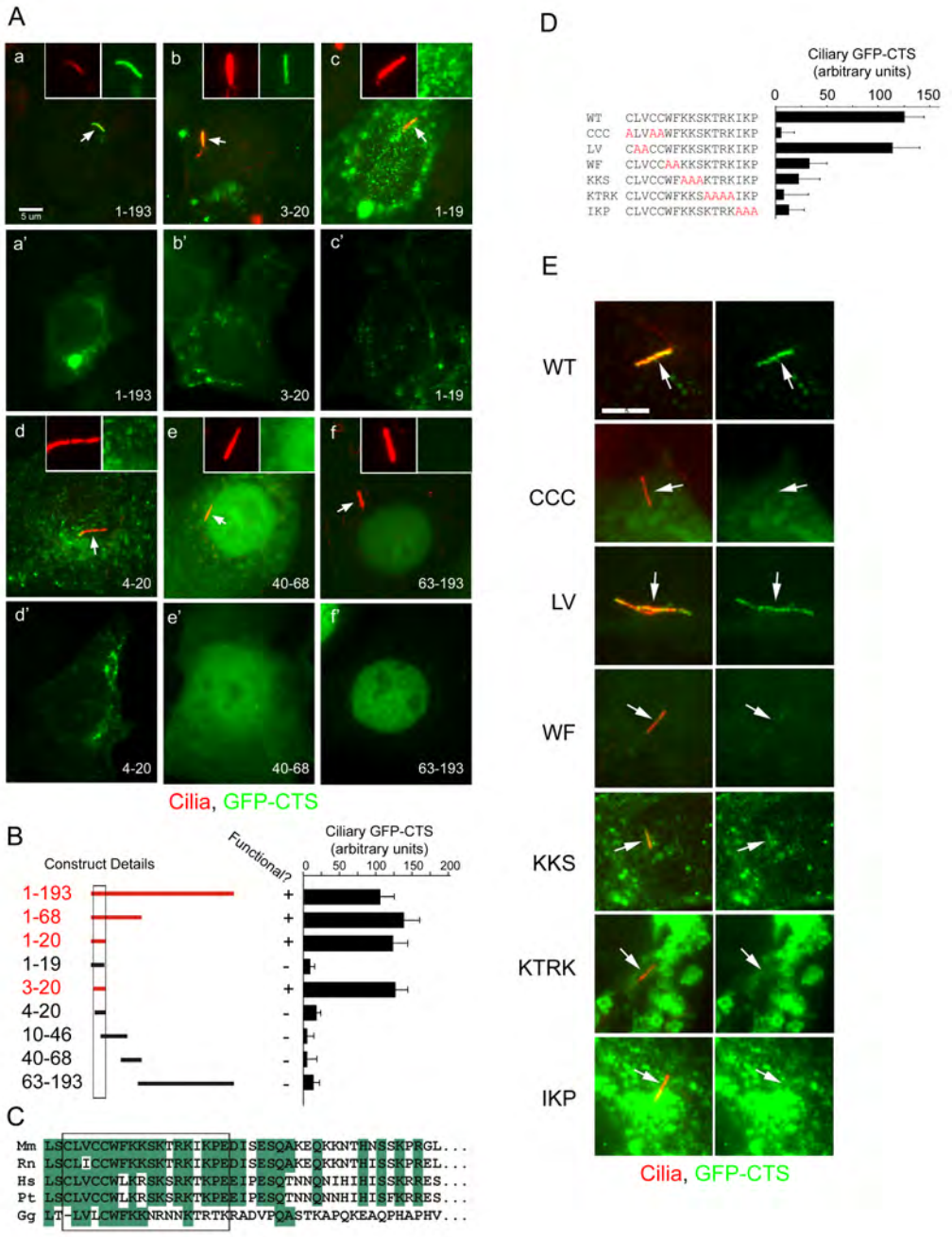


**Figure 3.2: Characterization of the CTS of fibrocystin.**

**Figure 3.2: Characterization of the CTS of fibrocystin. Aa-f**. Selected examples showing the distribution of sub fragments of the cytoplasmic tail. Two different cells are shown for each construct. The first image (**a-f**) shows a ciliated cell with the cilium marked with an arrow while the second image (**a'-f'**) shows a non-ciliated cell. Insets show the cilia (red) and GFP-CTS (green) channels alone. The amino acid fragments fused to GFP are listed at the bottom of each image and are graphically shown in **B**. Size bar in **Aa** is 5 mm and is relevant for all images in the panel. **B.** Graphical representation of the constructs and quantification of the ability of the constructs to function. The numbers on the left represent the amino acids included in the construct and the box denotes the limits of the CTS. The graph shows the mean amount of GFP fluorescence per μm in cilia from 25 transfected cells. Error bars are SEM. **C.** Alignment of the CTS (box) and surrounding sequence of vertebrate fibrocystins (mouse Mm, rat Rn, human Hs, chimp Pt, Chick Gg). **D,E.** Alanine scanning mutagenesis of the CTS. **D.** Sequence and quantification of the ability of the mutated CTSs to direct GFP to cilia. Quantification is as described for panel B. WT, wild type; CCC, LV, WF, KKS, KTRK, IKP indicate which amino acids were mutated in each construct. **E.** Images illustrating the cellular distribution of constructs described in D. Arrows mark cilia. Scale bar is 5 mm and is relevant for all images in the panel.

receptors (Berbari et al., 2008). To further our understanding of the CTS, we used alanine scanning mutagenesis to mutate small blocks of residues (Fig 3.2D, E). Quantification of the effects of these mutations (Fig 3.2D) shows that most residues are important for function. The CCC and KTRK residues are most critical since mutating these to alanines almost completely blocks CTS function. At the other extreme, the LV mutation does little to the CTS function while the other mutations reduce the ability to traffic to cilia but do not completely block function.

While we did not detect any significant homology between the fibrocystin CTS and other non-fibrocystin sequences, we noted similarity between the CTS amino acid composition and a lipid raft targeting sequence in SNAP25 (Salaun et al., 2005) (Fig 3.3A). This suggested that the punctate spots to which the CTS localized might be lipid rafts. To test this, live CTS-GFP expressing cells were labeled with fluorescent cholera toxin B (Fig 3.3B). Cholera toxin B binds GM1 gangliosides and is a marker for membrane domains enriched in these lipids. In non-ciliated cells, there is strong colocalization between the CTS-GFP spots and the cholera toxin binding sites (Fig 3.3Ba). The colocalization also is observed if the cholera toxin is cross linked with an antibody and then fixed (Fig 3.3Bb). Cholera toxin B labels the cilium (Fig 3.3Bc) confirming previous reports that this organelle is enriched in GM1 gangliosides (Janich and Corbeil, 2007). SNAP25 has been reported to localize to cilia (Low et al., 1998) but the lipid raft targeting sequence of SNAP25 was not sufficient to target GFP to cilia (Fig 3.3Bd) indicating that a lipid raft targeting sequence alone is not sufficient for ciliary targeting.

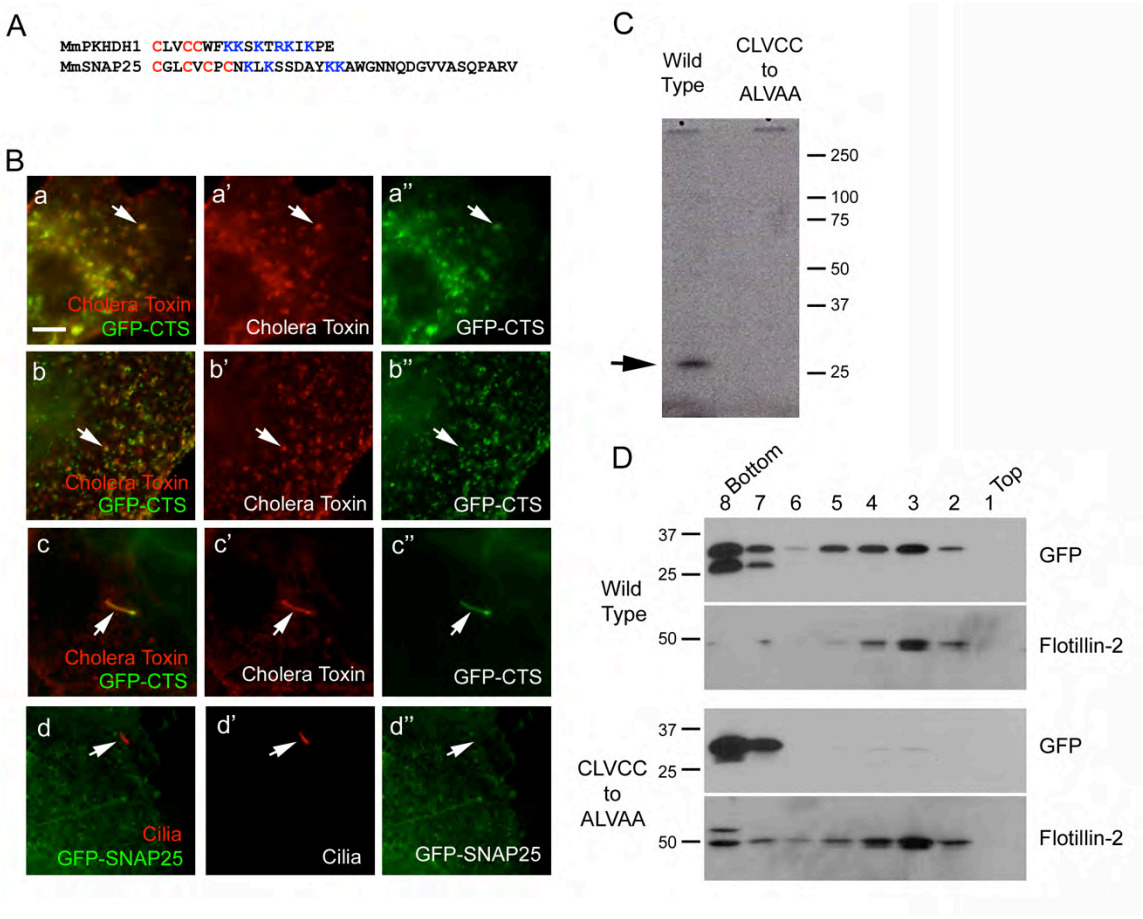


**Figure 3.3: The CTS is associated with lipid.**

**Figure 3.3: The CTS is associated with lipid.** **A.** Comparison of the CTS from fibrocystin to the lipid raft targeting sequence of SNAP25 [19]. **B.** Colocalization of GFP-CTS with lipid rafts. **Ba.** Live cells stained with Alexa-594 conjugated cholera toxin. In non-ciliated cells, cholera toxin shows extensive colocalization with the GFP-CTS in the cell body; the arrow points at one example. **Bb.** Cholera toxin was crosslinked by antibody before fixation, which caused the toxin and GFP to cluster (arrow). **Bc.** In ciliated cells, GFP and cholera toxin colocalize in the cilium (arrow). **Bd.** The lipid raft targeting sequence of Snap25 does not target GFP to the cilium (arrow). Size bar is 5 mm and is relevant for all images. **C.** Tritiated palmitate is incorporated into the wild type but not the cysteine-mutated CTS (arrow). **D.** The CTS cysteines mediate interaction with membranes. Cells expressing either wild type or cysteine-mutated CTS-GFP were lysed and fractionated by an OptiPrep gradient.

Cysteine residues near blocks of basic amino acids are often palmitoylated (Bijlmakers and Marsh, 2003). The fibrocystin CTS contains three cysteine residues followed by a block of basic residues (Fig 3.3A) and mutational analysis indicated that these cysteines are critical to CTS function (Fig 3.2D). To test if the CTS cysteines are palmitoylated, we grew cells expressing either the wild type or the CCC mutated GFP-CTS in radioactive palmitate, immunoprecipitated the GFP-CTS and looked for the incorporation of isotope. The wild type protein but not the CCC mutated version incorporated radioactive palmitate (Fig 3.3C). This indicates that the CTS includes a palmitoylation motif and since the mutation of the cysteines blocks function, this suggests that palmitoylation is important for targeting this protein to the cilia. Acylations like palmitoylation and myristoylation are common modifications of ciliary membrane proteins. The opsin photoreceptor contains two cysteine residues that are palmitoylated and needed for proper targeting to the cilium (Tam et al., 2000). A *Trypanosome* ciliary calcium binding protein contains a palmitoylated cysteine and a myristoylated glycine (Godsel and Engman, 1999) that are needed for targeting to the cilium.

It is likely that the palmitoylated cysteines of fibrocystin serve to link the GFP-CTS to lipid membranes and this is responsible for the puncta that are observed in non-ciliated cells. The fact that the GFP-CTS is evenly distributed in the cells when the cysteines are mutated (Fig 3.2E) supports this idea but we tested this more directly by floatation analysis. Membranes from cells expressing either wild type or the CCC mutated GFP-CTS were loaded on the bottom of an OptiPrep gradient and centrifuged. Membranes floated up and carried along the lipid raft marker flotillin-2. The wild type

GFP-CTS was also carried up whereas the CCC mutated protein remained at the bottom where it was loaded (Fig 3.3D). This indicates that the palmitoylated cysteines link the GFP-CTS to the membrane. Thus, even though the protein no longer contains a transmembrane domain, it remains associated with the membrane. To understand the cellular compartment to which the GFP-CTS localized, we labeled cells expressing the GFP-CTS with a variety of compartmental markers (Fig 3.4). No significant colocalization was seen with Golgi, lysosome, and most endosome markers but colocalization was seen with markers for the recycling endosome. This suggests that the palmitoylated GFP-CTS has affinity for the membranes of this compartment but whether the native protein is trafficked through the recycling endosome remains to be determined.

**Trafficking of the CTS is regulated by Rab8**

Work in frog retina indicates that Rab8 plays a key role in trafficking of opsin to the outer segment (Moritz et al., 2001) and recent work in mammalian cell culture has indicated that Rab8 and other Rab family proteins are critical for ciliary assembly (Nachury et al., 2007; Yoshimura et al., 2007). To test if Rab8 plays a role in the trafficking of the fibrocystin CTS, we generated cell lines expressing FLAG-tagged wild type Rab8, dominant negative Rab8T22N and constitutively active Rab8Q67L (Fig 3.5). These mutations are often used to perturb the GTP/GDP cycle of small G proteins. The T22N mutation is thought to keep the protein in the GDP-bound state, which binds guanine exchange factors to inhibit their activity on native substrates. The Q67L mutation reduces GTP hydrolysis keeping the protein in the GTP bound state (Feig, 1999). As previously reported (Nachury et al., 2007), wild-type FLAG-Rab8 and FLAG-

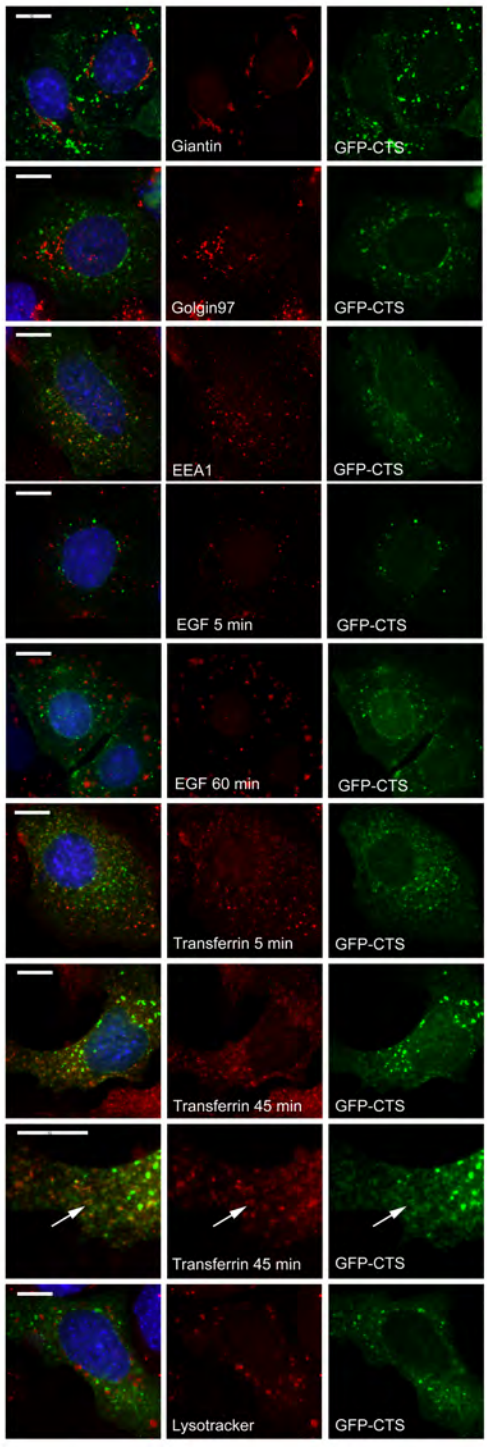


**Figure 3.4: Colocalization between the CTS-GFP and various markers of the endomembrane system.**

**Figure 3.4: Colocalization between the CTS-GFP and various markers of the endomembrane system.** IMCD3 cells expressing the GFP-CTS (JAF99) were fixed and stained with each of the antibodies listed (Giantin, Golgin97, EEA1), or were labeled with Lysotracker and then fixed, or were incubated with red fluorescent transferrin or EGF for 5 minutes, washed and then chased for the amount of time indicated before fixing. Size bars are 10 mm. Note that no significant colocalization was seen with markers of the cis-medial (Giantin) and trans (Golgin97) Golgi complex. Some markers of the endosomal compartment partially colocalized with the smaller GFP-CTS puncta. The most extensive colocalization is seen with endocytosed transferrin at late time points after a pulse chase (Transferrin 45 min). A 2X enlargement is shown to better visualize this co-localization. One example of a co-localizing region is marked with an arrow. Endocytosed EGF showed minimal colocalization at either early (EGF 5 min) or late (EGF 60 min) time points and minimal colocalization was seen with the early endosome antigen (EEA1) and with a lysosome marker (Lysotracker). This suggests that the GFP-CTS localizes to the recycling endosome as both transferrin and EGF traffic to early endosomes after endocytosis but from the early endosome, transferrin moves to the recycling endosome whereas EGF moves to the late endosome and then to the lysosome. The large GFP-CTS puncta near the nuclei did not colocalize with any markers suggesting that they may be aggregates. There was also a significant amount of the GFP-CTS in small puncta that did not localize with any of the markers. This pool may be in the plasma membrane since there was good colocalization with cholera toxin (Fig 2Ba, Bb).

Rab8Q67L localized to cilia while FLAG-Rab8T22N did not localize to the cilia that formed on these cells (Fig 3.5A). Cells expressing FLAG-tagged wild type Rab8 and Rab8Q67L ciliated fairly well but cells expressing Rab8T22N did not ciliate nearly as well (wild type 68%+/-12; T22N 2.7%+/-0.6; Q67L 46%+/-3.5). The fibrocystin GFP-CTS did not traffic to the cilia that formed on the FLAG-Rab8T22N cells (Fig 3.5B, C) but was trafficked to cilia on cells expressing FLAG-Rab8 and FLAG-Rab8Q67L. Interestingly, the amount of the GFP-CTS trafficked to cilia was higher in cells that expressed the wild type FLAG-Rab8 than in cells that were not transfected or in cells expressing either of the mutant forms. This suggests that Rab8 is a limiting factor in the amount of GFP-CTS that can be trafficked to cilia. The observation that the mutant forms either do not show the enhancement (Q67L) or reduce the amount of trafficking (T22N) suggests that Rab8 needs the normal GTP/GDP cycle to function properly.

**The CTS interacts with Rab8**

Since Rab8 appeared to regulate the trafficking of the fibrocystin CTS, we sought to understand how this might be functioning and asked if Rab8 or other Rabs could be physically connected to the CTS (Fig 3.6). To do this, we co-expressed the cytoplasmic tail of fibrocystin with a series of Rab proteins (Rab6, Rab8, Rab11, Rab17, and Rab23) that have been implicated in trafficking of ciliary membrane proteins (Deretic and Papermaster, 1993; Moritz et al., 2001; Yoshimura et al., 2007). We also included IFT20, which is not a Rab protein, but is an IFT subunit that we have implicated in trafficking proteins to the ciliary membrane (Follit et al., 2008; Follit et al., 2006). None of these proteins were completely co-localized with the GFP-CTS in non-ciliated cells.

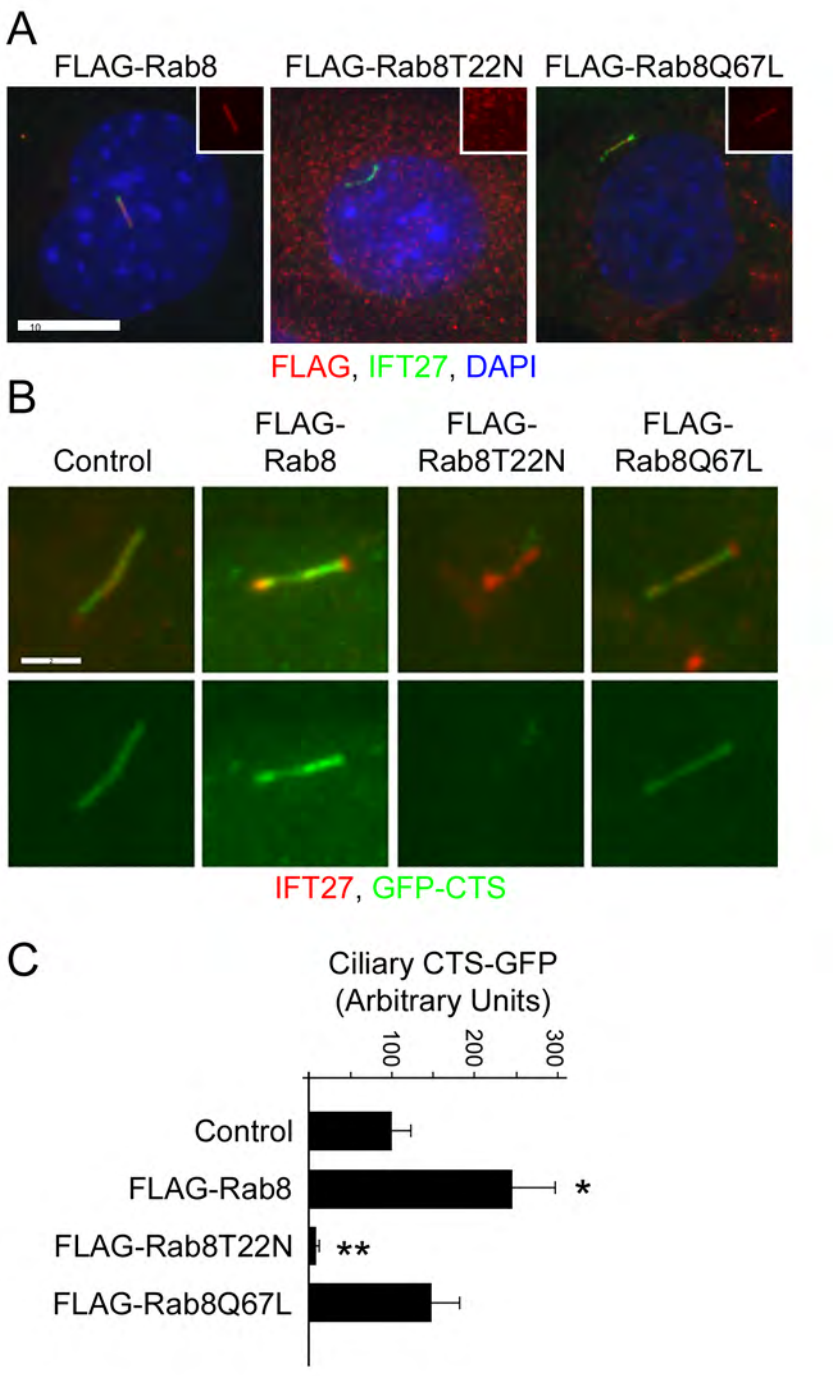


**Figure 3.5: Effect of Rab8 on the trafficking of the fibrocystin CTS.**

**Figure 3.5: Effect of Rab8 on the trafficking of the fibrocystin CTS. A**. FLAG-tagged Rab8 and Rab8Q67L are localized to cilia of IMCD3 cells while Rab8T22N is not. Insets show the red (FLAG) channels of the cilia. Scale bar is 10 mm and relevant for all images in panel. Insets show the FLAG-Rab8 channels alone. **B**. The fibrocystin CTS targets GFP to cilia in control cells and cells expressing wild type FLAG-Rab8 and FLAG-Rab8Q67L but not in cells expressing FLAG-Rab8T22N. Scale bar is 2 mm and relevant for all images in panel. **C.** Quantification of ciliary GFP-CTS fluorescence. Quantification was done as described in Fig 1. Error bars are SEM. Significance as compared to control: * <0.02; ** <0.001.

However, Rab8 showed some colocalization while Rab11 and Rab17 showed the most colocalization (Fig 3.6). The colocalization with Rab11 and Rab17 is consistent with the results of the compartmental analysis (Fig 3.4) as these two G-proteins localize to the recycling endosome (Zerial and McBride, 2001). Rab8 was the only one of these Rabs to localize to cilia (Fig 3.5B, and not shown). The ability of these proteins to interact with the GFP-CTS was tested by a co-immunoprecipitation assay. In this assay, the GFP-CTS was co expressed with each of the FLAG-tagged Rabs in mouse kidney cells. The Rabs were precipitated via the FLAG tag and the precipitates probed for the GFP-CTS. No interaction was seen between the GFP-CTS and Rab6, Rab11, Rab17, Rab23 or IFT20 but a significant amount of the GFP-CTS was precipitated by Rab8 (Fig 3.7A). This analysis was carried out with the entire cytoplasmic tail and so we asked if the Rab8 binding site overlapped the essential 18 residue CTS motif within the tail. To do this, we tested selected deletion constructs described in Fig 3.2B. The Rab8 binding site is located within the 18 residues minimal CTS as fragments that contain this sequence are co-precipitated (Fig 3.7B 1-193, 1-68, 3-20) whereas the C-terminal 130 residues (Fig 3.7B 63-193), which does not target to cilia (Fig 3.2A,B), is not precipitated. The CTS is not simply an Rab8 binding site as deletions of single residues from either end of the minimal CTS blocked the ability of the peptide to direct GFP to the cilium (Fig 3.2A, B) but did not block the binding to Rab8 (Fig 3.7B 1-19, 4-20).

We next examined the effect of the alanine scanning mutations on the ability of the CTS to be co-precipitated by Rab8. Interestingly, there is a good correlation between the function of the CTS to traffic to the cilium (Fig 3.2D) and its ability to bind to Rab8

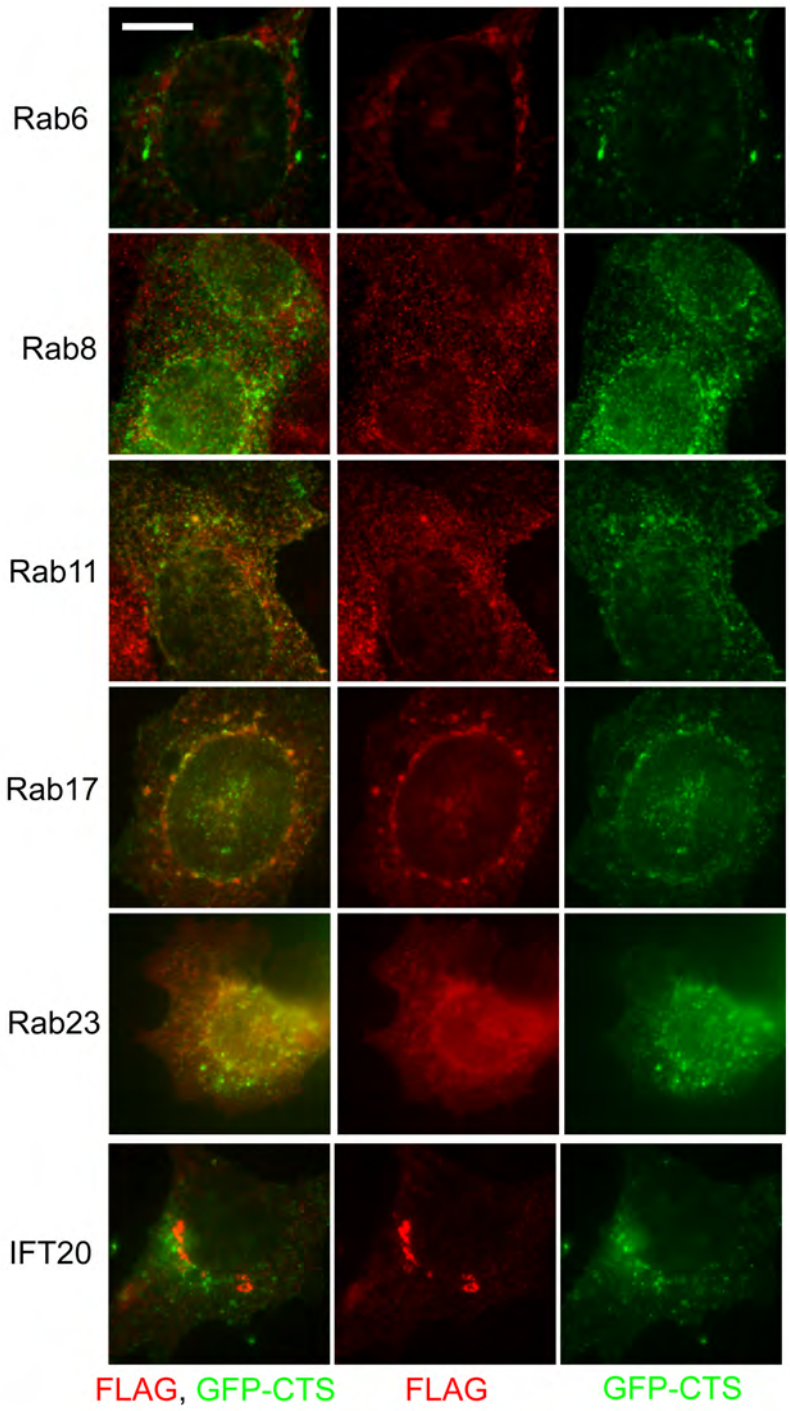


**Figure 3.6: Fluorescence images of cells expressing the FLAG-tagged Rab proteins used in Figure 3.7 with the GFP-CTS.**

**Figure 3.6: Fluorescence images of cells expressing the FLAG-tagged Rab proteins used in Figure 3.7 with the GFP-CTS.** Note that most do not show significant colocalization with the GFP-CTS. The most significant overlap with the GFP-CTS is seen with Rab11and Rab17. Scale bar is 10 mm and relevant for all images in panel.

(Fig 3.7C). For example, the LV mutation does little to block function of the CTS and this mutated protein binds Rab8. On the other hand, The CCC and KTRK mutations are most disruptive to the CTS and most significantly decrease binding to Rab8. Other mutations had intermediate effects on the targeting ability and have intermediate effects on the ability to bind Rab8. The KKS mutation is an exception as this is fairly detrimental to CTS function but still binds to Rab8. This suggests that additional proteins may bind the CTS and require these residues for activity.

To begin to understand if the interactions between the CTS and Rab8 may be regulated by the GTP/GDP state of Rab8, we compared the ability of the constitutively active and dominant negative mutations of Rab8 to bind to the CTS. Interestingly, the dominant negative form bound more CTS than either the wild type protein or the constitutively active form. This suggests that exchange of a GDP with a GTP would release Rab8 from the CTS. This behavior is different from classic Rab effectors, which bind more strongly when bound to GTP (Zerial and McBride, 2001) but is similar to what was previously observed in the interaction between Rab5 and the angiotensin receptor (Seachrist et al., 2002). In the case of the angiotensin receptor, it was proposed that the receptor anchors Rab5-GDP on the surface of the carrier vesicle so that once GTP is exchanged for GDP, efficient vesicle fusion could occur. Similarly, the fibrocystin CTS may bind Rab8-GDP to increase its local concentration in order to allow for efficient execution of the next step in transport when GTP exchange occurs. Based on work in frog photoreceptors, it is likely that the regulated step is the fusion of carrier vesicles at the base of the cilium as expression of dominant negative Rab8 mutant caused small

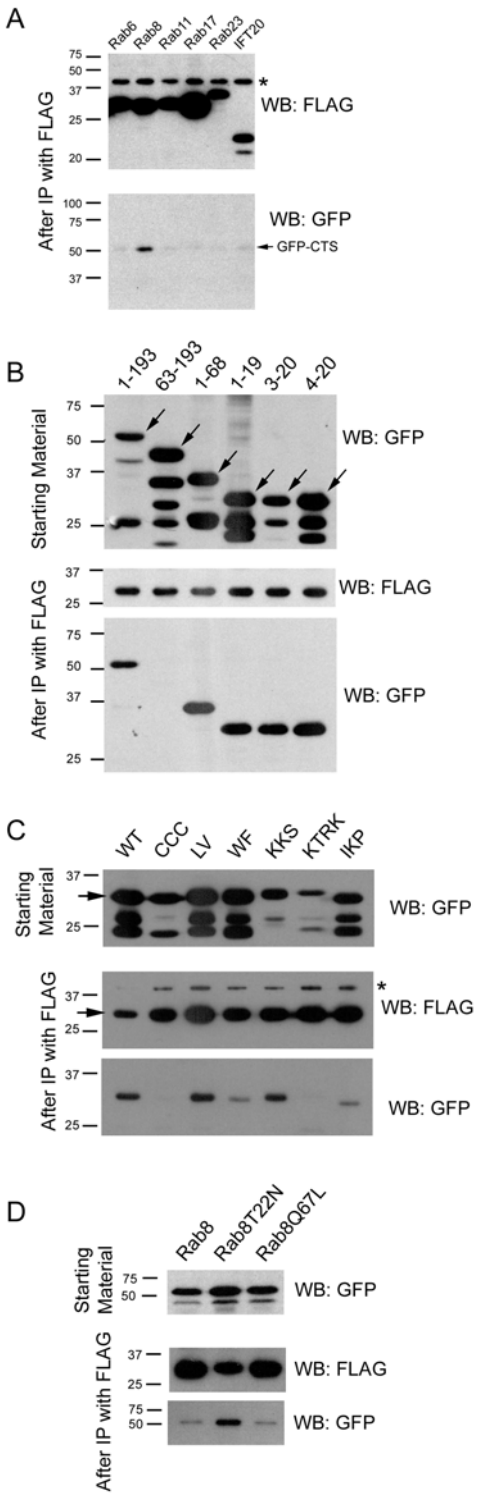


**Figure 3.7: Rab8 interacts with the fibrocystin CTS.**

**Figure 3.7: Rab8 interacts with the fibrocystin CTS.** **A**. FLAG-tagged Rab proteins were co-expressed with the GFP-CTS (1-193) and precipitated. The precipitates were analyzed by western blot with FLAG and GFP antibodies. * marks a non-specific band precipitated by the FLAG antibody. Positive interactions have a band in the GFP western blot. **B**. The deletion constructs (Fig 1B) were tested for the ability to interact with Rab8. Arrows mark the predicted size of the full length proteins. **C.** The alanine scan mutations (Fig 1D) were examined for their ability to interact with Rab8. Arrows mark the predicted size of the full length proteins; * marks a non-specific band precipitated by the FLAG antibody. **D**. The ability of Rab8T22N and Rab8Q67L mutants to bind the GFP-CTS were compared to wild type Rab8 in an analogous assay.

vesicles to accumulate around the base of photoreceptors (Moritz et al., 2001). This process may be regulated by the BBSome as the guanine exchange factor Rabin8 is associated with the BBSome and this protein would be expected to exchange GDP with a GTP on Rab8 (Nachury et al., 2007).

**Comparison of ciliary targeting to apical and basolateral targeting**

Compared to trafficking to the ciliary membrane, much more is known about trafficking to apical and basal-lateral membranes (Rodriguez-Boulan et al., 2005). Basolateral targeting sequences consist of short motifs that interact with the adaptor protein complexes that bind to clathrin coats as part of the sorting mechanism. Apical targeting motifs are much more diverse and do not share significant sequence homology with each other but have been proposed to function by directing proteins to lipid rafts that are preferentially sorted to the apical membrane (van Meer and Simons, 1988). Ciliary targeting is similar to apical targeting in that no sequence similarity is seen between the known CTSs (Pazour and Bloodgood, 2008) and at least for fibrocystin and the *Trypanosome* calcium binding protein (Tyler et al., 2009), association with a lipid raft appears to be required for proper targeting. Thus, it appears that ciliary targeting is related to apical targeting but has additional components to direct the proteins into the ciliary membrane. It is interesting to note that on vertebrate epithelial cells the ciliary membrane is a sub domain of the apical membrane and so perhaps it is logical that trafficking to these two domains share similar features.

## Materials and Methods

### Plasmids

The cytoplasmic tail of mouse fibrocystin (accession # NM_153179.2) was amplified from mouse kidney cDNA using GGGAATTCGCTTTGACTGTGACATTTTCAGTCCTAG and GGGAATTCTTACTGGATGGTTTCTGGTGG and fused to the CD8 open reading frame to create JAF16. The CD8 open reading frame was amplified from pCMS-CD8-NR1C (gift of H. Xia, Stanford Univ.) (Xia et al., 2001). JAF16 contains the last 503 residues of fibrocystin fused in frame to the CD8 extracellular domain. The fusion junction reads LDFACDefALTVTF with the first 6 residues being derived from CD8, the last 6 from MmPKHD1 and the two in the middle are from the restriction enzyme site. Likewise mouse kidney cDNA was amplified with GGGAATTCCTGAGCTGTCTCGTTTGCTG and GGGAATTCTTACTGGATGGTTTCTGGTGG and cloned into the EcoRI site of pEGFP-C2 (BD Biosciences Clontech, Mountain View, CA) to create pJAF99. This plasmid contains the last 193 amino acids of fibrocystin fused in frame to the C-terminal end of GFP. Deletion constructs were generated by similarly amplifying smaller fragments and cloning them into this vector. Point mutations were generated by inverse PCR. All plasmids were confirmed by DNA sequencing. Rab8, Rab8T22N and Rab8Q67L were cloned into p3XFLAG-myc-CMV26 (Sigma, St. Louis MO) for expression in mammalian cells.

**Miscellaneous Methods**

All cell culture work used mouse kidney IMCD3 (Rauchman et al., 1993) cells cultured in 47.5% DME, 47.5% F12 supplemented with 5% Fetal Bovine Serum (FBS) and penicillin/streptomycin (Cellgro, Herndon, VA) at 37˚ C in 5% $CO_2$. For transfection, cells were electroporated using a GenePulser Xcell (Bio-Rad, Hercules, CA) (200 volts, 50 ms pulse, 4 mm cuvette). Stable cell lines were selected with 400 µg/ml of G418 (Sigma). Clonal lines were isolated by dilution cloning after drug selection.

Percent ciliation was determined by counting cilia on cells stained with an IFT27 antibody after being grown for 48 hours in low serum (0.25%). Results reported are percent cilia +/- standard deviation from three independent experiments where >500 cells were counted.

Endocytosis assays were performed on IMCD3 cells electroporated with JAF99 48 hours after electroporation. Cells were washed with KRH (125 mM NaCl, 5 mM KCl, 1.3 mM $CaCl_2$, 1.2 mM $MgSO_4$, 25 mM HEPES pH 7.4, 2 mM sodium pyruvate and 0.5% bovine serum albumin) incubated with Alexa568-labeled EGF or Transferrin for 5 min at 37° C, washed with KRH and then incubated at 37 C in KRH (Leonard et al., 2008). Coverslips were periodically removed and fixed during the chase period.

For visualization of lipid domains, live cells grown in glass-bottom dishes (MatTec, Ashland, MA) were incubated for 10 min at 37° C with Alexa-594 conjugated cholera toxin B (Molecular Probes/Invitrogen, Carlsbad CA). Excess toxin was washed out and the cells were imaged at 37° C in medium lacking Phenol Red. Alternatively, cells were incubated for 10 min at 4° C with the cholera toxin, followed by 15 additional min at 4°

C with cholera toxin antibody before fixing and staining following manufacturer's specifications (Vybrant Lipid Raft Labeling Kit, Molecular Probes).

Lipids were floated using the protocol of Macdonald and Pike (Macdonald and Pike, 2005). Briefly, cells were lysed by passing them through a needle, the post nuclear supernatant was mixed with OptiPrep (Sigma) to a final concentration of 25%, placed at the bottom of a centrifuge tube, and a gradient of 0-20% OptiPrep was layered on top. The gradient was centrifuged at 52,000 x g for 90 min and fractions were collected and analyzed by western blotting.

To determine if the CTS was palmitoylated, IMCD3 cells were electroporated with the wild type (1-22) and equivalent cysteine-mutated GFP-CTS (1-22CCC) constructs. After 24hr, the medium was changed to one containing dialyzed serum (GIBCO/Invitrogen) supplemented with 0.25 mCi of tritiated palmitate (PerkinElmer, Waltham MA). After 16 hr, cells were lysed and the GFP-CTS was precipitated with the JL8 GFP antibody (BD Biosciences Clontech) and the eluates were separated by SDS-PAGE. The gel was then fixed in 2:9:9 acetic acid:methanol:water for 1hr, followed by 1M sodium salicylate for 30 min, dried and exposed to film.

Immunoprecipitations were performed using anti-FLAG resin. To do this, cells expressing the tagged constructs were rinsed with cold PBS, lysed in Cell Lytic M + 0.1 % NP40 (Sigma), 0.1% CHAPSO (BioRad), with Complete Protease Inhibitor (Roche, Basel Switzerland) at 4° C and clarified by centrifugation (18,000 g for 10 min). Clarified lysates were incubated with Agarose beads coupled with FLAG M2 antibody (Sigma) for one hour. FLAG beads were washed 3 times with Wash Buffer (50 mM Tris,

150 mM NaCl, pH 7.4) plus 1% NP40. Bound FLAG proteins were eluted with 200 μg/ml 3X FLAG peptide (Sigma). Purified proteins were separated by SDS-PAGE and electrophoretically transferred to Immobilon-P (Millipore, Billerica MA). After transfer, the membranes were incubated with antibodies to GFP (JL8, BD Biosciences Clontech) and FLAG (F1804, Sigma) followed by an HRP-conjugated anti-mouse IgG antibody (Pierce, Rockford, IL). The HRP-conjugates were detected on film (BioMax XAR, Kodak, Rochester NY) after LumiGLO (KPL, Gaithersburg MD) treatment.

**Immunofluorescence Microscopy**

Cells were transfected by electroporation and seeded on coverslips. After 24 hr, serum was reduced to 0.25% to promote ciliation and the cells grown for an additional 24-96 hr before being fixed with paraformaldehyde and stained with primary antibodies as described (Follit et al., 2006). Primary antibodies were detected by Alexa-350, Alexa-488, and Alexa-594 (Molecular Probes, Eugene OR) labeled secondary antibodies. Primary antibodies included anti-acetylated tubulin (611β1, Sigma), anti-FLAG (Sigma), anti-CD8(Zymed, San Francisco CA), EEA1 (gift of S. Corvera, Univ. Massachusetts Medical School), Giantin (gift of M. Fritzler, Univ. of Calgary), Golgin97 (CDF4, Molecular Probes), Flotillin-2 (BD Biosciences, San Jose CA) and mouse IFT20 and IFT27 (Follit et al., 2006).

Wide-field images were acquired by an Orca ER camera (Hamamatsu) on a microscope (Axiovert 200M; Carl Zeiss, Inc.) equipped with a 100 × Plan-Apochromat 1.4 NA objective (Carl Zeiss, Inc.). If comparisons are to be made between images, the photos were taken with identical conditions and manipulated equally. For the

quantification of GFP in the cilia, the length, area, and mean fluorescence intensity of the cilia was measured using the measurement tools of Openlab (Improvision). Numbers reported are fluorescence intensity per micron of length.

## Acknowledgements

We thank Drs. N. Kennedy for assistance with the palmitoylation assay, D. Navaroli for assistance with the endocytosis assays, J. Jonassen for statistical analysis and H. Xia (Stanford Univ.) M. Fritzler (Univ. of Calgary) and S. Corvera (Univ. Mass Med.) for reagents. This work was supported by grants from the NIH GM060992, the Worcester Foundation for Biomedical Research, and the Polycystic Kidney Foundation.

# CHAPTER IV

## Arf4 Is Required for Mammalian Development but Dispensable for Ciliary Assembly

John A. Follit, Julie A. Jonassen[1] and Gregory J. Pazour

Program in Molecular Medicine
University of Massachusetts Medical School
Biotech II, Suite 213
373 Plantation Street
Worcester, MA 01605

[1]Department of Microbiology and Physiological Systems
University of Massachusetts Medical School
55 Lake Avenue North
Worcester MA 01655

## Abstract

The primary cilium is a sensory organelle, defects in which cause a wide range of human diseases including retinal degeneration, polycystic kidney disease and birth defects. The sensory functions of cilia require specific receptors to be targeted to the ciliary subdomain of the plasma membrane. Arf4 has been proposed to sort cargo destined for the cilium at the Golgi complex and deemed a key regulator of ciliary protein trafficking. In this work, we show that Arf4 binds to the ciliary targeting sequence (CTS) of fibrocystin. Knockdown of Arf4 indicates that it is not absolutely required for trafficking of the fibrocystin CTS to cilia as steady-state CTS levels are unaffected. However we did observe a delay in delivery of newly synthesized CTS from the Golgi complex to the cilium when Arf4 was reduced. *Arf4* mutant mice are embryonic lethal and die at mid-gestation shortly after node formation. Nodal cilia appeared normal and functioned properly to break left-right symmetry in *Arf4* mutant embryos. At this stage of development Arf4 expression is highest in the visceral endoderm but we did not detect cilia on these cells. In the visceral endoderm, the lack of Arf4 caused defects in cell structure and apical protein localization. This work suggests that while Arf4 is not required for ciliary assembly, it is important for the efficient transport of fibrocystin to cilia, and also plays critical roles in non-ciliary processes.

## Author Summary

Primary cilia are ubiquitous sensory organelles that play vital roles in an ever-growing class of human diseases termed ciliopathies including obesity, retinal degeneration and polycystic kidney disease. The proper function of the primary cilium relies on a cell's ability to target and concentrate specific receptors to the ciliary membrane – a unique subdomain of the plasma membrane yet little is known about how receptors are trafficked to the primary cilium. Mutations affecting the ciliary localized receptor fibrocystin (*PKHD1*) cause autosomal recessive polycystic kidney disease, which affects approximately 1:20,000 individuals. Previously we identified a motif located in the cytoplasmic domain of fibrocystin that is required for its ciliary localization. In this work we demonstrate that the ciliary targeting sequence (CTS) of fibrocystin interacts with the small G protein Arf4 and this interaction is important for the efficient delivery of the CTS to cilia in cultured cells. Disruption of *Arf4* in mice results in defects in the non-ciliated visceral endoderm and death at mid-gestation indicating Arf4 has vital functions in addition to ciliary protein trafficking.

## Introduction

Cilia play diverse motility and sensory functions throughout the eukaryotic kingdom, but play especially critical roles in vertebrates where severe defects lead to embryonic lethality while mild defects cause a wide range of syndromes affecting every organ system. Both the motility and sensory functions of cilia are important for health and development, but it is now recognized that sensory defects underlie the most severe maladies affecting humans. The sensory functions of cilia rely on a cell's ability to target and concentrate a specific set of receptors to the ciliary membrane. While contiguous with the plasma membrane of the cell, the ciliary membrane is a distinct compartment to which the cell targets and concentrates a unique complement of proteins (Pazour and Bloodgood, 2008; Rohatgi and Snell, 2010). The list of membrane proteins found in the ciliary compartment is constantly growing; among the most studied ciliary proteins are the polycystins and fibrocystin that are defective in human polycystic kidney disease, rhodopsins and opsins that are critical for vision and the patched and smoothened receptors of the hedgehog pathway.

The mechanism that targets membrane proteins specifically to the ciliary compartment is an active area of study but very little is definitively known (Nachury et al., 2010). It appears that ciliary membrane proteins contain cis-acting motifs that cause them to be localized to cilia. We identified one of these ciliary targeting sequences (CTS) in fibrocystin, the gene product of the human autosomal recessive polycystic kidney disease gene (*PKHD1*) (Follit et al., 2010; Onuchic et al., 2002; Ward et al., 2002;

Ward et al., 2003). Like many other CTSs, the fibrocystin CTS contains lipid-modified residues that target the protein to lipid rafts, which appears to be part of the ciliary trafficking pathway. We proposed that this sequence might interact with proteins that are important for sorting or transport to the ciliary membrane compartment. In support of this idea, we found that the fibrocystin CTS interacted with Rab8, a protein widely recognized as important to ciliary membrane protein trafficking (Follit et al., 2010; Nachury et al., 2007; Yoshimura et al., 2007). In the present work we asked if the fibrocystin CTS could interact with Arf4 as work of Deretic and colleagues has shown that this protein interacts with the CTS of opsin and is important for the formation of rhodopsin carrier vesicles at the Golgi complex (Deretic et al., 2005; Mazelova et al., 2009).

Arf4 is a small G protein in the Arf subfamily of Ras-related small G proteins. Mice have six members of this family while humans have lost Arf2 and have five members. Arf1 and Arf6 have been best studied and are thought to organize membrane protein cargos into coated vesicles for transport to specific lipid domains in the cell (D'Souza-Schorey and Chavrier, 2006; Donaldson and Jackson, 2011; Gillingham and Munro, 2007; Nie and Randazzo, 2006). Arf1 forms coated vesicles at the Golgi complex crucial for trafficking between the ER and Golgi and throughout the cell while Arf6 is thought to operate at the plasma membrane and regulate endosomal-membrane traffic. Arf4, which is thought to have evolved from an Arf1-like precursor when metazoans arose, is a relatively unstudied member of the family (D'Souza-Schorey and Chavrier, 2006; Gillingham and Munro, 2007; Nie and Randazzo, 2006). Arf4 was first proposed

to be important for ciliary trafficking when it was found to interact with the C-terminal tail of rhodopsin where the CTS is localized (Deretic et al., 2005). Depletion of Arf4 from an *in vitro* budding assay showed that it was important for the formation of rhodopsin carrier vesicles (Mazelova et al., 2009). The CTSs of rhodopsins are contained in the last five amino acids (QV[S/A]PA) at the C-terminal end of the protein. The V and P residues are mutated in human patients with autosomal dominant retinitis pigmentosa. These residues were found to be important in an *in vitro* assay for the formation of rhodopsin carrier vesicles, thus the sequence has become known as a VXPX motif. A similar RVXP motif is present in the CNGB1b subunit of the CNG channel, another ciliary-localized protein (Jenkins et al., 2006). The VXPX sequence is part of the CTS in polycystin-1 and polycystin-2 and it is hypothesized that VXPX motifs function as Arf4 binding sites for transport to the cilium (Donaldson and Jackson, 2011; Geng et al., 2006; Ward et al., 2011).

In this work we ask if Arf4 plays a role in trafficking the fibrocystin CTS to the cilium and probe the function of Arf4 *in vivo* by analyzing a mutant mouse. Although the fibrocystin CTS does not contain a VXPX motif, it does bind to Arf4. Arf4 is not required for the trafficking of the fibrocystin CTS to cilia, but knockdown of Arf4 increases the time needed for the protein to travel from the Golgi complex to the cilium. Deletion of *Arf4* in the mouse does not affect the formation or function of nodal cilia, but causes embryonic lethality at mid-gestation, probably due to trafficking defects in the visceral endoderm.

## Results

### Arf4 interacts with the ciliary targeting sequence of fibrocystin

Fibrocystin (polyductin), the human autosomal recessive polycystic kidney disease gene product, is targeted to cilia by an 18-residue ciliary targeting sequence (CTS) located in the cytoplasmic C-terminal tail of the protein. Previously we showed that this sequence interacted with Rab8 and proposed that it may function by interacting with proteins involved in the sorting and transport of ciliary membrane proteins (Follit et al., 2010). Recent work indicates that Arf4 is required for trafficking of other ciliary proteins including rhodopsin and the polycystins (Deretic et al., 2005; Mazelova et al., 2009; Ward et al., 2011). Arf4 is one of six members of the Arf subfamily of small G proteins. Our previous analysis showed that in non-ciliated cells, the GFP-CTS localized to small puncta that appeared to be lipid microdomains rich in GM1 gangliosides. Interestingly, Arf4 exhibited significant co-localization with the CTS-GFP in these puncta while the rest of the Arf family did not (Fig 4.1A). To determine if this colocalization represented a physical interaction, we immunoprecipitated each of the Arfs and asked if the CTS-GFP was co-precipitated. Arf4 strongly precipitated the CTS, while the other Arfs either precipitated no CTS (Arf1, 3, 5, 6) or only a small amount (Arf2) (Fig 4.1B). Because *ARF2* is a pseudogene in humans we did not pursue the Arf2 interaction any further. The failure of the CTS to interact with Arf5 suggests that the Arf4 interaction is likely to be specific as Arf4 and Arf5 share over 90% identity at the amino acid level.

To further characterize the interaction between Arf4 and the CTS we tested the ability of a series of CTS deletion constructs to interact with Arf4 in the co-expression

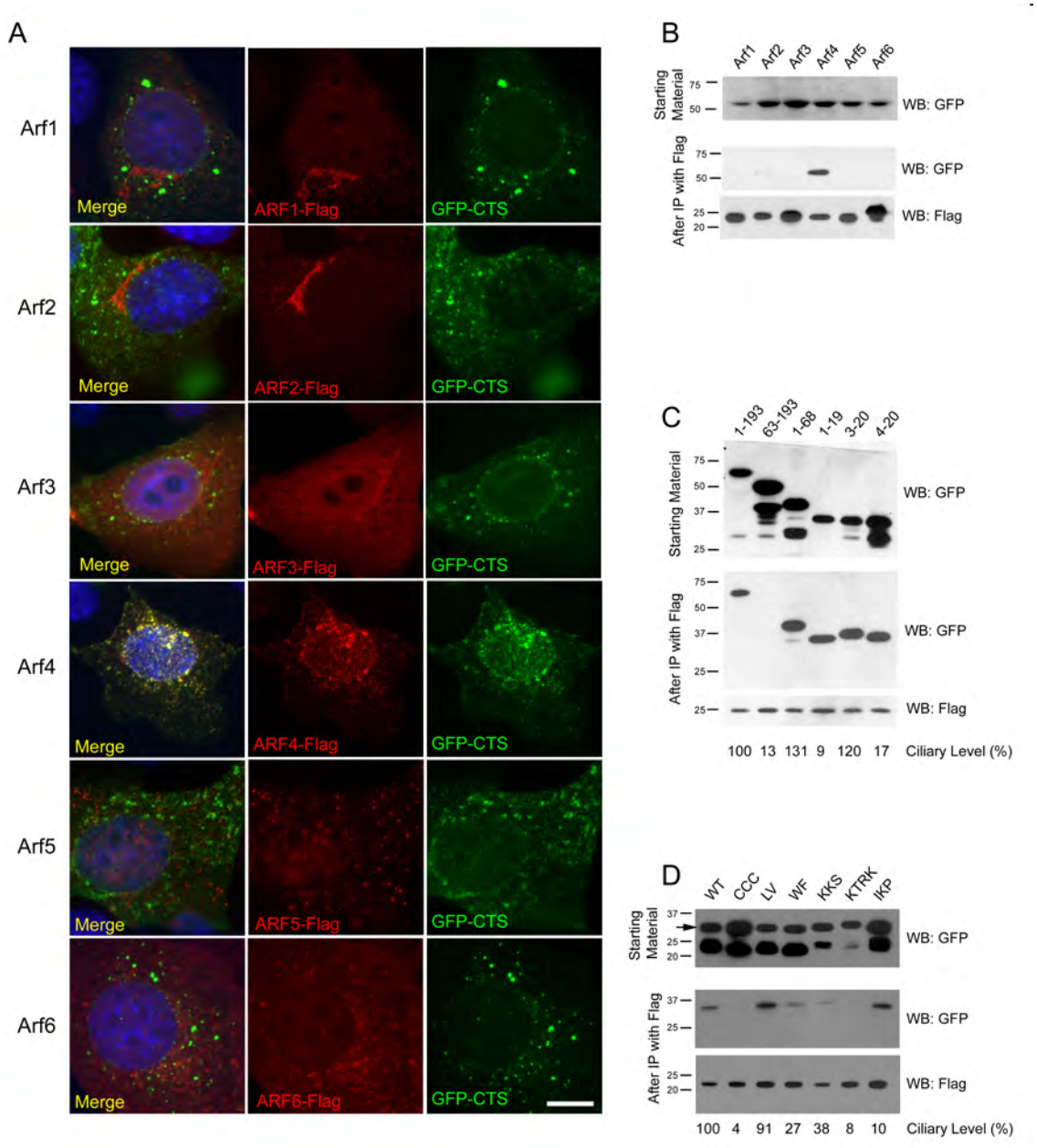


**Figure 4.1: Arf4 interacts with the ciliary targeting sequence of fibrocystin.**

**Figure 4.1: Arf4 interacts with the ciliary targeting sequence of fibrocystin.**
**A.** Mouse IMCD3 cells co-transfected with FLAG-tagged Arf proteins and GFP-tagged CTS; DAPI (blue) anti-FLAG (red) and GFP (green). Scale bar is 10 μm. Note extensive colocalization of Arf4 and CTS-GFP. **B.** FLAG IPs from cells shown in **A** were analyzed by western blot after SDS-PAGE. The top panel shows GFP-CTS expressed in the starting material. The bottom panel indicates that each of the 6 Arf proteins was precipitated. Only Arf4 brought down significant amounts of GFP-CTS (middle panel). **C.** Selected CTS deletion constructs were co-expressed with Arf4-FLAG. Following FLAG IP, Arf4 (bottom panel) precipitated the full-length intracellular tail of fibrocystin (1-193) and also precipitated truncations including the CTS but not the 63-193 construct, which lacks the CTS. Deletions to the CTS that prevent ciliary trafficking (1-19) and (4-20) also bound Arf4. Ciliary Level is a relative measure of the ability of the fusion protein to traffic to cilia with the control construct set to 100%. Data are from [7]. **D.** Alanine scanning mutant CTSs were co-expressed with Arf4-FLAG. After Arf4 precipitation (bottom panel), WT, LV and IKP mutant CTSs were brought down (middle panel). Mutations that completely prevented ciliary targeting of the CTS (CCC and KTRK) failed to interact with Arf4. Ciliary Level is as described in **C.**

immunoprecipitation assay (Fig 4.1C). In this assay, the CTS is sufficient for binding as the 3-20 construct was precipitated by Arf4 while the 63-193 construct, which lacks the CTS, was not bound. The 1-19 and 4-20 constructs also interact with Arf4 but do not target to cilia, indicating the CTS has functions in addition to Arf4 binding.

Next we examined the ability of Arf4 to interact with a series of alanine-scanning mutations within the CTS (Fig 4.1D). In general, the ability of Arf4 to bind the CTS correlated with the ability of the CTS to traffic to cilia. For example, mutations affecting the palmitoylated cysteines (CCC>AAA) or conserved basic residues (KTRK>AAAA) prevent ciliary targeting and likewise inhibit Arf4 binding. Mutations that exhibit little effect on the ciliary targeting of the CTS (LV>AA) similarly do not affect Arf4 binding. However the concordance was not perfect as the (IKP>AAA) mutation blocked ciliary targeting but had little effect on Arf4 binding, again supporting the idea that while the CTS is an Arf4 binding site, this is not its entire function.

Arf4 cycles between GTP and GDP bound states. To explore the role of this cycling on the ciliary trafficking of the CTS we measured the affects of constitutively active and dominant negative Arf4 on ciliary targeting and interaction with the CTS (Fig 4.2). Constitutively active Arf4 (Q67L) co-localized with IFT20 at the Golgi Complex while wild type or dominant negative (T13N, T48N) Arf4 displayed a punctate distribution in the cytoplasm (Fig 4.2A). The mutant forms of Arf4 retained the ability to bind the CTS (Fig 4.2E). Expression of dominant negative Arf4 reduced the percent of ciliated cells (Fig 4.2B) and ciliary length (Fig 4.2C). Surprisingly, over-expression of any Arf4 constructs completely inhibited CTS trafficking to the cilium (Fig 4.2D). These

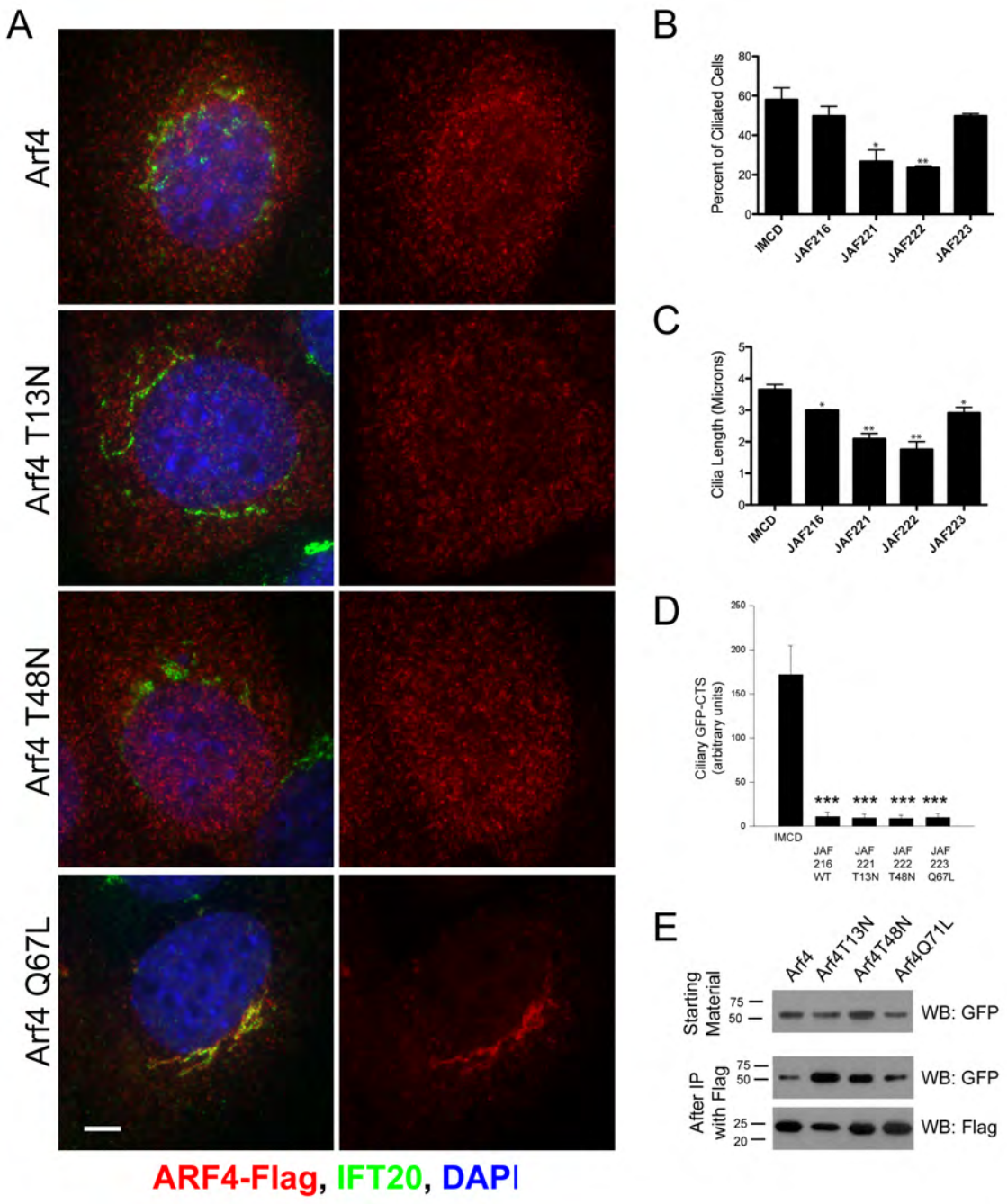


**Figure 4.2: Arf4 expression inhibits CTS trafficking.**

**Figure 4.2: Arf4 expression inhibits CTS trafficking.**
**A.** Mouse kidney cells stably expressing wild type (top row), dominant negative (T13N, T48N) and constitutively active (Q67L) Arf4-FLAG (red) stained with IFT20 (green) and DAPI (blue). Constitutively active (Q67L) localizes to the Golgi complex while wild type and dominant negative Arf4 are dispersed in the cytoplasm. **B.** Expression of dominant negative (T13N, T48N) Arf4 reduced the percent of ciliated cells. * $p<0.05$, ** $p<0.01$ as compared to IMCD cells not transfected with an Arf4-FLAG construct **C.** Dominant negative Arf4 (T13N, T48N) causes a reduction in ciliary length. * $p<0.05$, ** $p<0.01$ as compared to IMCD cells not transfected with an Arf4-FLAG construct **D.** Expression of any Arf4 constructs prevents ciliary trafficking of GFP-CTS. *** $p<0.001$ as compared to IMCD cells not transfected with an Arf4-FLAG construct. **B-D**, error bars are standard error of the mean. **E.** Co-immunoprecipitation experiments demonstrate that GFP-CTS interacts with FLAG-tagged Arf4 wild type and mutant proteins.

data indicate that increases in Arf4 levels prevent ciliary trafficking of the CTS possibly by sequestering it in the cytoplasm.

**Arf4 is required for efficient delivery of the fibrocystin c-terminal tail to the cilium**

Prior studies in frog photoreceptors (Deretic et al., 2005; Mazelova et al., 2009) and cultured mammalian cells (Ward et al., 2011) suggest that Arf4 functions at the Golgi complex to direct rhodopsin and polycystin-1 to the cilium. Our initial immunofluorescence and biochemical results suggested that Arf4 may also be required for the ciliary targeting of fibrocystin. To test the role of Arf4 in the trafficking of fibrocystin, we developed a pulse chase assay to measure its movement through the endomembrane system and delivery to the cilium. To do this, we created a chimeric molecule containing the extracellular domain of CD8 fused to the C-terminal tail of fibrocystin (including the transmembrane domain) with a SNAP tag (Keppler et al., 2003) on the C-Terminal end (Fig 4.3A). The extracellular domain of CD8 contains a signal sequence that when combined with the transmembrane domain of fibrocystin produces a type 1 membrane protein with membrane topology the same as native fibrocystin except that the large (3,851 residue) extracellular domain is replaced with the CD8 epitope. The SNAP tag is a fragment of the DNA repair protein $O^6$-alkylguanine-DNA alkyltransferase that can be covalently modified with benzyl guanine derivatives and allows for pulse chase experiments (Farr et al., 2009; Milenkovic et al., 2009). We developed a protocol to follow the movement of this chimeric protein through the endo-membrane system. At the beginning of the experiment all existing SNAP sites are blocked with a non-fluorescent benzyl-guanine so that only newly synthesized protein

will be labeled by the fluorescent benzyl-guanine. The newly synthesized SNAP-CTS is first detected in the endoplasmic reticulum as expected for a trans-membrane receptor. The protein then moves to the Golgi complex where it can be trapped using a 19°C temperature block (Saraste et al., 1986). Shifting the cells back to 37°C allows the accumulated protein to exit the Golgi and traffic to the cilium where it can be detected within 30 min of release.

To determine if Arf4 is involved in trafficking of the CTS, cells expressing the CD8-CTS-SNAP construct were treated with siRNA to reduce the level of Arf4. Arf4 mRNA level was reduced greater than 90% as compared to cells treated with a control scrambled siRNA (Fig 4.3B). The Arf4 knockdown did not affect the percent of ciliated cells nor did it affect ciliary length (data not shown). Arf4 knockdown did not affect the total amount of CD8-CTS-SNAP in the cilium as measured by CD8 fluorescence (Fig 4.3D). To determine if the reduction of Arf4 affected the rate of delivery to the cilium, we measured the time that it takes for the CD8-CTS-SNAP construct to move from the Golgi complex to the cilium by using the pulse chase protocol described above. Newly synthesized protein was accumulated in the Golgi complex by a 19°C block and then released by shifting cells to 37°C (Fig 4.3C, D). In control cells, after release from the Golgi block the CD8-SNAP-CTS moves quickly to the cilium and is detectable at the 1 hr time point with the ciliary level peaking at about 2 hrs post block (Fig 4.3C, insets). In contrast, when Arf4 is depleted, little CD8-CTS-SNAP is detectable in the cilium within the first two hrs after release from Golgi block but protein is detectable at 4hrs. These

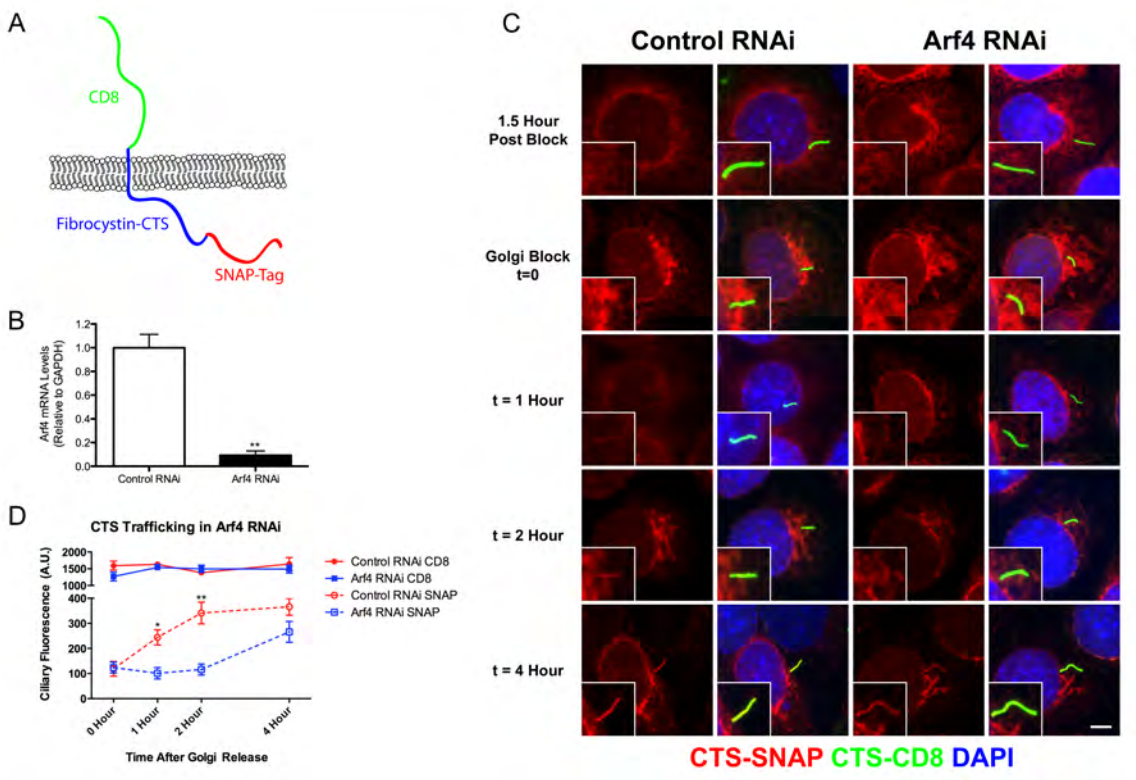


**Figure 4.3: Arf4 knockdown delays CTS trafficking to the primary cilium.**

**Figure 4.3: Arf4 knockdown delays CTS trafficking to the primary cilium.**
**A.** Diagram of the CD8-CTS-SNAP construct used in the trafficking assays. The extracellular domain of CD8 (green) is fused to fibrocystin (blue) just N-terminal to its transmembrane domain and the SNAP-tag (red) is fused to the C-terminus of fibrocystin. **B.** siRNA mediated knockdown of Arf4 results in a >90% reduction in Arf4 mRNA abundance as indicated by qRT-PCR. **C.** Immunofluorescence images showing CTS-SNAP trafficking in control (left two columns) and Arf4 knockdown (right two columns) cells. Mouse kidney cells stably expressing CD8-CTS-SNAP were blocked with non-fluorescent SNAP substrate, allowed 1.5 hr to synthesize new CD8-CTS-SNAP (1.5 Hour Post Block, top row), treated with cycloheximide and incubated at 19° C for 2hr to accumulate CD8-CTS-SNAP at the Golgi complex (Golgi Block t=0, second row). At t=0 cells were returned to 37° C for the indicated amount of time (bottom 3 rows). At indicated times, cells were fixed and stained with DAPI (blue) anti-CD8 (green) and TMR-SNAP (red). Scale bar is 5 μm. Insets are 2X enlargements of the cilium. **D.** Quantification of the delivery of CD8-CTS-SNAP to cilia. Starting at the time of temperature shift from 19° C to 37° C (t=0), the ciliary levels of CD8 and SNAP were measured by fluorescence microscopy. CD8 staining (green) is present at similar levels in the control and knockdown cells at all time points. Newly synthesized CD8-CTS-SNAP (red) is seen in control cilia within 1 hr of release. An increase is observed at 2 hr and the amount of SNAP label plateaus at 4 hr. Knockdown of Arf4 delays delivery such that little label is detected in the cilia until the 4hr time point. Differences were significant at t=1, 2 (t=0 NS; t=1 * $p<0.05$; t=2 ** $p<0.005$; t=4 NS). The mean CD8 fluorescence (solid line) and SNAP fluorescence (dotted line) were plotted from three independent experiments in which 50 cilia were quantitated for each condition (Arf4 knockdown and control) at each time point. Error bars represent standard error of the mean.

data indicate Arf4 is not absolutely required for the delivery of the CTS to the cilium but does play a kinetic role in the steps between the Golgi complex and the cilium.

**Arf4 mutant mice are embryonic lethal**

Our initial data indicate that Arf4 interacts with the CTS of fibrocystin and this interaction is required for the efficient delivery of newly synthesized CTS to the cilium. Data in the literature suggest that Arf4 is important for the trafficking of rhodopsin and the polycystins to cilium and it has been suggested that it is a global regulator of ciliary cargo (Deretic et al., 2005; Mazelova et al., 2009; Ward et al., 2011). To test the idea of whether Arf4 was a global regulator of ciliary protein trafficking we created an *Arf4* knockout mouse with the prediction that if it plays this role, the mouse should have ciliopathy phenotypes. Embryonic stem cells harboring a LacZ insertion in the *Arf4* locus just downstream of exon 3 were obtained from the Sanger Institute and used to create an *Arf4* knockout mouse (Fig 4.4). The allele we generated expresses less than 1% of control *Arf4* mRNA and is, at minimum, a strong hypomorph (Fig 4.4C).

Mice lacking cilia typically die mid-gestation around day e10 with a failure to undergo embryonic turning and have severe disruptions in left-right patterning (Nonaka et al., 1998). Similar to this, the *Arf4* mutant mice are embryonic lethal at mid-gestation with no live embryos detected after day e9.5 (Fig 4.4D). At e9.5 the mutant embryos were smaller than either wild type or heterozygous embryos and never completed embryonic turning to assume the characteristic fetal body position that is observed in almost all wild type and heterozygote embryos by this time (Fig 4.4A,B).

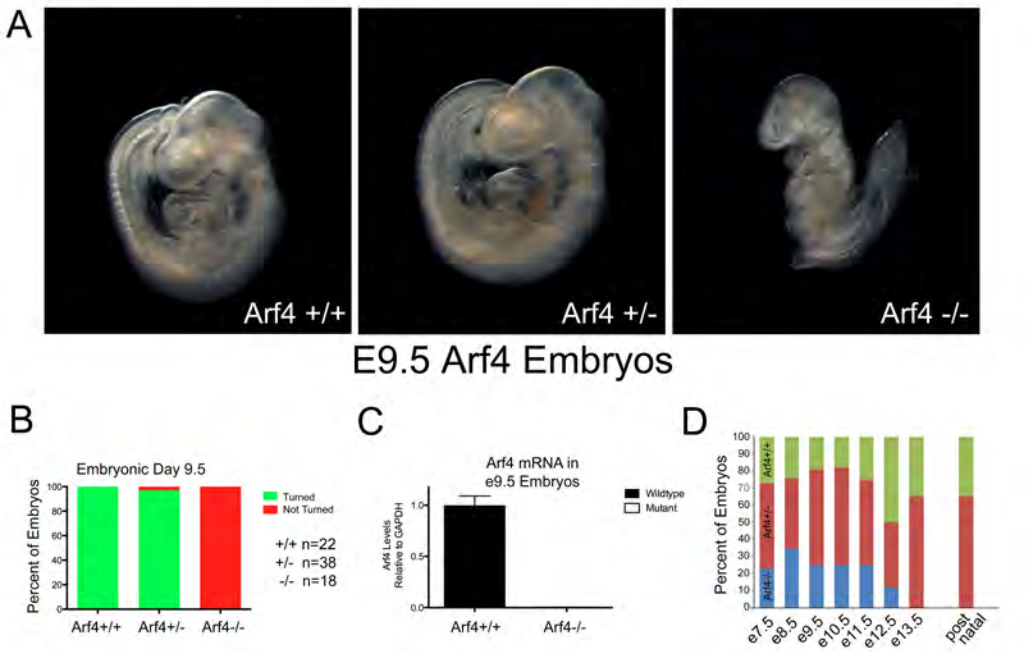


**Figure 4.4: Arf4 mutant mice are embryonic lethal.**

**Figure 4.4: Arf4 mutant mice are embryonic lethal.**
**A, B.** By e9.5, wild type and most heterozygous mice complete embryonic turning and adopt the normal fetal orientation. At this time point, Arf4 mutants are smaller and have not completed embryonic turning. **C.** qRT-PCR analysis indicates that mean Arf4 mRNA abundance in the mutant embryos is <1% of controls; error bars depict standard error of the mean. **D.** Genotype distribution as a function of age (+/+ green; +/- red; -/- blue). Arf4 mutant embryos are present until e12.5, however all mutant embryos dissected after e9.5 were dead and being resorbed.

To investigate if Arf4 affects ciliary assembly we performed scanning electron microscopy (SEM) of the node, which is thought to be the first ciliated structure in the embryo. To preclude differences caused by a developmental delay in the mutant embryos, embryos from multiple litters were dissected and those at the 3-4 somite stages were examined by SEM (Fig 4.5A). No differences were observed in either length or number of cilia present on the mutant nodes as compared to wild type or heterozygous embryos (Fig 4.5B, C) indicating that Arf4 is not required for ciliary assembly. Nodal cilia beat to create a leftward flow required to break the left/right symmetry of the developing embryo (Nonaka et al., 1998). This leads to asymmetric gene expression patterns on the left versus right side of the embryos and eventually leads to the right-right pattern of the abdominal and visceral organs. One of the earliest physical manifestations is the looping of the heart tube, which under normal conditions adopts a characteristic C-loop by day 9.5. The developing heart in *Arf4* mutant embryos always adopts a C-loop indicating the nodal cilia present in the *Arf4* mutant embryos are functional in breaking left/right symmetry (Fig 4.5D, E).

**Arf4 expression is highest in the visceral endoderm**

*Arf4* mutant mice die at approximately embryonic day 9.5. This embryonic lethality is not associated with left-right defects suggesting that ciliary dysfunction is not the cause, a finding corroborated by our failure to detect structural or functional defects in the nodal cilia. To identify the site of pathology, we took advantage of the β-galactosidase insertion that was used to generate this allele and performed X-Gal staining to identify the sites of high *Arf4* expression (Fig 4.6). As expected, no staining was observed in the

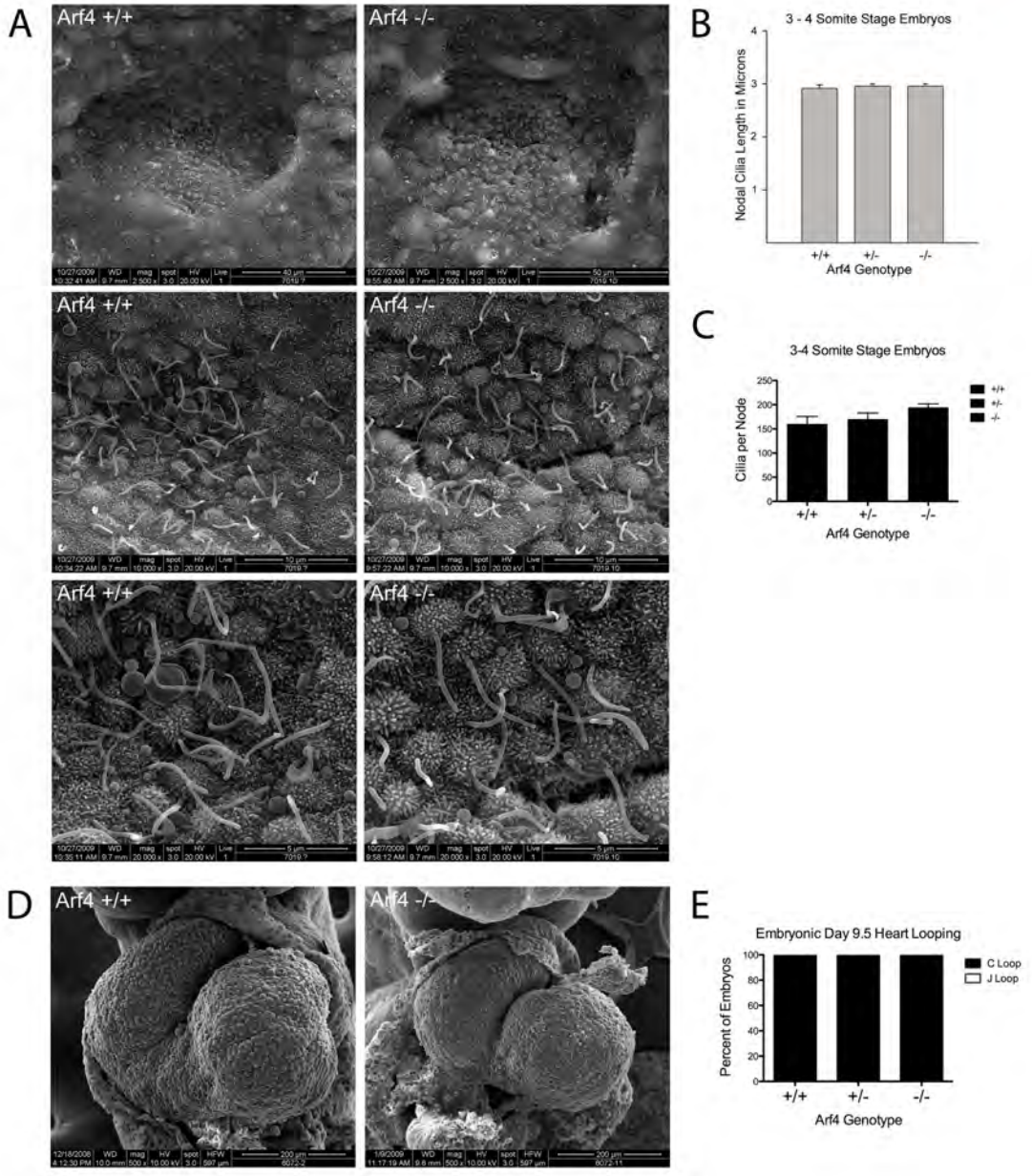


**Figure 4.5: Arf4 mutant mice have functional nodal cilia.**

**Figure 4.5: Arf4 mutant mice have functional nodal cilia.**
**A.** SEM of 3-4 somite developmentally matched embryos at 2,500X (top), 10,000X (middle) and 20,000X (bottom) magnification showing nodal cilia in wild type (left column) and Arf4 mutant (right column) embryos. **B.** Nodal cilia length is not significantly affected by the Arf4 mutation. Mean cilia length from 3-4 somite stage embryos is plotted (N=3 each genotype); error bars are standard error of the mean. **C.** Total number of nodal cilia is not significantly affected in the Arf4 mutants. Mean number of cilia per node (N=3 for each genotype) is plotted; error bars are standard error of the mean. **D.** SEM of developing heart tube at e9.5 showing normal heart looping in wild type (left) and Arf4 mutant (right) embryos. **E.** Heart looping analysis of e9.5 embryos shows that all had normally looped hearts (n=22, 38, 18 for +/+, +/-, -/-).

wild type embryos. Both the heterozygous and homozygous mutants showed staining at all three time points examined, with the staining concentrated in the extra-embryonic tissues (Figure 4.6). To better understand what cells were labeled, e9.5 embryos were stained and then sectioned (Figure 4.6D). In the heterozygote and mutant, the majority of the stain was seen in the outer cell layer of the yolk sac, which is the visceral endoderm (Figure 2.6D). The mutant embryos also showed some staining within the epiblast, which is probably the definitive endoderm. The yolk sac consists of two layers; the outer visceral endoderm is composed of highly polarized cells covered with microvilli on their apical surface, while the inner mesoderm gives rise to the developing blood islands in early development of the circulatory system (Zohn and Sarkar, 2010).

**Arf4 is required for visceral endoderm function**

As *Arf4* is most highly expressed within the visceral endoderm during development, we examined this tissue further by immunofluorescence and electron microscopy (Fig 4.7). To determine if these tissues were ciliated, we stained yolk sacs and sectioned embryos for cilia, and imaged by confocal microscopy. We did not detect cilia on the visceral endoderm at embryonic day 8.5 or 9.5. However cilia are present on the adjacent inner layer of mesoderm cells in both wild type and mutant embryos at these stages in development (Fig 4.7A, B).

The visceral endoderm serves as the major secretory and absorptive tissue of the developing embryo prior to placental formation (Bielinska et al., 1999). As expected for a highly absorptive tissue, the visceral endoderm has a well-developed brush border on the apical surface and large lysosomes that facilitate uptake and breakdown of

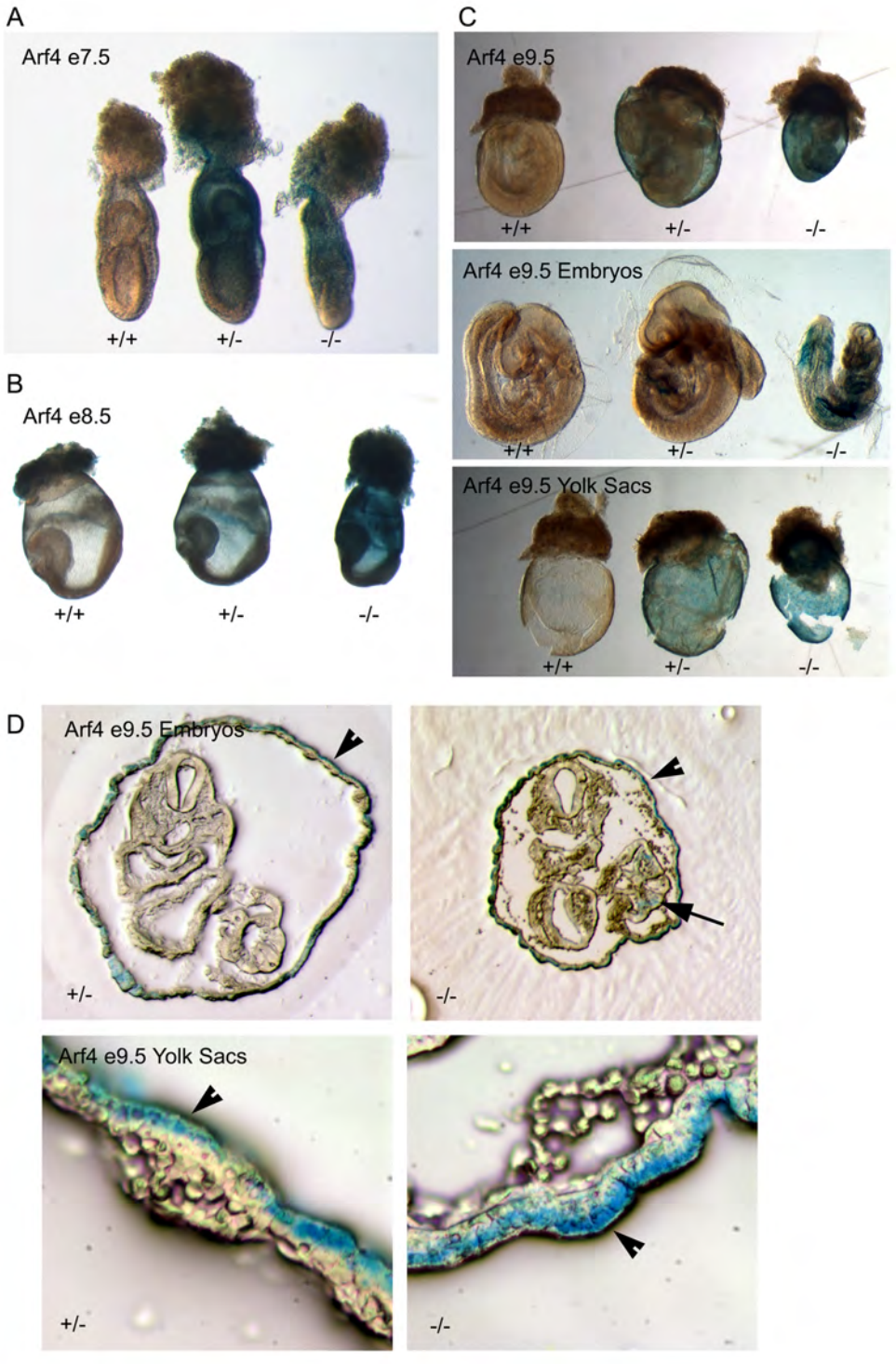


**Figure 4.6: Arf4 expression is concentrated in the visceral endoderm during development.**

**Figure 4.6: Arf4 expression is concentrated in the visceral endoderm during development.**

**A-C.** β-Gal staining indicates Arf4 expression at e7.5 (**A**) e8.5 (**B**) and e9.5 (**C**) is highest in the extra-embryonic tissues (yolk sac) of the developing embryo (blue in heterozygote and mutant). This is most clearly seen in **C**, where e9.5 embryos have been photographed before (top row) and after dissection of the epiblast (middle row) from the yolk sac (bottom row). Mutant animals show β-gal staining in the epiblast but little staining of the epiblast is seen in the heterozygote. **D.** Sections through e9.5 embryos show that β-Gal activity is concentrated in the visceral endoderm (outermost cell layer of the yolk sac, arrowheads) in both heterozygous and mutant embryos. Some staining is observed in the epiblast of the mutant embryo, which is likely in the definitive endoderm (arrow).

macronutrients from the maternal blood supply (Fig 4.7C). In *Arf4* mutants the apical/basolateral polarity appears intact and the brush border remains, but the microvilli are less organized. In addition, bulbous misshapen microvilli are often observed along with small vesicles that are surrounded by a fuzzy coat, which is not seen on the microvilli (Fig 4.7C, middle row). The cell-cell contacts also appear to be compromised as more space is seen between the mutant cells by TEM; moreover microprojections that form the interdigitations between the lateral surfaces of adjacent cells can be observed by SEM on the apical surface of the mutants but not the controls (Fig 4.7C, bottom row). *Arf4* mutant embryos lack the large lysosomes suggesting that visceral endoderm function may be compromised.

The visceral endoderm carries out its absorptive function by localizing megalin (Lrp2) and other scavenger receptors on its apical surface. These receptors bind to substrates such as vitamins, lipoproteins and signaling molecules [reviewed in (May et al., 2007)], which are then internalized and transcytosed or broken down in the lysosome. Trafficking defects within the visceral endoderm result in embryonic lethality and are often associated with mislocalization of megalin (Lighthouse et al., 2011; Nada et al., 2009). At e8.5, megalin is normally concentrated along the apical surface of the visceral endoderm (Fig 4.7D). Arf4 mutants have significantly reduced megalin staining at the apical surface and some of the protein appears in the cytoplasm. This suggests megalin trafficking is disrupted in *Arf4* mutants and supports the ultrastructural studies of the visceral endoderm that indicate nutrient uptake is compromised within this cell layer.

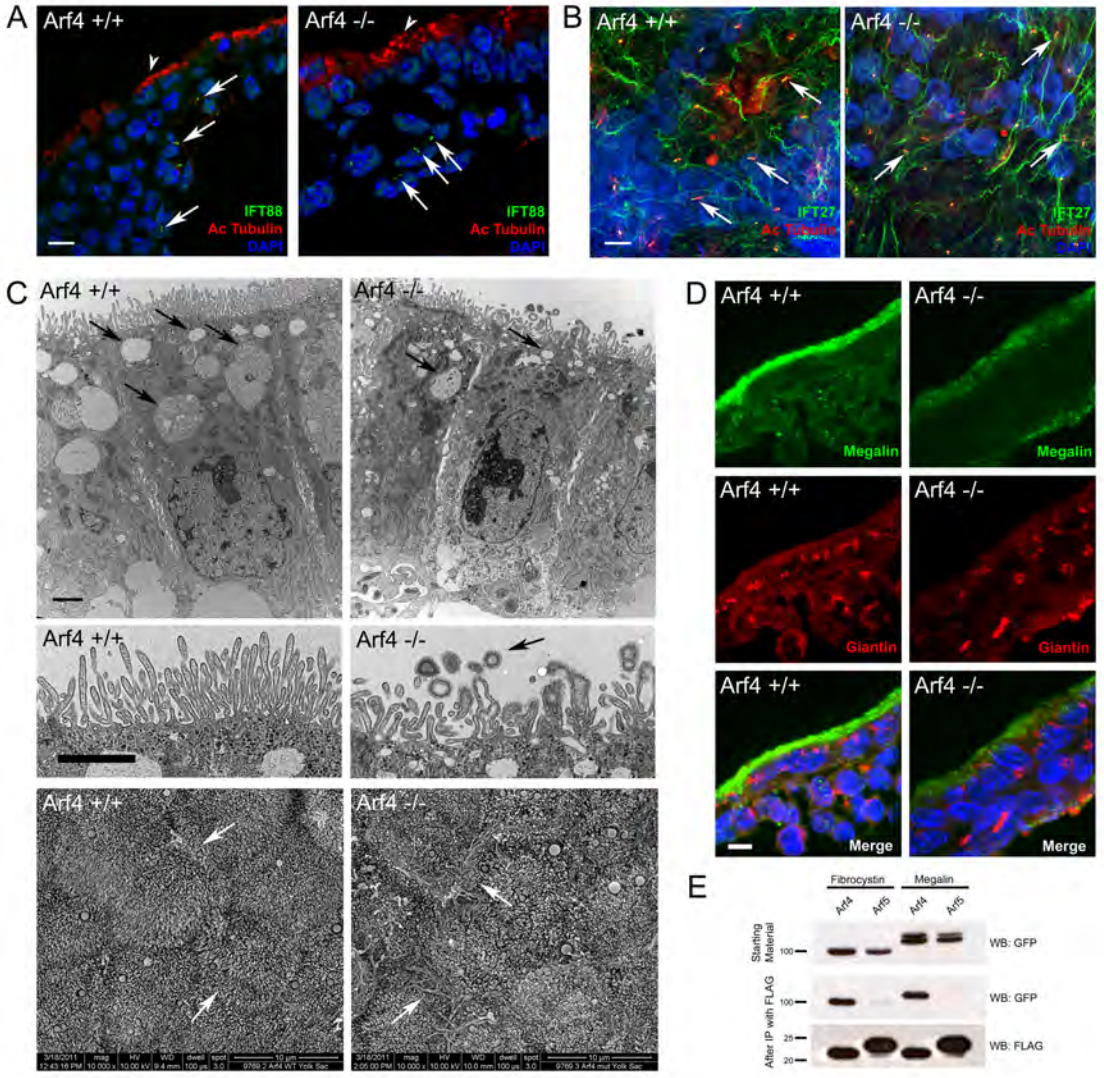


**Figure 4.7: Arf4 mutant embryos have defects in the visceral endoderm.**

**Figure 4.7: Arf4 mutant embryos have defects in the visceral endoderm.**
**A.** Confocal images of the visceral endoderm (arrowhead, outermost cell layer) and adjacent mesoderm (inner cell layers) of e8.5 embryo sections. Cilia (arrows) stained with acetylated tubulin (red) and IFT88 (green) are present on mesodermal cells in both mutant and wild type embryos. No cilia were observed on the visceral endoderm. Scale bar is 5 μM. **B.** Confocal images of flat mounted yolk sacs from e9.5 embryos stained with acetylated tubulin (red) and IFT27 (green). Numerous cilia (arrows) are present on the mesoderm in both wild type and mutant embryos. Scale bar is 5 μM**. C.** Thin section TEM images of the visceral endoderm at e8.5 of wild type (left) and Arf4 mutant (right) embryos. Healthy visceral endoderm is filled with large lysosomes (arrows, top panel), which in the mutants are reduced in number and size. The microvilli on the apical surface of the visceral endoderm (middle panel) are abnormally organized and shaped in the mutant, and are associated with small coated vesicles (arrow) not seen in the controls. Scale bar is 2 μM for all TEM images. The abnormally shaped microvilli are better observed by SEM (bottom panels). In controls, the microvilli have a uniform diameter while the tips are bulbous in the mutants. In addition, cell/cell contacts appear to be compromised in the mutants, as the microprojections that normally form the interdigitations between the lateral surfaces of the cells are visible on the apical surface (regions of cell/cell contact are marked with arrows). **D.** Megalin staining (green) is normally concentrated at the apical surface of the visceral endoderm of e8.5 embryos. Mutants have significantly reduced megalin staining. Golgi organization (giantin, red) does not appear to be affected. **E.** Co-IP experiments showing GFP tagged fibrocystin (left two columns) and megalin (right two columns) expressed in cell lysates (GFP blot, top panel) along with FLAG tagged Arf4 (lanes 1 & 3) or Arf5 (lanes 2 & 4). Following immunoprecipitation of Arf4 and Arf5 (FLAG blot, bottom panel), Arf4 brought down fibrocystin and megalin (GFP blot, middle panel, lane 1 and 3) while Arf5 did not precipitate either fibrocystin or megalin (GFP blot, lanes 2 & 4, middle panel).

Megalin is a type 1 membrane protein with a large extra cellular domain, single transmembrane span and a short cytoplasmic C-terminal tail similar to the structure of fibrocystin. Because of the similarity in structure and the observation that *Arf4* mutant embryos have reduced megalin on the apical surface of the visceral endoderm, we asked if Arf4 interacts with megalin. To test if Arf4 interacts with megalin we replaced the large extracellular domain of megalin with CD8a and fused a SNAP and GFP to the c-terminal end of megalin creating a construct similar to the fibrocystin construct (Figure 4.23). Co-immunoprecipitation indicates Arf4 interacts with the intracellular domain of megalin (Fig 4.7E). Similar to what we observed with fibrocystin, the highly similar protein Arf5 did not interact with megalin. These data suggest Arf4 is involved in not just trafficking of ciliary cargo but also a larger class of trans-membrane receptors – including megalin.

## Discussion

The primary cilium is a sensory organelle and its proper function relies on the correct complement of receptors localized specifically in the ciliary membrane. Little is known about how proteins are sorted to the ciliary compartment but understanding this process is critical as defects in the signaling functions of primary cilia underlie a diverse group of human pathologies known collectively as ciliopathies. These diseases range from developmental defects of the brain, heart and other organs to chronic ailments including retinal degeneration, obesity and polycystic kidney disease. To study ciliary protein

sorting, we focused on analysis of the trafficking of the transmembrane protein fibrocystin to the primary cilium. Mutations in the fibrocystin gene (*PKHD1*) are responsible for autosomal recessive polycystic kidney disease, a disorder afflicting approximately 1 in 20,000 individuals and a cause of significant mortality during the first year of life (Harris and Torres, 2009; Pazour, 2004). The ciliary targeting sequence of fibrocystin is an 18 amino acid sequence contained in the cytoplasmic tail (Follit et al., 2010). We had previously shown that the CTS interacts with the small G protein Rab8. In this work we studied the interaction of the CTS with another small G protein, Arf4. Arf proteins group vesicular cargo and through interactions with coat proteins form transport vesicles (D'Souza-Schorey and Chavrier, 2006; Donaldson and Jackson, 2011; Nie and Randazzo, 2006). The proposed sorting ability of Arf proteins make them attractive candidates as specificity factors and recent work suggests Arf4 is involved in targeting rhodopsin and polycystin-1 to the cilium (Deretic et al., 2005; Mazelova et al., 2009; Ward et al., 2011). We found that Arf4 was capable of interacting with the fibrocystin CTS in a co-immunoprecipitation assay. The interaction is specific as Arf4 is the only member of this highly conserved family that precipitated significant amounts of the CTS. The analysis of deletion and alanine scanning mutants within the cytoplasmic tail of fibrocystin showed that the Arf4 interaction site was localized within the CTS. The ability of Arf4 to bind to the mutated CTSs roughly correlated to the ability of the CTS to enter the cilium suggesting that the Arf4/CTS interaction was functionally important.

Using SNAP-tagging technology we found that Arf4 is not absolutely required for the delivery of the fibrocystin targeting construct to cilia as the steady state level of the protein was not affected by knockdown of Arf4. This is in contrast to the reported effect of knockdown on the trafficking of polycystin-1 where Arf4 knockdown significantly reduced ciliary levels of polycystin-1 (Ward et al., 2011). However, in our hands, the delivery of newly synthesized fibrocystin fusion protein was slower in the knockdown cells indicating that Arf4 is needed for the efficient delivery to primary cilia. The delayed, but eventual delivery of the CTS to the cilium may be a result of residual Arf4 protein (~10% of the mRNA remains in the knockdown cells) or it may indicate an alternative pathway to the cilium that does not utilize Arf4. Smoothened appears to enter the ciliary compartment by first traveling to the plasma membrane before moving into the cilium (Milenkovic et al., 2009) and so it is possible that this route can also be utilized by fibrocystin.

Our work, and work from others, indicates that Arf4 may play a key role in sorting transmembrane receptors to the cilium. This suggests that Arf4 may be an important player in human diseases such as retinal degeneration and polycystic kidney disease. To better understand the function of Arf4 and its possible role in ciliopathies, we created an *Arf4* knockout mouse. If the primary function of Arf4 is specific to cilia, we would expect the mutant mice to exhibit phenotypes in common with established mutations that affect cilia. Mice with strong defects in ciliary assembly die at mid-gestation with severe left-right abnormalities while those with more mild ciliary defects survive longer and display phenotypes indicative of hedgehog signaling dysfunction.

*Arf4* mutant mice die at embryonic day 9.5, which is similar to the time when mice with severe ciliary assembly defects die. However, ciliary assembly is normal in the embryonic node and the nodal cilia are functional as all embryos broke left-right symmetry properly and formed a C-looped heart. We did not examine polycystin-2 levels on the nodal cilia, but the fact that the embryos broke symmetry properly suggests that it would not have been severely affected (Pennekamp et al., 2002). The embryonic lethality but lack of ciliary defects suggested that Arf4 might have functions in addition to the ciliary targeting of transmembrane proteins. Expression analysis between embryonic day 7 and 10, around the time that the *Arf4* mutant embryos were dying, indicated that the major site of *Arf4* expression was in the visceral endoderm. Examination of the visceral endoderm indicates that this tissue is not ciliated at this time in development although cilia are present on the adjacent mesoderm. The visceral endoderm is the major secretory and absorptive tissue of the developing embryo prior to chorioallantoic placenta formation (Zohn and Sarkar, 2010) and defects within this cell layer often result in embryonic lethality (Lighthouse et al., 2011; Nada et al., 2009). *Arf4* mutant embryos have multiple defects within the visceral endoderm. Ultrastructural analysis of the visceral endoderm indicates *Arf4* mutant embryos have defects in cell-cell contacts and organization of the brush border, but most strikingly, they lack the large lysosomes normally present in healthy tissue. The absence of lysosomes could be a direct effect of the *Arf4* mutation, but is more likely an indirect consequence of a failure to absorb nutrients from the adjacent maternal blood supply. A failure to uptake nutrients is consistent with the observed growth restriction evident by embryonic day 7 and likely

accounts for the lethality around day 9. The apical surface of the visceral endoderm is covered with microvilli that contain a number of scavenger receptors that bind ligands including vitamins and lipoproteins required by the developing embryo. We examined the distribution of one of these receptors, megalin, within the visceral endoderm. Megalin is normally localized to the apical surface of the developing visceral endoderm however in *Arf4* mutants, megalin fails to localize to the apical surface. Megalin is a large single span transmembrane receptor with membrane topology similar to fibrocystin. Co-immunoprecipitation assays indicate that Arf4 can interact with megalin similar to what we observed between Arf4 and fibrocystin. This interaction and the observed defects in megalin trafficking in the *Arf4* mutant suggest that Arf4 is required to target megalin to the apical surface.

RNAi studies suggested that the Arf family of proteins was highly redundant and it was not predicted that the genetic loss of any one would have a strong phenotype (Kudelko et al., 2012). The observation that *Arf4* null mice die mid gestation indicates that this is not correct. To date, *Arf6* is the only other Arf family member that has been mutated in the mouse. Like *Arf4*, *Arf6* null mice die during development, although they survive longer than the *Arf4* mice. The major defect in *Arf6* null mice was in the liver, where the lack of Arf6 caused increased rates of apoptosis resulting in a significantly smaller liver with lethality around embryonic day 15 (Suzuki et al., 2006). The fact that both *Arf4* and *Arf6* mice survive through early gestation suggests that neither of these genes are essential genes at the cellular level, but do play critical functions in particular cells at particular times in development. In the case of the *Arf4* mouse, the major defect

was in the visceral endoderm, a tissue with a very high rate of internalization and trafficking of lipid and protein molecules. It is possible that this is the first point in development that requires this level of internalization and trafficking. The analysis of a floxed allele will be of interest to determine if Arf4 is required in adult cells with a high rate of flux such as the intestine or kidney proximal tubule, or even the rod and cone photoreceptor cells where a high flux is needed to maintain the outer segment.

The literature on Arf4 has mostly focused on proposed roles in trafficking proteins to the ciliary membrane compartment. However, our finding that the highest level of expression is in the visceral endoderm, which is not ciliated at the time of high expression, suggests that Arf4 has functions outside the targeting of ciliary cargo. This is consistent with two recent studies finding that class II Arfs (Arf4, Arf5) play roles in the trafficking of dense core vesicles (Sadakata et al., 2012; Sadakata et al., 2010) and secretion of Dengue virus particles (Kudelko et al., 2012). In the case of the dense core vesicle transport, Arf4 and Arf5 interacted with two calcium dependent activator proteins for secretion (CAPS1 and CAPS2). This interaction was required for the efficient trafficking of dense core vesicles as knockdown of either Arf4/5 or CAPS1/2 significantly reduced chromogranin secretion (Sadakata et al., 2012; Sadakata et al., 2010). In the case of Dengue virus production, Arf4 and Arf5 were required for the secretion of subviral particles and the Arfs were thought to act though an interaction with prM glycoprotein of the virus. Interestingly, the prM glycoprotein contains a VXPX motif in the C-terminus similar to the Arf4 binding site in rhodopsin (Deretic et al., 2005). However mutation of the VXPX motif did not disrupt interaction with Arf4

indicating that it is not the binding site (Kudelko et al., 2012). This is consistent with our finding that Arf4 binds to the CTS of fibrocystin, which does not contain a VXPX motif and studies of nephrocystin-3, which contains a VXPX motif that is not necessary for ciliary targeting (Nakata et al., 2012).

In conclusion, we have shown that Arf4 plays a role in the efficient transport of the fibrocystin CTS to the cilium, but it is not required for ciliary assembly and in the mouse has critical functions in non-ciliated cells. Thus, our work, and other published work, suggests that Arf4 function is not restricted to ciliary assembly but rather plays a broader role in cellular trafficking.

## Materials and Methods

### Ethics Statement

Mouse work was approved by the University of Massachusetts Medical School IACUC.

### Mouse Breeding

An *Arf4*-mutant ES cell line was obtained from the Sanger Center and used to generate *Arf4*$^{Gt(AY0614)Wtsi}$ mutant mice. The animals used in this study were a mix of 129 and C57Bl6 backgrounds. Embryonic ages were determined by timed mating with the day of the plug being embryonic day 0.5. Genotyping was carried out with the following primer pairs: Arf4-1 AGCAGCCTCATTGTCCTAGC + Arf4-2 CCTCCCCACAATTCAACAAT (product size = 189 bp in wildtype) and Geo-3 GATCGGCCATTGAACAAGAT + Geo-4 CAATAGCAGCCAGTCCCTTC (product size = 280 bp in mutant).

### Mammalian Cell Culture

IMCD3 (ATCC) were grown in 47.5% DMEM 47.5% F12, 5% fetal bovine serum, with penicillin and streptomycin at 37° C in 5% $CO_2$. Cells were transfected by electroporation (Bio-Rad, Hercules CA). Stable cell lines were selected by supplementing the medium with 400 μg/ml of G418 (Sigma, St. Louis, MO). Clonal lines were selected by dilution cloning after drug selection.

**Electron Microscopy**

For scanning electron microscopy (SEM), timed pregnant females were euthanized by approved IACUC protocols, embryos dissected in DMEM/F12 supplemented with 5% fetal bovine serum, fixed overnight in 2.5% glutaraldehyde in 0.1M sodium cacodylate. Fixed embryos were rinsed twice with 0.1M sodium cacodylate, osmicated in 1% osmium tetroxide, dehydrated in a graded ethanol series and critical point dried (Autosamdri-815, Series A, Tousimis Research Corp.). Dried embryos were sputter coated with iridium to a thickness of 3 nm (Cressington 208 HR Sputter Coater, Ted Pella, Redding, CA, USA) and examined in a scanning electron microscope (FEI Quanta 200 FEG SEM) (SanAgustin et al., 2009). For comparison of nodal cilia, embryos were developmentally matched by counting somite number.

For transmission electron microscopy (TEM), samples were fixed, osmicated and dehydrated as described above. Dehydrated samples were then infiltrated first with two changes of 100% propylene oxide and then with a 50%/50% propylene oxide / SPI-Pon 812 resin mixture. The following day, three changes of fresh 100% SPI-Pon 812 resin were done before the samples were polymerized at 68$^{o}$C in plastic capsules. The samples were then reoriented and thin sections were placed on copper support grids and contrasted with Lead citrate and Uranyl acetate. Sections were examined using a Phillips CM10 TEM with 80Kv accelerating voltage, and images were captured using a Gatan TEM CCD camera.

**Immunofluorescence Microscopy**

Cells for immunofluorescence microscopy were grown, fixed, and stained as described (Follit et al., 2008). For visceral endoderm immunofluorescence, e8.5 embryos were fixed for 15 minutes at room temperature with 4% paraformaldehyde in PBS rinsed twice in PBS, equilibrated in 30% sucrose overnight and embedded in Tissue Freezing Media (Triangle Biomedical Sciences). Cryosections (10 μm) were blocked for 1 hour in 1% bovine serum albumin, incubated with primary antibodies overnight at 4°C.

Primary antibodies included anti acetylated-tubulin (611B1, Sigma, St. Louis MO), anti-FLAG (Sigma), anti-MmIFT20, anti-MmIFT88 (Pazour et al., 2002a), MmIFT27 (Keady et al., 2012), anti-golgin97 (CDF4, Molecular Probes) anti-BIP (clone 40, BD Transduction Laboratories), anti-Rab11 (clone 47, BD Transduction Laboratories), anti-TfR (clone H68.4, Invitrogen), anti-giantin (Nozawa et al., 2002) and anti-megalin (P-20, Santa Cruz Biotechnology).

Widefield images were acquired by an Orca ER camera (Hamamatsu, Bridgewater, NJ) on a Zeiss Axiovert 200 M microscope equipped with a Zeiss 100× plan-Apochromat 1.4 NA objective. Images were captured by Openlab (Improvision, Waltham, MA) and adjusted for contrast in Adobe Photoshop. If comparisons are to be made between images, the photos were taken with identical conditions and manipulated equally. For the quantification of SNAP and CD8 in the cilia, the length, area, and average fluorescence intensity of the cilia was measured using the measurement tools of Openlab. To determine significance of differences, data from three independent experiments were subjected to an unpaired Student's T test. Confocal images were

acquired by a Nikon TE-2000E2 inverted microscope equipped with a Solamere Technology modified Yokogawa CSU10 spinning disk confocal scan head. Z-stacks were acquired at 0.2 μm or 0.5 μm intervals and converted to single planes by maximum projection with MetaMorph software. Bright field images were acquired using a Zeiss Axioskop 2 Plus equipped with an Axiocam HRC color digital camera and Axiovision 4.0 acquisition software.

**SNAP Trafficking Assays**

The construct (pJAF270) used for SNAP trafficking assays was constructed by fusing the extracellular domain of mouse CD8a (Xia et al., 2001) to the last 17 extracellular residues of mouse fibrocystin through the first 27 intracellular residues, the SNAP tag was cloned onto the c-terminal end of the CTS creating CD8-CTS-SNAP. Mouse kidney cells stably expressing CD8-CTS-SNAP were incubated with 0.04 μM cell permeable non-fluorescent BG-Block (New England Biolabs) for 30 minutes to block all SNAP epitopes. Following 3 washes with complete growth media cells were allowed to synthesize new CD8-CTS-SNAP for 1.5 hrs before the addition of HEPES pH 7.4 to 20 mM and cycloheximide to 150 μg/ml, then shifted to 19°C for two hrs to accumulate CD8-CTS-SNAP at the Golgi complex. Cells were returned to 37° and allowed to traffic CD8-CTS-SNAP for the indicated periods of time before being fixed and stained.

For siRNA knockdown, cells were transfected by RNAiMAXX (Invitrogen) with SMARTpool siRNA (Dharmacon) targeting Arf4 (L-060271) or a non-targeting control (D-001810) and assayed for knockdown 48 hours post transfection.

**Protein Analysis**

FLAG-tagged Arf1-6 (pJAF215, pJAF213, pJAF214, pJAF216, pJAF210, pJAF211), were constructed by PCR amplifying the open reading frames and inserting them into p3XFLAG-CMV-14 (Sigma, St. Louis, MO). Point mutations in Arf4 ($Arf4^{T31N}$ = pJAF221, $Arf4^{T48N}$ = pJAF222, $Arf4^{Q71L}$ = pJAF223) were generated by inverse PCR using the Quick Change II site directed mutagenesis kit (Stratagene) starting from pJAF216. Cells were transfected with FLAG-tagged Arf and GFP-tagged CTS deletion and alanine scanning mutants used in (Follit et al., 2010), CD8-PKHD1 (pJAF268), or CD8-Megalin (pJAF281) and 48 hours later, FLAG immunoprecipitation was carried out as described in (Follit et al., 2008).

**Beta-galactosidase Staining of Mouse Embryos**

Embryos were fixed in 0.2% glutaraldehyde, 2% formalin, 5mM EGTA and 2mM $MgCl_2$ in 0.1M phosphate buffer pH 7.3 for 10 minutes at room temperature then rinsed three times in wash buffer containing 0.1% sodium deoxycholate, 0.2% IGEPAL, 2mM $MgCl_2$ in 0.1M phosphate buffer for 30 minutes each wash. Fixed embryos were stained overnight at 37° C in 1mg/ml X-gal, 5mM potassium ferrocyanide, 5mM potassium ferricyanide diluted in wash buffer.

**mRNA Analysis**

RNA was isolated from individual e9.5 embryos or from IMCD3 cells using RNeasy kits (Qiagen), including on-column DNA digestion. First strand cDNA was synthesized from 100-500 ng of total RNA using a SuperScript II First-Strand Synthesis System

(Invitrogen, Carlsbad, CA) and random hexameric primers. Quantitative real-time PCR primers were designed to produce amplicons between 100–150 nucleotides in length, using the online primer3 web PCR primer tool (http://fokker.wi.mit.edu/primer3/input.htm) and the IDT Primer Express software tool (http://www.idtdna.com/Scitools/Applications/Primerquest/). Primers were synthesized by Integrated DNA Technologies Inc (Coralville, IA) and are listed in Table 1. qRT-PCR analysis was performed using an ABI Prism 7500 sequence detection system (Applied Biosystems, Foster City, CA). Each reaction contained 5-12.5 ng first strand cDNA, 0.1 μM each specific forward and reverse primers and 1× Power SYBR Green (Applied Biosystems, Foster City, CA) in a 15 μl volume. Arf4 mRNA expression was normalized to GAPDH mRNA abundance and compared between mutant and control animals with an unpaired Student t-test.

**Table 4.1: qPCR Primers**

| Primer Name | Sequence | Tm | Amplicon |
|---|---|---|---|
| MmARF4exon3FOR | TTCACAGTATGGGATGTTGGTGGTCA | 59.9 | 133 |
| MmARF4exon4REV | GCACAGCTGCTCCTTCCTGGATT | 61.7 | |
| MmGAPDHExon3FOR | GCAATGCATCCTGCACCACCA | 61.1 | 138 |
| MmGAPDHExon4rREV | TTCCAGAGGGGCCATCCACA | 61.1 | |

## Acknowledgements

We thank Drs. S. Jones (Transgenic Mouse Core) G. Hendricks, L. Strittmatter (Electron Microscopy Core) and P. Furcinitti (Digital Imaging Core) for assistance during this work. We thank Drs. K. Tremblay (UMass Amherst) and J. Rivera (UMass Worcester) for helpful discussion during this project. This work was supported by the National Institutes of Health (GM060992 to GJP) and the Order of the Eagles (GJP). JAJ is a member of the Harvard Center for PKD Research (P50 DK074030). Core resources supported by the Diabetes Endocrinology Research Center grant DK32520 were also used.

# CHAPTER 5

## Discussion

The body of work presented in this thesis explores how membrane proteins are targeted to the cilium. The sensory functions of primary cilia rely on the unique complement of receptors localized to this distinct subdomain of the plasma membrane. Ciliary dysfunction is known to cause a number of pleiotropic human diseases including polycystic kidney disease, retinal degeneration, obesity and congenital birth defects. A better understanding of the mechanisms controlling ciliary protein targeting may lead to the development of potential therapeutics to treat these ciliopathies. Here, we summarize the pertinent research findings discussed in this thesis and hypothesize the next steps in understanding protein targeting to the cilium.

### GMAP210 and IFT20 as a ciliary sorting module

Intraflagellar transport (IFT) proteins are known to transport soluble axonemal precursors required to build a cilium. It is unknown if IFT proteins are also required for the transport of transmembrane cargo. IFT20 is the only IFT subunit known to localize to the Golgi apparatus in addition to the canonical ciliary localization of IFT subunits. The unique localization of IFT20 suggested it might be involved in the sorting of cargo destined for the cilium and initial knockdown of IFT20 caused a reduction in the ciliary levels of polycystin-2.

Chapter II of this thesis builds on these findings by identifying the binding partner of IFT20 at the Golgi apparatus, GMAP210. The novel GMAP210/IFT20 complex represents a pool of IFT20 that is independent from established IFT Complex B in and around the cilium. Previous findings indicated IFT20 was required for the delivery of the ciliary membrane protein polycystin-2 to the cilium. To investigate if GMAP210 was likewise required for ciliary protein trafficking we created a knockout mouse. GMAP210 knockout mice die just after birth due to defects in lung and heat development. The structure of the Golgi apparatus was not affected by the lack of GMAP210 as previous cell culture studies suggested, however the absence of GMAP210 prevented IFT20 from localizing to the Golgi apparatus. Mouse embryonic kidney cells isolated from the GMAP210 null mice exhibited reduced ciliary polycystin-2 levels suggesting GMAP210 and IFT20 are required for the targeting of this protein to the cilium. Re-introduction of full-length GMAP210 restores IFT20 localization to the Golgi apparatus and also rescues polycystin-2 levels at the cilium.

## Implications and future directions of GMAP210/IFT20 research

The findings discussed in Chapter II support the hypothesis that IFT20 binds GMAP210 at the Golgi apparatus and these proteins are involved in targeting proteins to the cilium. Interestingly, the GMAP210 knockout mouse phenotype differs greatly from IFT20 null mice that die embryonically at approximately day 9.5 due to a number of ciliary related defects in heart development and laterality. Further research is needed to explore the common or disparate functions of IFT20 and GMAP210. The use of a Cre/Lox system to

create tissue specific knockouts of each protein would aid in discerning the specific roles of each of these proteins during development. Specifically, knockouts in the heart and lung, the two organs greatly affected by the loss of GMAP210, would provide critical information regarding the lethality of these mice. Targeted deletion of IFT20 in mouse kidney epithelia results in massive cystogenesis by postnatal day 21. A similar deletion of GMAP210 is needed to investigate if the loss of polycystin-2 observed in mouse embryonic kidney cells lacking GMAP210 would cause a similar cystic phenotype in adult kidneys.

Another implication of the data presented in Chapter II is that IFT20 marks vesicles containing ciliary cargo destined for the cilium. GMAP210 is present at the Golgi apparatus where it binds IFT20. GMAP210 is not seen in or around the primary cilium suggesting it remains at the Golgi apparatus while IFT20 has been shown to dynamically traffic between the Golgi apparatus and the cilium. This suggests that IFT20 may decorate vesicles leaving the Golgi apparatus and help direct them to the cilium. Once at the cilium, IFT20 could then interact with known IFT Complex B subunits and incorporate the transmembrane cargo into the ciliary membrane. This provocative model is interesting but needs to be rigorously tested. Crucial experiments are needed to isolate the hypothesized IFT20 vesicles. These vesicles are predicted to be devoid of GMAP210 (a resident Golgi apparatus protein) and also lack the canonical IFT complex B proteins present in and around the cilium. The identification of IFT20 binding partners at both the Golgi apparatus and the cilium provide key tools required to identify a possibly ciliary-targeted vesicle fraction decorated with IFT20 and en route to the cilium.

## Identification of a fibrocystin ciliary targeting sequence

To better understand the mechanism of ciliary protein trafficking we chose to study a known ciliary membrane protein fibrocystin. Mutations within fibrocystin are known to cause autosomal recessive polycystic kidney disease, which affects 1:20,000 live births and is a significant source of neonate lethality. Chapter III identifies an 18 amino acid sequence present in the cytoplasmic tail of fibrocystin that is necessary and sufficient to direct a heterologous protein (GFP) to the cilium in cultured kidney cells. Alanine scanning mutagenesis identified three palmitoylated cysteine residues that target the CTS to lipid microdomains and are required for the ciliary trafficking of the CTS. We suggest lipid modification, in this case palmitoylation, is likely an important first step in sorting membrane proteins to the primary cilium – a possibility we will discuss in more detail below.

## The fibrocystin CTS interacts with Rab8 and Arf4

We hypothesized that the CTS of fibrocystin functions to bind the intracellular sorting machinery required to direct fibrocystin to the cilium. To identify proteins that interact with the CTS we performed a series of co-immuoprecipitation assays with proteins implicated in ciliary protein trafficking. We identified an interaction between the small G protein Rab8 (Chapter III) and Arf4 (Chapter IV) and the CTS of fibrocystin. Rab8 and Arf4 binding roughly correlated with the ability of CTS constructs to enter the cilium suggesting these interactions were important for the trafficking of the CTS to the cilium.

However, binding of Rab8 or Arf4 did not always correlate with CTS trafficking to cilia and these exceptions are discussed below.

We used dominant negative and constitutively active forms of Rab8 (Chapter III) and Arf4 (Chapter IV) to explore the function of these proteins in the trafficking of the CTS. Wildtype or constitutively active Rab8 localized to the cilium and allowed the CTS to enter cilia while the dominant negative form of Rab8 was concentrated in the cytoplasm and prevented the CTS from entering the cilium. The function of Arf4 mutations is less clear as any overexpression of Arf4 wildtype or mutant proteins prevented the CTS from entering cilia (Figure 4.2). Knockdown of Arf4 did not block CTS trafficking to the cilium but did result in a delay in CTS delivery and suggested Arf4 is required for the efficient delivery of fibrocystin to the cilium. These data support the model presented in Figure 5.1.

## Palmitoylation, lipid microdomains and CTS trafficking

The work presented in Chapter III identified a ciliary targeting sequence contained in the cytoplasmic tail of fibrocystin. These experiments identified a palmitoylated 18 amino acid motif that is necessary and sufficient to target GFP to cilia in cultured kidney cells. One limitation to this sequence is that it lacks at transmembrane domain and not subjected to the normal trafficking pathway through the cell. An improved fibrocystin construct was designed and used in trafficking assays described in Chapter IV that showed Arf4 is required for the efficient delivery of this construct to cilia.

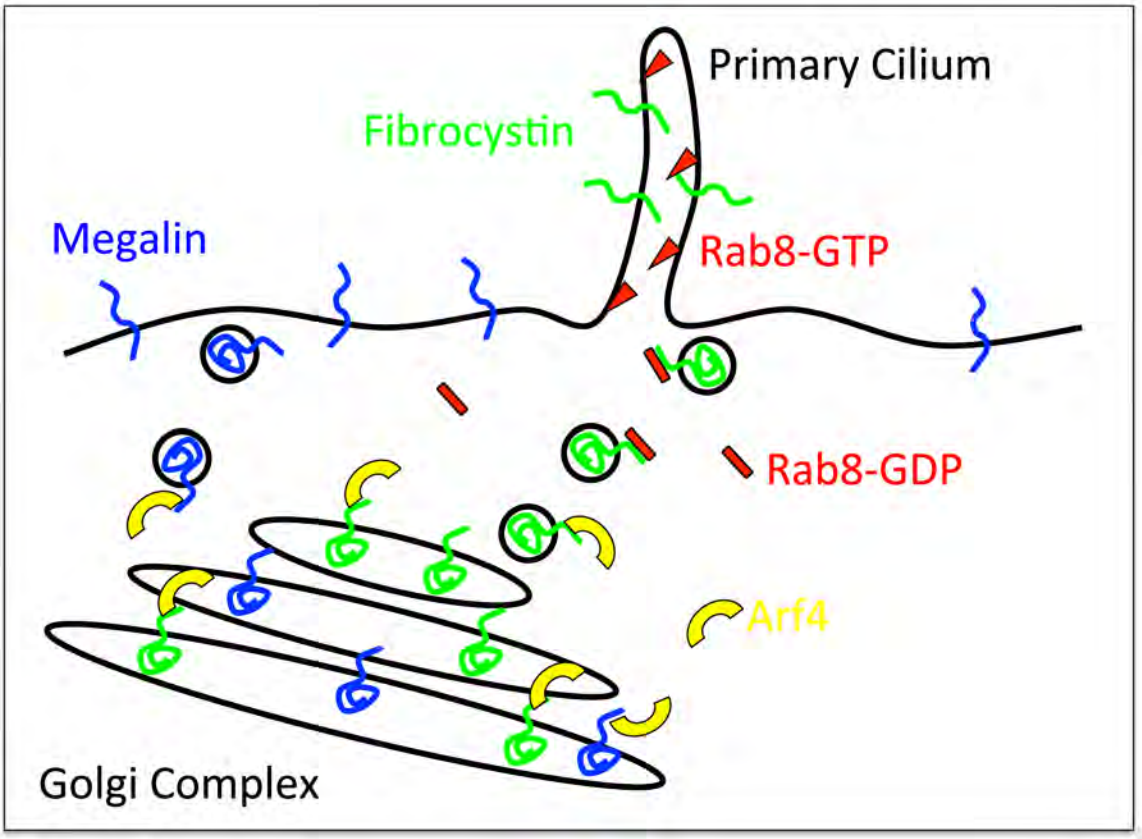


**Figure 5.1: Model of Rab8 and Arf4 trafficking.**

**Figure 5.1: Model of Rab8 and Arf4 trafficking.** Rab8 interacts with and controls the ciliary levels of the fibrocystin CTS. Arf4 also interacts with the CTS of fibrocystin likely at the Golgi apparatus and is required for the efficient delivery of the CTS to the cilium. Arf4 also interacts with the cytoplasmic domain of megalin and is required for megalin localization to the apical plasma membrane in the visceral endoderm of mice.

Initial alanine scanning mutagenesis suggested that a group of cysteines were absolutely required for the trafficking of the soluble CTS to the cilium. However, as this sequence lacked a transmembrane domain these results are difficult to interpret. It is likely the palmitoylated cysteines provide the only membrane association with this CTS. We speculated that mutating the cysteine residues to alanines prevented the CTS from associating to membranes, which prevented the sequence from interacting with Rab8 (Chapter III) and Arf4 (Chapter IV) and prevented the CTS from being targeted to the cilium.

To test the requirement of the palmitoylated cysteines in the context of a transmembrane containing construct I mutated the cysteines residues to alanines in the construct described in Figure 4.3A. Surprisingly, the cysteine residues are not required for the interaction with Arf4 (Figure 5.2E). However, the palmitoylated cysteines are required for the targeting of this construct to cilia (Figure 5.2 A-D). This suggests the palmitoylated cysteine residues did not simply provide membrane association to the original CTS construct but serve a crucial function in targeting the CTS to the cilium. The palmitoylation of these cysteines is required to concentrate the CTS in lipid microdomains discussed in Chapter III. Further experiments are needed to investigate the function of the CTS in the context of a transmembrane containing construct to test whether lipid microdomain targeting is an initial step in trafficking the CTS of fibrocystin.

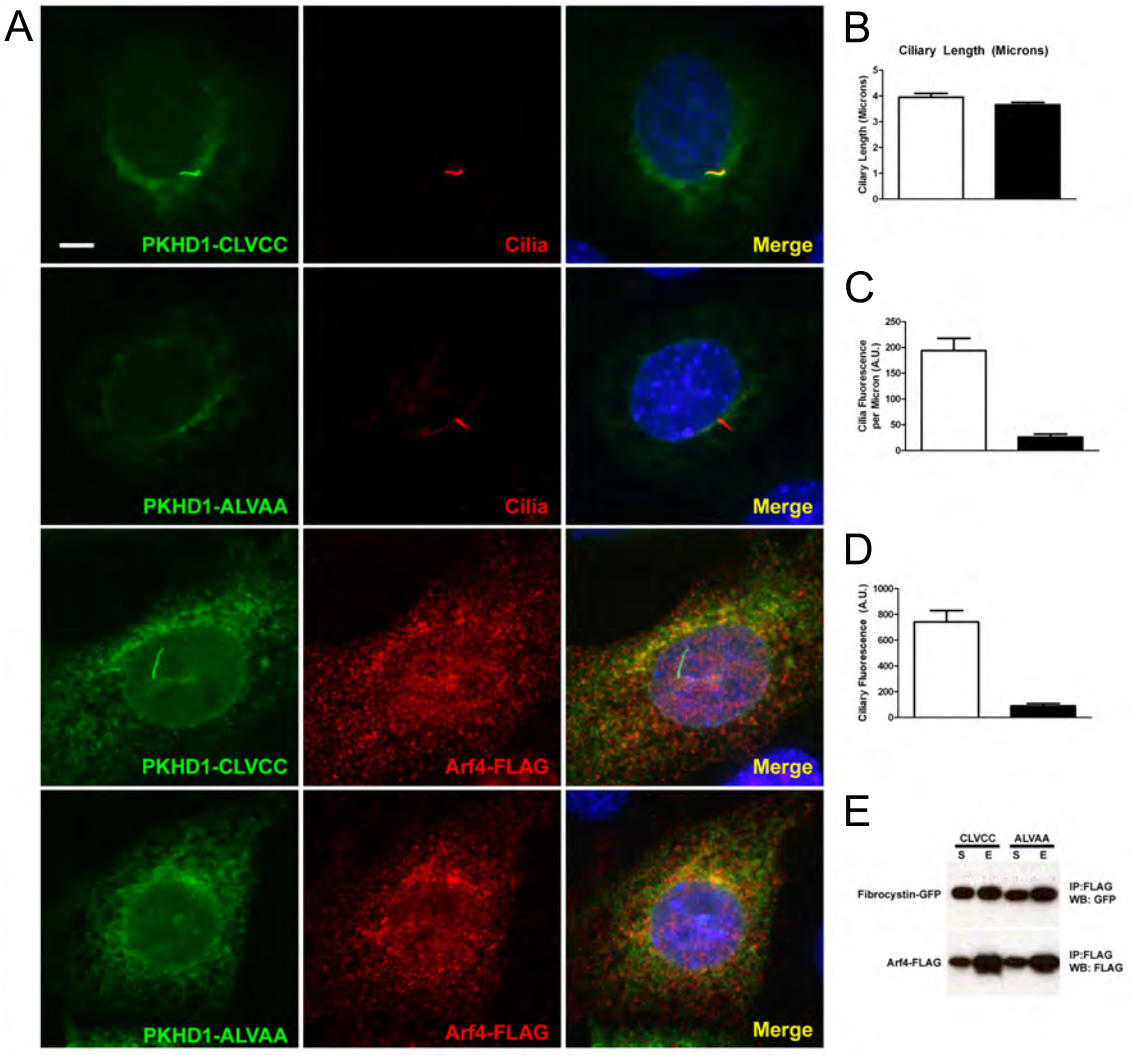


**Figure 5.2: Palmitoylated cysteines required for proper CTS localization but dispensable for Arf4 binding.**

**Figure 5.2: Palmitoylated cysteines required for proper CTS localization but dispensable for Arf4 binding. A.** IMCD3 cells expressing the CD8-CTS-SNAP-GFP wildtype (JAF270) or triple cysteine mutant (JAF280) and Arf4-FLAG (JAF216) were fixed and stained with antibodies to CD8 (green) and FLAG (red). **B.** Cilia length is not effected by expression of JAF270 or JAF280. **C.** Quantification of the ciliary intensity per micron of wildtype CD8-CTS-SNAP-GFP (JAF270) and triple cysteine mutant CD8-CTS-SNAP-GFP (JAF280). **D.** Total ciliary fluorescence of JAF270 and JAF280. **E.** FLAG-tagged Arf4 brings down both wildtype CTS (JAF270) and triple cysteine mutant CTS (JAF280).

## Protein interactions and CTS trafficking

Chapter III and IV described specific protein interactions between the CTS and two small G proteins, Rab8 and Arf4. We speculated that these interactions play critical roles in the trafficking of the CTS to the cilium. Mutations affecting the GTP-binding state of Rab8 and Arf4 had different effects on the trafficking of the CTS to the cilium (Chapter III, IV).

It is important to point out that simply binding to Rab8 or Arf4 alone is not sufficient to target the CTS to the cilium as mutations that prevented the ciliary localization of the CTS still bound Rab8 and Arf4 (Figure 3.2, 3.7, 4.1). This suggests there are additional steps required for the ciliary targeting of the CTS that are not explained by the interactions with Rab8 or Arf4. The initial characterization of the CTS and alanine scanning mutagenesis was performed in a construct that lacked a transmembrane domain. It may be useful to repeat these experiments with the new fibrocystin construct to elucidate residues that are required for palmitoylation and those which may be playing a direct role in Rab8 or Arf4 binding.

Furthermore, it is not known if the interaction between Rab8 and Arf4 is direct or mediated through an adaptor protein or what coat or coats may be involved in ciliary protein trafficking. Future experiments should focus on identifying additional proteins that interact with the CTS including potential coat or adaptor proteins as this may help explain the observed differences between the ciliary targeting of the CTS and binding to the small G proteins Rab8 and Arf4.

## The role of Arf4 in ciliary vs. general trafficking

Chapter IV described a unique interaction between Arf4 and the CTS of fibrocystin. Extensive biochemical and immunofluorescence data indicated Arf4 was required for the efficient delivery of the CTS to the cilium. Additional work in the field of ciliary protein trafficking suggested Arf4 functioned as a global regulator of ciliary protein trafficking. Based on our work and the work of others we chose to study the function of Arf4 further and created and Arf4 knockout mouse (Chapter IV).

Arf4 null mice are embryonic lethal. This indicates Arf4 is essential for mammalian development its unique function cannot be provided by the other 5 members of the Arf family as suggested by tissue culture based studies. We predicted the Arf4 mutant mice would have defects similar mice with known mutations affecting ciliary function. Examination of nodal cilia indicated that Arf4 mutant mice had no defects in ciliary assembly or nodal cilia function as left/right symmetry was properly broken. Instead, Arf4 is most highly expressed in the developing visceral endoderm – a non-ciliated tissue.

Careful examination of the visceral endoderm revealed multiple defects including a failure to localize the scavenger protein megalin to the apical surface of these cells. Arf4 is likely affecting the trafficking of a large number of proteins within the visceral endoderm, which led to the observed embryonic lethality at day 9.5. The studies performed in the Arf4 knockout mice provide clear evidence that Arf4 has functions outside of ciliary protein trafficking.

Additional studies are required to more completely understand the role of Arf4 in ciliary protein targeting. It remains to be seen if Arf4 plays a role in the trafficking of ciliary proteins like rhodopsin and fibrocystin in the mouse. Targeted deletion of Arf4 in the eye and kidney would be required to circumvent the embryonic lethality of the Arf4 null mice. It will be exciting to see if tissue specific disruption of Arf4 will result in phenotypes consistent with ciliary dysfunction like blindness or cystic kidney disease.

## Closing remarks

An interesting thing happens when biochemistry and experiments performed in tissue culture dishes meet the field of developmental biology. Although initial experiments pointed to Arf4 playing a specific role in the trafficking of ciliary membrane proteins, the Arf4 knockout mouse proves this hypothesis naïve at best and at worst just plain wrong.

I believe my graduate experience to be unique, but in all likelihood it was probably more similar to the countless students that came before me then I can appreciate at this time. Working in Greg's lab provided me fertile ground to explore new realms of science and taught me valuable lessons regarding the scientific process. Science is not static, the best hypotheses are fluid and proteins care not for what you believe they're function to be – that is merely transference of your own limitations. Objectivity is easy in theory but requires work to practice. In the end, trust the data – it's telling you something – you just have to listen…

# BIBLIOGRAPHY


Abe, A., N. Emi, M. Tanimoto, H. Terasaki, T. Marunouchi, and H. Saito. 1997. Fusion of the platelet-derived growth factor receptor beta to a novel gene CEV14 in acute myelogenous leukemia after clonal evolution. *Blood*. 90:4271-4277.

Alberts, B. 1994. Molecular biology of the cell. Garland Pub., New York. xliii, 1294, 1267 p. pp.

Bae, Y.K., H. Qin, K.M. Knobel, J. Hu, J.L. Rosenbaum, and M.M. Barr. 2006. General and cell-type specific mechanisms target TRPP2/PKD-2 to cilia. *Development*. 133:3859-3870.

Barr, F.A., and J. Egerer. 2005. Golgi positioning: are we looking at the right MAP? *The Journal of cell biology*. 168:993-998.

Ben-Shachar, G., R.A. Arcilla, R.V. Lucas, and F.J. Manasek. 1985. Ventricular trabeculations in the chick embryo heart and their contribution to ventricular and muscular septal development. *Circulation research*. 57:759-766.

Berbari, N.F., A.D. Johnson, J.S. Lewis, C.C. Askwith, and K. Mykytyn. 2008. Identification of ciliary localization sequences within the third intracellular loop of G protein-coupled receptors. *Molecular biology of the cell*. 19:1540-1547.

Berson, E.L., B. Rosner, C. Weigel-DiFranco, T.P. Dryja, and M.A. Sandberg. 2002. Disease progression in patients with dominant retinitis pigmentosa and rhodopsin mutations. *Investigative ophthalmology & visual science*. 43:3027-3036.

Bhowmick, R., M. Li, J. Sun, S.A. Baker, C. Insinna, and J.C. Besharse. 2009. Photoreceptor IFT complexes containing chaperones, guanylyl cyclase 1 and rhodopsin. *Traffic*. 10:648-663.

Bielinska, M., N. Narita, and D.B. Wilson. 1999. Distinct roles for visceral endoderm during embryonic mouse development. *The International journal of developmental biology*. 43:183-205.

Bijlmakers, M.J., and M. Marsh. 2003. The on-off story of protein palmitoylation. *Trends in cell biology*. 13:32-42.

Bloodgood, R.A. 1990. Ciliary and Flagellar Membranes. Springer, New York. 431 pp.

Bokel, C., S. Dass, M. Wilsch-Brauninger, and S. Roth. 2006. Drosophila Cornichon acts as cargo receptor for ER export of the TGFalpha-like growth factor Gurken. *Development*. 133:459-470.

Bonner, A.E., W.J. Lemon, and M. You. 2003. Gene expression signatures identify novel regulatory pathways during murine lung development: implications for lung tumorigenesis. *Journal of medical genetics*. 40:408-417.

Bouck, G.B. 1971. The structure, origin, isolation, and composition of the tubular mastigonemes of the Ochromas flagellum. *The Journal of cell biology*. 50:362-384.

Brailov, I., M. Bancila, M.J. Brisorgueil, M.C. Miquel, M. Hamon, and D. Verge. 2000. Localization of 5-HT(6) receptors at the plasma membrane of neuronal cilia in the rat brain. *Brain research*. 872:271-275.

Bridges, J.P., and T.E. Weaver. 2006. Use of transgenic mice to study lung morphogenesis and function. *ILAR journal / National Research Council, Institute of Laboratory Animal Resources*. 47:22-31.

Chapin, H.C., and M.J. Caplan. 2010. The cell biology of polycystic kidney disease. *The Journal of cell biology*. 191:701-710.

Chen, Y., P.L. Chen, C.F. Chen, Z.D. Sharp, and W.H. Lee. 1999. Thyroid hormone, T3-dependent phosphorylation and translocation of Trip230 from the Golgi complex to the nucleus. *Proceedings of the National Academy of Sciences of the United States of America*. 96:4443-4448.

Cole, D.G. 2003. The intraflagellar transport machinery of Chlamydomonas reinhardtii. *Traffic*. 4:435-442.

Cole, D.G., D.R. Diener, A.L. Himelblau, P.L. Beech, J.C. Fuster, and J.L. Rosenbaum. 1998. Chlamydomonas kinesin-II-dependent intraflagellar transport (IFT): IFT particles contain proteins required for ciliary assembly in Caenorhabditis elegans sensory neurons. *The Journal of cell biology*. 141:993-1008.

Corbit, K.C., P. Aanstad, V. Singla, A.R. Norman, D.Y. Stainier, and J.F. Reiter. 2005. Vertebrate Smoothened functions at the primary cilium. *Nature*. 437:1018-1021.

D'Souza-Schorey, C., and P. Chavrier. 2006. ARF proteins: roles in membrane traffic and beyond. *Nature reviews. Molecular cell biology*. 7:347-358.

Deretic, D. 2006. A role for rhodopsin in a signal transduction cascade that regulates membrane trafficking and photoreceptor polarity. *Vision research*. 46:4427-4433.

Deretic, D., and D.S. Papermaster. 1993. Rab6 is associated with a compartment that transports rhodopsin from the trans-Golgi to the site of rod outer segment disk formation in frog retinal photoreceptors. *Journal of cell science*. 106 ( Pt 3):803-813.

Deretic, D., A.H. Williams, N. Ransom, V. Morel, P.A. Hargrave, and A. Arendt. 2005. Rhodopsin C terminus, the site of mutations causing retinal disease, regulates trafficking by binding to ADP-ribosylation factor 4 (ARF4). *Proceedings of the National Academy of Sciences of the United States of America*. 102:3301-3306.

Donaldson, J.G., and C.L. Jackson. 2011. ARF family G proteins and their regulators: roles in membrane transport, development and disease. *Nature reviews. Molecular cell biology*. 12:362-375.

Dotti, C.G., and K. Simons. 1990. Polarized sorting of viral glycoproteins to the axon and dendrites of hippocampal neurons in culture. *Cell*. 62:63-72.

Drin, G., V. Morello, J.F. Casella, P. Gounon, and B. Antonny. 2008. Asymmetric tethering of flat and curved lipid membranes by a golgin. *Science*. 320:670-673.

Emmer, B.T., D. Maric, and D.M. Engman. 2010. Molecular mechanisms of protein and lipid targeting to ciliary membranes. *Journal of cell science*. 123:529-536.

Fan, S., V. Fogg, Q. Wang, X.W. Chen, C.J. Liu, and B. Margolis. 2007. A novel Crumbs3 isoform regulates cell division and ciliogenesis via importin beta interactions. *The Journal of cell biology*. 178:387-398.

Farr, G.A., M. Hull, I. Mellman, and M.J. Caplan. 2009. Membrane proteins follow multiple pathways to the basolateral cell surface in polarized epithelial cells. *The Journal of cell biology*. 186:269-282.

Feig, L.A. 1999. Tools of the trade: use of dominant-inhibitory mutants of Ras-family GTPases. *Nature cell biology*. 1:E25-27.

Fliegauf, M., T. Benzing, and H. Omran. 2007. When cilia go bad: cilia defects and ciliopathies. *Nature reviews. Molecular cell biology*. 8:880-893.

Follit, J.A., L. Li, Y. Vucica, and G.J. Pazour. 2010. The cytoplasmic tail of fibrocystin contains a ciliary targeting sequence. *The Journal of cell biology*. 188:21-28.

Follit, J.A., J.T. San Agustin, F. Xu, J.A. Jonassen, R. Samtani, C.W. Lo, and G.J. Pazour. 2008. The Golgin GMAP210/TRIP11 anchors IFT20 to the Golgi complex. *PLoS genetics*. 4:e1000315.

Follit, J.A., R.A. Tuft, K.E. Fogarty, and G.J. Pazour. 2006. The intraflagellar transport protein IFT20 is associated with the Golgi complex and is required for cilia assembly. *Molecular biology of the cell*. 17:3781-3792.

Follit, J.A., F. Xu, B.T. Keady, and G.J. Pazour. 2009. Characterization of mouse IFT complex B. *Cell motility and the cytoskeleton*. 66:457-468.

Freshney, R.I. 2000. Culture of Animal Cells: A Manual of Basic Technique. Wiley-Liss, New York. 600 pp.

Geng, L., D. Okuhara, Z. Yu, X. Tian, Y. Cai, S. Shibazaki, and S. Somlo. 2006. Polycystin-2 traffics to cilia independently of polycystin-1 by using an N-terminal RVxP motif. *Journal of cell science*. 119:1383-1395.

Gillingham, A.K., and S. Munro. 2007. The small G proteins of the Arf family and their regulators. *Annual review of cell and developmental biology*. 23:579-611.

Gillingham, A.K., A.H. Tong, C. Boone, and S. Munro. 2004. The GTPase Arf1p and the ER to Golgi cargo receptor Erv14p cooperate to recruit the golgin Rud3p to the cis-Golgi. *The Journal of cell biology*. 167:281-292.

Gilula, N.B., and P. Satir. 1972. The ciliary necklace. A ciliary membrane specialization. *The Journal of cell biology*. 53:494-509.

Godsel, L.M., and D.M. Engman. 1999. Flagellar protein localization mediated by a calcium-myristoyl/palmitoyl switch mechanism. *The EMBO journal*. 18:2057-2065.

Hamblet, N.S., N. Lijam, P. Ruiz-Lozano, J. Wang, Y. Yang, Z. Luo, L. Mei, K.R. Chien, D.J. Sussman, and A. Wynshaw-Boris. 2002. Dishevelled 2 is essential for cardiac outflow tract development, somite segmentation and neural tube closure. *Development*. 129:5827-5838.

Hamon, M., E. Doucet, K. Lefevre, M.C. Miquel, L. Lanfumey, R. Insausti, D. Frechilla, J. Del Rio, and D. Verge. 1999. Antibodies and antisense oligonucleotide for probing the distribution and putative functions of central 5-HT6 receptors. *Neuropsychopharmacology : official publication of the American College of Neuropsychopharmacology*. 21:68S-76S.

Han, R.N., S. Babaei, M. Robb, T. Lee, R. Ridsdale, C. Ackerley, M. Post, and D.J. Stewart. 2004. Defective lung vascular development and fatal respiratory distress in endothelial NO synthase-deficient mice: a model of alveolar capillary dysplasia? *Circulation research*. 94:1115-1123.

Handel, M., S. Schulz, A. Stanarius, M. Schreff, M. Erdtmann-Vourliotis, H. Schmidt, G. Wolf, and V. Hollt. 1999. Selective targeting of somatostatin receptor 3 to neuronal cilia. *Neuroscience*. 89:909-926.

Harris, P.C., and V.E. Torres. 2009. Polycystic kidney disease. *Annual review of medicine*. 60:321-337.

Henderson, D.J., H.M. Phillips, and B. Chaudhry. 2006. Vang-like 2 and noncanonical Wnt signaling in outflow tract development. *Trends in cardiovascular medicine*. 16:38-45.

Hiesberger, T., E. Gourley, A. Erickson, P. Koulen, C.J. Ward, T.V. Masyuk, N.F. Larusso, P.C. Harris, and P. Igarashi. 2006. Proteolytic cleavage and nuclear translocation of fibrocystin is regulated by intracellular Ca2+ and activation of protein kinase C. *The Journal of biological chemistry*. 281:34357-34364.

Hoffman, J.I., and S. Kaplan. 2002. The incidence of congenital heart disease. *Journal of the American College of Cardiology*. 39:1890-1900.

Hou, X., M. Mrug, B.K. Yoder, E.J. Lefkowitz, G. Kremmidiotis, P. D'Eustachio, D.R. Beier, and L.M. Guay-Woodford. 2002. Cystin, a novel cilia-associated protein, is disrupted in the cpk mouse model of polycystic kidney disease. *The Journal of clinical investigation*. 109:533-540.

Huang, K., D.R. Diener, A. Mitchell, G.J. Pazour, G.B. Witman, and J.L. Rosenbaum. 2007. Function and dynamics of PKD2 in Chlamydomonas reinhardtii flagella. *The Journal of cell biology*. 179:501-514.

Infante, C., F. Ramos-Morales, C. Fedriani, M. Bornens, and R.M. Rios. 1999. GMAP-210, A cis-Golgi network-associated protein, is a minus end microtubule-binding protein. *The Journal of cell biology*. 145:83-98.

Ishikawa, H., and W.F. Marshall. 2011. Ciliogenesis: building the cell's antenna. *Nature reviews. Molecular cell biology*. 12:222-234.

Janich, P., and D. Corbeil. 2007. GM1 and GM3 gangliosides highlight distinct lipid microdomains within the apical domain of epithelial cells. *FEBS letters*. 581:1783-1787.

Jekely, G., and D. Arendt. 2006. Evolution of intraflagellar transport from coated vesicles and autogenous origin of the eukaryotic cilium. *BioEssays : news and reviews in molecular, cellular and developmental biology*. 28:191-198.

Jenkins, P.M., T.W. Hurd, L. Zhang, D.P. McEwen, R.L. Brown, B. Margolis, K.J. Verhey, and J.R. Martens. 2006. Ciliary targeting of olfactory CNG channels requires the CNGB1b subunit and the kinesin-2 motor protein, KIF17. *Current biology : CB*. 16:1211-1216.

Jin, H., S.R. White, T. Shida, S. Schulz, M. Aguiar, S.P. Gygi, J.F. Bazan, and M.V. Nachury. 2010. The conserved Bardet-Biedl syndrome proteins assemble a coat that traffics membrane proteins to cilia. *Cell*. 141:1208-1219.

Jonassen, J.A., J. San Agustin, J.A. Follit, and G.J. Pazour. 2008. Deletion of IFT20 in the mouse kidney causes misorientation of the mitotic spindle and cystic kidney disease. *The Journal of cell biology*. 183:377-384.

Jones, C., V.C. Roper, I. Foucher, D. Qian, B. Banizs, C. Petit, B.K. Yoder, and P. Chen. 2008. Ciliary proteins link basal body polarization to planar cell polarity regulation. *Nature genetics*. 40:69-77.

Kahn, R.A., L. Volpicelli-Daley, B. Bowzard, P. Shrivastava-Ranjan, Y. Li, C. Zhou, and L. Cunningham. 2005. Arf family GTPases: roles in membrane traffic and microtubule dynamics. *Biochemical Society transactions*. 33:1269-1272.

Keady, B.T., Y.Z. Le, and G.J. Pazour. 2011. IFT20 is required for opsin trafficking and photoreceptor outer segment development. *Molecular biology of the cell*. 22:921-930.

Keady, B.T., R. Samtani, K. Tobita, M. Tsuchya, J.T. SanAgustin, J.A. Follit, J.A. Jonassen, R. Subramanian, C.W. Lo, and G.J. Pazour. 2012. IFT25 Links the Signal-Dependent Movement of Hedgehog Components to Intraflagellar Transport. *Developmental Cell*.

Keppler, A., S. Gendreizig, T. Gronemeyer, H. Pick, H. Vogel, and K. Johnsson. 2003. A general method for the covalent labeling of fusion proteins with small molecules in vivo. *Nature biotechnology*. 21:86-89.

Kim, D.W. 2003. Characterization of Grp1p, a novel cis-Golgi matrix protein. *Biochemical and biophysical research communications*. 303:370-378.

Kim, D.W., M. Sacher, A. Scarpa, A.M. Quinn, and S. Ferro-Novick. 1999. High-copy suppressor analysis reveals a physical interaction between Sec34p and Sec35p, a protein implicated in vesicle docking. *Molecular biology of the cell*. 10:3317-3329.

Kovacs, J.J., E.J. Whalen, R. Liu, K. Xiao, J. Kim, M. Chen, J. Wang, W. Chen, and R.J. Lefkowitz. 2008. Beta-arrestin-mediated localization of smoothened to the primary cilium. *Science*. 320:1777-1781.

Kozminski, K.G., K.A. Johnson, P. Forscher, and J.L. Rosenbaum. 1993. A motility in the eukaryotic flagellum unrelated to flagellar beating. *Proceedings of the National Academy of Sciences of the United States of America*. 90:5519-5523.

Kudelko, M., J.B. Brault, K. Kwok, M.Y. Li, N. Pardigon, J.S. Peiris, R. Bruzzone, P. Despres, B. Nal, and P.G. Wang. 2012. Class II ADP-ribosylation factors are required for efficient secretion of dengue viruses. *The Journal of biological chemistry*. 287:767-777.

Leonard, D., A. Hayakawa, D. Lawe, D. Lambright, K.D. Bellve, C. Standley, L.M. Lifshitz, K.E. Fogarty, and S. Corvera. 2008. Sorting of EGF and transferrin at the plasma membrane and by cargo-specific signaling to EEA1-enriched endosomes. *Journal of cell science*. 121:3445-3458.

Li, C., J. Xiao, K. Hormi, Z. Borok, and P. Minoo. 2002. Wnt5a participates in distal lung morphogenesis. *Developmental biology*. 248:68-81.

Lighthouse, J.K., L. Zhang, J.C. Hsieh, T. Rosenquist, and B.C. Holdener. 2011. MESD is essential for apical localization of megalin/LRP2 in the visceral endoderm. *Developmental dynamics : an official publication of the American Association of Anatomists*. 240:577-588.

Low, S.H., P.A. Roche, H.A. Anderson, S.C. van Ijzendoorn, M. Zhang, K.E. Mostov, and T. Weimbs. 1998. Targeting of SNAP-23 and SNAP-25 in polarized epithelial cells. *The Journal of biological chemistry*. 273:3422-3430.

Macdonald, J.L., and L.J. Pike. 2005. A simplified method for the preparation of detergent-free lipid rafts. *Journal of lipid research*. 46:1061-1067.

May, P., E. Woldt, R.L. Matz, and P. Boucher. 2007. The LDL receptor-related protein (LRP) family: an old family of proteins with new physiological functions. *Annals of medicine*. 39:219-228.

Mazelova, J., L. Astuto-Gribble, H. Inoue, B.M. Tam, E. Schonteich, R. Prekeris, O.L. Moritz, P.A. Randazzo, and D. Deretic. 2009. Ciliary targeting motif VxPx directs assembly of a trafficking module through Arf4. *The EMBO journal*. 28:183-192.

Menezes, L.F., Y. Cai, Y. Nagasawa, A.M. Silva, M.L. Watkins, A.M. Da Silva, S. Somlo, L.M. Guay-Woodford, G.G. Germino, and L.F. Onuchic. 2004. Polyductin, the PKHD1 gene product, comprises isoforms expressed in plasma membrane, primary cilium, and cytoplasm. *Kidney international*. 66:1345-1355.

Milenkovic, L., M.P. Scott, and R. Rohatgi. 2009. Lateral transport of Smoothened from the plasma membrane to the membrane of the cilium. *The Journal of cell biology*. 187:365-374.

Moritz, O.L., B.M. Tam, L.L. Hurd, J. Peranen, D. Deretic, and D.S. Papermaster. 2001. Mutant rab8 Impairs docking and fusion of rhodopsin-bearing post-Golgi membranes and causes cell death of transgenic Xenopus rods. *Molecular biology of the cell*. 12:2341-2351.

Nachury, M.V., A.V. Loktev, Q. Zhang, C.J. Westlake, J. Peranen, A. Merdes, D.C. Slusarski, R.H. Scheller, J.F. Bazan, V.C. Sheffield, and P.K. Jackson. 2007. A core complex of BBS proteins cooperates with the GTPase Rab8 to promote ciliary membrane biogenesis. *Cell*. 129:1201-1213.

Nachury, M.V., E.S. Seeley, and H. Jin. 2010. Trafficking to the ciliary membrane: how to get across the periciliary diffusion barrier? *Annual review of cell and developmental biology*. 26:59-87.

Nada, S., A. Hondo, A. Kasai, M. Koike, K. Saito, Y. Uchiyama, and M. Okada. 2009. The novel lipid raft adaptor p18 controls endosome dynamics by anchoring the MEK-ERK pathway to late endosomes. *The EMBO journal*. 28:477-489.

Nakata, K., D. Shiba, D. Kobayashi, and T. Yokoyama. 2012. Targeting of Nphp3 to the primary cilia is controlled by an N-terminal myristoylation site and coiled-coil domains. *Cytoskeleton (Hoboken)*.

Nauli, S.M., Y. Kawanabe, J.J. Kaminski, W.J. Pearce, D.E. Ingber, and J. Zhou. 2008. Endothelial cilia are fluid shear sensors that regulate calcium signaling and nitric oxide production through polycystin-1. *Circulation*. 117:1161-1171.

Nie, Z., and P.A. Randazzo. 2006. Arf GAPs and membrane traffic. *Journal of cell science*. 119:1203-1211.

Nonaka, S., Y. Tanaka, Y. Okada, S. Takeda, A. Harada, Y. Kanai, M. Kido, and N. Hirokawa. 1998. Randomization of left-right asymmetry due to loss of nodal cilia generating leftward flow of extraembryonic fluid in mice lacking KIF3B motor protein. *Cell*. 95:829-837.

Nozawa, K., C.A. Casiano, J.C. Hamel, C. Molinaro, M.J. Fritzler, and E.K. Chan. 2002. Fragmentation of Golgi complex and Golgi autoantigens during apoptosis and necrosis. *Arthritis research*. 4:R3.

Onuchic, L.F., L. Furu, Y. Nagasawa, X. Hou, T. Eggermann, Z. Ren, C. Bergmann, J. Senderek, E. Esquivel, R. Zeltner, S. Rudnik-Schoneborn, M. Mrug, W. Sweeney, E.D. Avner, K. Zerres, L.M. Guay-Woodford, S. Somlo, and G.G. Germino. 2002. PKHD1, the polycystic kidney and hepatic disease 1 gene, encodes a novel large protein containing multiple immunoglobulin-like plexin-transcription-factor domains and parallel beta-helix 1 repeats. *American journal of human genetics*. 70:1305-1317.

Pan, J., and W.J. Snell. 2003. Kinesin II and regulated intraflagellar transport of Chlamydomonas aurora protein kinase. *Journal of cell science*. 116:2179-2186.

Papermaster, D.S., B.G. Schneider, and J.C. Besharse. 1985. Vesicular transport of newly synthesized opsin from the Golgi apparatus toward the rod outer segment. Ultrastructural immunocytochemical and autoradiographic evidence in Xenopus retinas. *Investigative ophthalmology & visual science*. 26:1386-1404.

Pazour, G.J. 2004. Intraflagellar transport and cilia-dependent renal disease: the ciliary hypothesis of polycystic kidney disease. *Journal of the American Society of Nephrology : JASN*. 15:2528-2536.

Pazour, G.J., N. Agrin, J. Leszyk, and G.B. Witman. 2005. Proteomic analysis of a eukaryotic cilium. *The Journal of cell biology*. 170:103-113.

Pazour, G.J., S.A. Baker, J.A. Deane, D.G. Cole, B.L. Dickert, J.L. Rosenbaum, G.B. Witman, and J.C. Besharse. 2002a. The intraflagellar transport protein, IFT88, is essential for vertebrate photoreceptor assembly and maintenance. *The Journal of cell biology*. 157:103-113.

Pazour, G.J., and R.A. Bloodgood. 2008. Targeting proteins to the ciliary membrane. *Current topics in developmental biology*. 85:115-149.

Pazour, G.J., B.L. Dickert, Y. Vucica, E.S. Seeley, J.L. Rosenbaum, G.B. Witman, and D.G. Cole. 2000. Chlamydomonas IFT88 and its mouse homologue, polycystic kidney disease gene tg737, are required for assembly of cilia and flagella. *The Journal of cell biology*. 151:709-718.

Pazour, G.J., J.T. San Agustin, J.A. Follit, J.L. Rosenbaum, and G.B. Witman. 2002b. Polycystin-2 localizes to kidney cilia and the ciliary level is elevated in orpk mice with polycystic kidney disease. *Current biology : CB*. 12:R378-380.

Pazour, G.J., C.G. Wilkerson, and G.B. Witman. 1998. A dynein light chain is essential for the retrograde particle movement of intraflagellar transport (IFT). *The Journal of cell biology*. 141:979-992.

Pazour, G.J., and G.B. Witman. 2003. The vertebrate primary cilium is a sensory organelle. *Current opinion in cell biology*. 15:105-110.

Pennekamp, P., C. Karcher, A. Fischer, A. Schweickert, B. Skryabin, J. Horst, M. Blum, and B. Dworniczak. 2002. The ion channel polycystin-2 is required for left-right axis determination in mice. *Current biology : CB*. 12:938-943.

Pernet-Gallay, K., C. Antony, L. Johannes, M. Bornens, B. Goud, and R.M. Rios. 2002. The overexpression of GMAP-210 blocks anterograde and retrograde transport between the ER and the Golgi apparatus. *Traffic*. 3:822-832.

Phillips, H.M., J.N. Murdoch, B. Chaudhry, A.J. Copp, and D.J. Henderson. 2005. Vangl2 acts via RhoA signaling to regulate polarized cell movements during development of the proximal outflow tract. *Circulation research*. 96:292-299.

Phillips, H.M., H.J. Rhee, J.N. Murdoch, V. Hildreth, J.D. Peat, R.H. Anderson, A.J. Copp, B. Chaudhry, and D.J. Henderson. 2007. Disruption of planar cell polarity signaling results in congenital heart defects and cardiomyopathy attributable to early cardiomyocyte disorganization. *Circulation research*. 101:137-145.

Piperno, G., and K. Mead. 1997. Transport of a novel complex in the cytoplasmic matrix of Chlamydomonas flagella. *Proceedings of the National Academy of Sciences of the United States of America*. 94:4457-4462.

Powers, J., and C. Barlowe. 2002. Erv14p directs a transmembrane secretory protein into COPII-coated transport vesicles. *Molecular biology of the cell*. 13:880-891.

Qin, H., D.T. Burnette, Y.K. Bae, P. Forscher, M.M. Barr, and J.L. Rosenbaum. 2005. Intraflagellar transport is required for the vectorial movement of TRPV channels in the ciliary membrane. *Current biology : CB*. 15:1695-1699.

Qin, H., J.L. Rosenbaum, and M.M. Barr. 2001. An autosomal recessive polycystic kidney disease gene homolog is involved in intraflagellar transport in C. elegans ciliated sensory neurons. *Current biology : CB*. 11:457-461.

Rauchman, M.I., S.K. Nigam, E. Delpire, and S.R. Gullans. 1993. An osmotically tolerant inner medullary collecting duct cell line from an SV40 transgenic mouse. *The American journal of physiology*. 265:F416-424.

Rios, R.M., A. Sanchis, A.M. Tassin, C. Fedriani, and M. Bornens. 2004. GMAP-210 recruits gamma-tubulin complexes to cis-Golgi membranes and is required for Golgi ribbon formation. *Cell*. 118:323-335.

Rodriguez-Boulan, E., G. Kreitzer, and A. Musch. 2005. Organization of vesicular trafficking in epithelia. *Nature reviews. Molecular cell biology*. 6:233-247.

Rohatgi, R., L. Milenkovic, and M.P. Scott. 2007. Patched1 regulates hedgehog signaling at the primary cilium. *Science*. 317:372-376.

Rohatgi, R., and W.J. Snell. 2010. The ciliary membrane. *Current opinion in cell biology*. 22:541-546.

Rosenbaum, J.L., and G.B. Witman. 2002. Intraflagellar transport. *Nature reviews. Molecular cell biology*. 3:813-825.

Rosenthal, J., V. Mangal, D. Walker, M. Bennett, T.J. Mohun, and C.W. Lo. 2004. Rapid high resolution three dimensional reconstruction of embryos with episcopic fluorescence image capture. *Birth defects research. Part C, Embryo today : reviews*. 72:213-223.

Ross, A.J., H. May-Simera, E.R. Eichers, M. Kai, J. Hill, D.J. Jagger, C.C. Leitch, J.P. Chapple, P.M. Munro, S. Fisher, P.L. Tan, H.M. Phillips, M.R. Leroux, D.J. Henderson, J.N. Murdoch, A.J. Copp, M.M. Eliot, J.R. Lupski, D.T. Kemp, H. Dollfus, M. Tada, N. Katsanis, A. Forge, and P.L. Beales. 2005. Disruption of Bardet-Biedl syndrome ciliary proteins perturbs planar cell polarity in vertebrates. *Nature genetics*. 37:1135-1140.

Sadakata, T., Y. Sekine, M. Oka, M. Itakura, M. Takahashi, and T. Furuichi. 2012. Calcium-dependent activator protein for secretion 2 interacts with the class II ARF small GTPases and regulates dense-core vesicle trafficking. *The FEBS journal*. 279:384-394.

Sadakata, T., Y. Shinoda, Y. Sekine, C. Saruta, M. Itakura, M. Takahashi, and T. Furuichi. 2010. Interaction of calcium-dependent activator protein for secretion 1 (CAPS1) with the class II ADP-ribosylation factor small GTPases is required for dense-core vesicle trafficking in the trans-Golgi network. *The Journal of biological chemistry*. 285:38710-38719.

Salaun, C., G.W. Gould, and L.H. Chamberlain. 2005. The SNARE proteins SNAP-25 and SNAP-23 display different affinities for lipid rafts in PC12 cells. Regulation by distinct cysteine-rich domains. *The Journal of biological chemistry*. 280:1236-1240.

SanAgustin, J.T., J.A. Follit, G. Hendricks, and G.J. Pazour. 2009. Scanning electron microscopy to examine cells and organs. *Methods in cell biology*. 91:81-87.

Saraste, J., G.E. Palade, and M.G. Farquhar. 1986. Temperature-sensitive steps in the transport of secretory proteins through the Golgi complex in exocrine pancreatic cells. *Proceedings of the National Academy of Sciences of the United States of America*. 83:6425-6429.

Satir, P., and S.T. Christensen. 2007. Overview of structure and function of mammalian cilia. *Annual review of physiology*. 69:377-400.

Schneider, L., C.A. Clement, S.C. Teilmann, G.J. Pazour, E.K. Hoffmann, P. Satir, and S.T. Christensen. 2005. PDGFRalphaalpha signaling is regulated through the primary cilium in fibroblasts. *Current biology : CB*. 15:1861-1866.

Scholey, J.M. 2003. Intraflagellar transport. *Annual review of cell and developmental biology*. 19:423-443.

Schulz, S., M. Handel, M. Schreff, H. Schmidt, and V. Hollt. 2000. Localization of five somatostatin receptors in the rat central nervous system using subtype-specific antibodies. *Journal of physiology, Paris*. 94:259-264.

Seachrist, J.L., S.A. Laporte, L.B. Dale, A.V. Babwah, M.G. Caron, P.H. Anborgh, and S.S. Ferguson. 2002. Rab5 association with the angiotensin II type 1A receptor promotes Rab5 GTP binding and vesicular fusion. *The Journal of biological chemistry*. 277:679-685.

Seo, S., Q. Zhang, K. Bugge, D.K. Breslow, C.C. Searby, M.V. Nachury, and V.C. Sheffield. 2011. A novel protein LZTFL1 regulates ciliary trafficking of the BBSome and Smoothened. *PLoS genetics*. 7:e1002358.

Shinebourne, E.A., S.V. Babu-Narayan, and J.S. Carvalho. 2006. Tetralogy of Fallot: from fetus to adult. *Heart*. 92:1353-1359.

Short, B., A. Haas, and F.A. Barr. 2005. Golgins and GTPases, giving identity and structure to the Golgi apparatus. *Biochimica et biophysica acta*. 1744:383-395.

Skarnes, W.C., H. von Melchner, W. Wurst, G. Hicks, A.S. Nord, T. Cox, S.G. Young, P. Ruiz, P. Soriano, M. Tessier-Lavigne, B.R. Conklin, W.L. Stanford, and J. Rossant. 2004. A public gene trap resource for mouse functional genomics. *Nature genetics*. 36:543-544.

Slough, J., L. Cooney, and M. Brueckner. 2008. Monocilia in the embryonic mouse heart suggest a direct role for cilia in cardiac morphogenesis. *Developmental dynamics : an official publication of the American Association of Anatomists*. 237:2304-2314.

Smits, P., A.D. Bolton, V. Funari, M. Hong, E.D. Boyden, L. Lu, D.K. Manning, N.D. Dwyer, J.L. Moran, M. Prysak, B. Merriman, S.F. Nelson, L. Bonafe, A. Superti-Furga, S. Ikegawa, D. Krakow, D.H. Cohn, T. Kirchhausen, M.L. Warman, and D.R. Beier. 2010. Lethal skeletal dysplasia in mice and humans lacking the golgin GMAP-210. *The New England journal of medicine*. 362:206-216.

Stadtfeld, M., M. Ye, and T. Graf. 2007. Identification of interventricular septum precursor cells in the mouse embryo. *Developmental biology*. 302:195-207.

Suzuki, T., Y. Kanai, T. Hara, J. Sasaki, T. Sasaki, M. Kohara, T. Maehama, C. Taya, H. Shitara, H. Yonekawa, M.A. Frohman, T. Yokozeki, and Y. Kanaho. 2006. Crucial role of the small GTPase ARF6 in hepatic cord formation during liver development. *Molecular and cellular biology*. 26:6149-6156.

Takeda, S., S. Kadowaki, T. Haga, H. Takaesu, and S. Mitaku. 2002. Identification of G protein-coupled receptor genes from the human genome sequence. *FEBS letters*. 520:97-101.

Tam, B.M., O.L. Moritz, L.B. Hurd, and D.S. Papermaster. 2000. Identification of an outer segment targeting signal in the COOH terminus of rhodopsin using transgenic Xenopus laevis. *The Journal of cell biology*. 151:1369-1380.

Tao, B., S. Bu, Z. Yang, B. Siroky, J.C. Kappes, A. Kispert, and L.M. Guay-Woodford. 2009. Cystin localizes to primary cilia via membrane microdomains and a targeting motif. *Journal of the American Society of Nephrology : JASN*. 20:2570-2580.

Torkko, J.M., A. Manninen, S. Schuck, and K. Simons. 2008. Depletion of apical transport proteins perturbs epithelial cyst formation and ciliogenesis. *Journal of cell science*. 121:1193-1203.

Tyler, K.M., A. Fridberg, K.M. Toriello, C.L. Olson, J.A. Cieslak, T.L. Hazlett, and D.M. Engman. 2009. Flagellar membrane localization via association with lipid rafts. *Journal of cell science*. 122:859-866.

van Meer, G., and K. Simons. 1988. Lipid polarity and sorting in epithelial cells. *Journal of cellular biochemistry*. 36:51-58.

Vieira, O.V., K. Gaus, P. Verkade, J. Fullekrug, W.L. Vaz, and K. Simons. 2006. FAPP2, cilium formation, and compartmentalization of the apical membrane in polarized Madin-Darby canine kidney (MDCK) cells. *Proceedings of the National Academy of Sciences of the United States of America*. 103:18556-18561.

Wang, S., Y. Luo, P.D. Wilson, G.B. Witman, and J. Zhou. 2004. The autosomal recessive polycystic kidney disease protein is localized to primary cilia, with concentration in the basal body area. *Journal of the American Society of Nephrology : JASN*. 15:592-602.

Ward, C.J., M.C. Hogan, S. Rossetti, D. Walker, T. Sneddon, X. Wang, V. Kubly, J.M. Cunningham, R. Bacallao, M. Ishibashi, D.S. Milliner, V.E. Torres, and P.C. Harris. 2002. The gene mutated in autosomal recessive polycystic kidney disease encodes a large, receptor-like protein. *Nature genetics*. 30:259-269.

Ward, C.J., D. Yuan, T.V. Masyuk, X. Wang, R. Punyashthiti, S. Whelan, R. Bacallao, R. Torra, N.F. LaRusso, V.E. Torres, and P.C. Harris. 2003. Cellular and subcellular localization of the ARPKD protein; fibrocystin is expressed on primary cilia. *Human molecular genetics*. 12:2703-2710.

Ward, H.H., U. Brown-Glaberman, J. Wang, Y. Morita, S.L. Alper, E.J. Bedrick, V.H. Gattone, 2nd, D. Deretic, and A. Wandinger-Ness. 2011. A conserved signal and GTPase complex are required for the ciliary transport of polycystin-1. *Molecular biology of the cell*. 22:3289-3305.

Waters, A.M., and P.L. Beales. 2011. Ciliopathies: an expanding disease spectrum. *Pediatr Nephrol*. 26:1039-1056.

Wheatley, D.N. 1995. Primary cilia in normal and pathological tissues. *Pathobiology : journal of immunopathology, molecular and cellular biology*. 63:222-238.

Wu, Y., X.Q. Dai, Q. Li, C.X. Chen, W. Mai, Z. Hussain, W. Long, N. Montalbetti, G. Li, R. Glynne, S. Wang, H.F. Cantiello, G. Wu, and X.Z. Chen. 2006. Kinesin-2 mediates physical and functional interactions between polycystin-2 and fibrocystin. *Human molecular genetics*. 15:3280-3292.

Xia, H., Z.D. Hornby, and R.C. Malenka. 2001. An ER retention signal explains differences in surface expression of NMDA and AMPA receptor subunits. *Neuropharmacology*. 41:714-723.

Yoder, B.K., X. Hou, and L.M. Guay-Woodford. 2002. The polycystic kidney disease proteins, polycystin-1, polycystin-2, polaris, and cystin, are co-localized in renal cilia. *Journal of the American Society of Nephrology : JASN*. 13:2508-2516.

Yoshimura, S., J. Egerer, E. Fuchs, A.K. Haas, and F.A. Barr. 2007. Functional dissection of Rab GTPases involved in primary cilium formation. *The Journal of cell biology*. 178:363-369.

Zerial, M., and H. McBride. 2001. Rab proteins as membrane organizers. *Nature reviews. Molecular cell biology*. 2:107-117.

Zhang, M.Z., W. Mai, C. Li, S.Y. Cho, C. Hao, G. Moeckel, R. Zhao, I. Kim, J. Wang, H. Xiong, H. Wang, Y. Sato, Y. Wu, Y. Nakanuma, M. Lilova, Y. Pei, R.C. Harris, S. Li, R.J. Coffey, L. Sun, D. Wu, X.Z. Chen, M.D. Breyer, Z.J. Zhao, J.A. McKanna, and G. Wu. 2004. PKHD1 protein encoded by the gene for autosomal recessive polycystic kidney disease associates with basal bodies and primary cilia in renal epithelial cells. *Proceedings of the National Academy of Sciences of the United States of America*. 101:2311-2316.

Zohn, I.E., and A.A. Sarkar. 2010. The visceral yolk sac endoderm provides for absorption of nutrients to the embryo during neurulation. *Birth defects research. Part A, Clinical and molecular teratology*. 88:593-600.